Fracture Analysis of all composite made fuselage shell under random vibration loading

By

Kirubeil Awoke

A thesis submitted to the School of Graduate Studies of Addis Ababa Institute of Technology in partial fulfillment of the requirements of the Degree of Masters of Science in Mechanical Engineering

(Mechanical Design Stream)

Advisor

Prof. Idalberto Mendoza

July, 2011

Addis Ababa, Ethiopia

Addis Ababa Institute of Technology

School of Graduate Studies

Department of Mechanical Engineering

Mechanical Design Stream

"Fracture analysis of all composite made fuselage shell under random vibration loading."

By

Kerubeil Awoke

Approved by board examiners:

Prof. Idalberto Mendoza (Advisor)	24/01/2011 Date
Dr. Daniel Tilahun (Chairman, Examiner)	19/07/2011 Date
Dr.Ing Tamirat Tesfaye (Ext. Examiner)	06/09/2011 Date

Associate Deans office for Research & Graduate Program
Addis Ababa University
Addis Ababa Institute of Technology
06 Sept 2011

Acknowledgments

I would like to thank my supervisor, Prof. Idalberto Mendoza for his support, enthusiasm, guidance, assistance and wealth of ideas. He gave me good advice as a friend and supervisor in many moments of my life.

I also would like to express my appreciation to Measho and Lema who provided flexible working time to complete my thesis.

I would especially like to thank my classmates Mulugeta, Samrawit, and my friends. I cannot forget the times that we stayed to talk about different ideas in the coffee time and walking time.

I also would like to thank my friend Belay Olijera, who has made technical support and materials necessary for the thesis.

Finally, I wish to thank my families who have made all this possible: my mother and father, and my sisters and brothers and my friend Genet.

Abstract

Aircrafts and its airframes are subjected to various kinds of time dependent loadings; ranging from flight loads to ground maneuvering loads. In this thesis, the dynamic responses such as stress, strain or displacement near the crack tips on the all composite made fuselage structure when landing on various types of take off and landing pavement are assessed.

Finite element modeling and analysis for all composite made fuselages is done using the layered shell element 4 node 63. A crack of significant parameter is generated on the outer top part of the shell for initiation of fracture. One leg model of the landing gear is used to drive the required mathematical formulations. The crack tips responses to random excitation caused by road roughness are determined. The excitation includes smooth, pastured and ploughed take off and landing strips.

In all curves as the crack length increases the displacement and stresses response near the crack tips increases. We can see from the literature that the applied stress is directly proportional to the square root of the half crack length. This result was verified experimentally by Griffith for a wide range of crack length. This confirms both the analytical and experimental results obtained by Griffith's and other similar researchers.

From the curves we can observe that the shell responds relatively lowest stress and displacement response to class A than Class G and Class H pavement. Class H has the worst stress and strain response near crack tips and much affects and severs the thin structure. More over, stress and strain response to circumferential crack orientation is higher than the corresponding longitudinal one. This is probably due to the stress waves are perpendicular to the orientation of a crack, and which maximizes the local stress.

Generally, the shell structure has higher strength to weight ratio and has higher stress and strain carrying capability, trends should look for using shells as their primary structure. Moreover, in the event of forced and emergency landing, the pilot has recommended to land as much as possible on Class G pavement than Class H pavement so that the applied stress is optimized.

Key words: ***Composite, Shell fuselage, Crack, Random vibration analysis, Power spectral density, Ground induced excitations, pavement roughness data.***

Table of Contents

List of figures

List of tables

Nomenclature

a	*Half of crack length*
a_y	*Vertical component of aircraft acceleration*
$[B]$	*Strain displacement matrix*
c	*Depth of crack*
$c.g$	*Center of Gravity*
C_N	*Nose gear viscous damping*
C_M	*Main gear viscous damping*
Ct	*Damping of the tire*
$[C]$	*Structural damping matrix*
$[D]$	*Constitutive matrix*
E_x	*Young's modulus along the longitudinal direction*
E_y	*Young's modulus along the normal direction*
E_{xy}	*Young's modulus along the lateral direction*
f	*Frequency*
$\{F\}$	*Body force vector*
$\vec{F}(t)$	*Load vector or forcing function.*
$F(\omega)$	*Fourier transform of response* $f(t)$
F^B	*Body force vector*
F^S	*Surface load vector*
$f_{ij}^{I}(\varphi)$	*Beta or the geometric factors for mode I*
$f_{ij}^{II}(\varphi)$	*Beta or the geometric factors for mode II*
$f_{ij}^{III}(\varphi)$	*Beta or the geometric factors for mode III*
G_x	*Shear modulus along the longitudinal direction*

G_y	*Shear modulus along the normal direction*
G_{xy}	*Shear modulus along the lateral direction*
$h(\chi_r)$	*Profile of a runway is defined relative to a flat datum*
$h(\chi_r)$	*Current location of the aircraft during the taxiing process*
$h(t)$	*Runway profile*
$\dot{h}(t)$	*Rate of change with time of the profile*
h_N	*The profile values at the nose gear position*
h_M	*The profile values at the main gear positions*
h'_N	*The amplitude input excitations at the nose gear*
h'_M	*The amplitude input excitations at the main landing gears*
$H(\omega)$	*Transfer function matrix*
$[H^*(\omega)]$	*The complex conjugate of the transfer function*
K_N	*Nose gear stiffness*
K_M	*Main gear stiffness*
Kt	*Stiffness of the tire*
$K_I(t)$	*Mode-I Dynamic Stress Intensity Factor*
$K_{II}(t)$	*Mode-II Dynamic Stress Intensity Factor*
[K]	*Structural stiffness matrix*
L	*Lift force*
L	*The Lagrangian's*
l_M	*Length from main leg to the aircraft c.g position*
l_N	*Length from nose leg to the aircraft c.g position*
L_r	*Length of runways/pavements*
m	*Mass of aircraft*
Mt	*Mass of the tire*
[M]	*Structural mass matrix*

$[M_e]$	*Element mass matrix*
N	*Inertial load*
$[N]$	*Displacement transformation matrix*
$O(l)$	*Contribution of higher order terms on the stress field and T-stress*
r	*Distance from crack tip*
R_M	*Reaction forces at the main landing gears*
$S_g(\Omega)$	*Power spectral density of the road roughness based on spatial frequency*
$s_g(\omega)$	*Power spectral density of the road roughness based on temporal frequency*
$[S_F(\omega)]$	*The Spectral density function matrix of a load or excitation*
$[S_Z(\omega)]$	*The Spectral density function matrix of the responses*
$S_{xx}(\omega)$	*Power spectral density (PSD) of the excitation in terms of circular frequency*
t	*Time*
t	*The specific time that autocorrelation function is dependent*
T *-stress*	*Uniform non-singular stress, normal to the crack line*
T	*The kinetic energy*
u_r	*Radial component of displacement*
u_θ	*Angular component of displacement*
$\{u\}$	*Displacement vector for the element*
U	*The internal/strain energy*
U	*Displacement vectors*
$\dot{U}$	*Velocity vectors*
$\ddot{U}$	*Acceleration vectors*
v_y	*Vertical component of landing speed*
v_{land}	*Horizontal component of landing speed*

w	*Crack width*
W	*Aircraft weight*
W_E	*The external energy which is work done by external loads*
$X(\omega)$	*Fourier transform of excitation* $x(t)$
χ_r	*Distance along the runway measured with respect to a convenient origin*
χ_r	*Aircraft position at any instant, being defined with the centre of mass at distance from the runway origin*
χ_N	*Nose gear location from the reference origin*
χ_M	*Main gear location from the reference origin*
χ'_U	*Amplitudes of the responses of the un-sprung sprung mass*
χ'_S	*Amplitudes of the responses of the sprung mass*
χ_U	*The power spectral densities, PSD of the un-sprung masses*
χ_S	*The power spectral densities PSD of the sprung masses*
X_{Z11}	*Power spectral density functions of* χ_S
X_{Z22}	*Power spectral density functions of* χ_U
$X_{Z11}(\Omega)$	*The PSD function used as input for the FE analysis*
$X_{Z22}(\Omega)$	*The PSD function response of the structure*
y	*Displacement excitation*
y'	*The amplitude input excitations*
Z_C	*Heave relative to any horizontal datum*
Z'_C	*Amplitudes of the translational response of the aircraft at the center of gravity*
σ_{ij}	*Mixed mode distribution of stress near crack tip*
σ_r	*Radial component of stress*
σ_θ	*Angular component of stress*
$\tau_{r\theta}$	*Transverse shear stress component*

σ_1	*Principal stress along x direction*
σ_2	*Principal stress along y direction*
φ	*Polar coordinate angle*
X-Y-Z	*Earth fixed coordinate system*
x-y-z	*Body fixed coordinate system*
τ	*The period that autocorrelation function is dependent*
Ω	*Spatial frequency*
Ω_0	*Value of the spatial frequency which is equal to* $1/2\pi$ *cycles/m*
ω	*Circular frequency*
Δh_r	*Dip of depth*
θ	*Pitch relative to any horizontal datum*
θ'	*Amplitudes of the pitch response of the aircraft at the center of gravity*
Π	*The potential energy*
$\{\overline{\Phi}\}$	*Surface load vector*
$\{\phi\}$	*Nodal displacement vector*
$\{\varepsilon\}$	*Displacement matrix*
$\{\sigma\}$	*Stress vector*
ϖ_i	*The* i^{th} *Natural frequency*
γ_x	*Shear strain along the longitudinal direction*
γ_y	*Shear strain along the normal direction*
γ_{xy}	*Shear strain along the lateral direction*
ρ	*Mass density of the material*

Abbreviations

ANSYS	*Analysis software*
CAD	*Computer Aided Design*
CFRP	*Carbon Fiber Reinforced Plastic*
DDAM	*Dynamic Design Analysis Method*
DoF	*Degree of Freedom*
DSIF	*Dynamic Stress Intensity Factor*
FEM	*Finite Element Method*
FRF	*Frequency Response Function*
FT	*Fourier transforms*
IRI	*International Roughness Index*
ISO	*International organization for Standardization*
LEFM	*Linear Elastic Fracture Mechanic*
M	*Main subscript*
N	*Nose subscript*
MDoF	*Multiple degree of freedom*
MPRS	*Multi-point Response Spectrum*
PSD	*Power Spectral Density*
SAE	*Society of Automotive Engineers*
SPRS	*Single-point Response Spectrum*
2D	*Two dimensional*
3D	*Three dimensional*

Chapter One

1.1 Thesis Background

Our understandings of how materials fail and our ability to prevent such failures have increased considerably since World War II. Much remains to be learned, however, and existing knowledge of fracture mechanics is not always appropriately applied when especially for modern technological materials like composites. The combination of two or more materials can lead to a third material with highly desirable properties known as composite materials. The constituents of a composite material are usually combined on a macroscopic scale through physical rather than chemical means. Composite materials usually consist of a matrix and a reinforcing constituent. The matrix is often soft and ductile compared to the reinforcement. Various types of reinforcement are possible, including continuous fibers, chopped fibers, whiskers, flakes, and particulates [12].

In many practical applications, using composites is more efficient. For example, in highly competitive airline markets, one is continuously looking for ways to lower overall mass of the aircraft without decreasing the stiffness and strength of its components like thin shells or pressure vessel. This is possible by replacing conventional metal alloys with composite materials. Even if the composite material costs may be higher, the reduction in the number of parts in an assembly and the savings in the fuel costs make them more profitable [13].

The use of composite materials in all types of engineering structures has led to an increased interest in the theory, analysis, design and manufacturing of structural components. The last few decades have seen a major effort to develop composite material systems and analyze, and design structural components made from them.

The dynamic analysis of composite plates/shells plays an increasingly important role in the design of structures in mechanical, civil and aerospace engineering applications. A thorough study of the dynamic behaviors of these structures is essential in assessing their full potential. Therefore, it is necessary to develop appropriate physical and mathematical models capable of accurately predicting their dynamic responses.

The presence of cracks in structural elements or mechanical components is, to a certain point, a common case in industrial installations. Such cracks are due to excessive loads and fatigue during service or even manufacturing and installation defects, which are a cause of reduction in structural integrity. To evaluate the effect of the presence of cracks in structural components, fracture mechanics theory is used; its origins can be referred to Griffith [2]. This is adequate when quasistatic conditions are present and the material shows linear elastic behavior.

Dynamic fracture mechanics is the subfield of fracture mechanics concerned with fracture phenomena in which inertia plays a role. Dynamic processes in a cracked body fall into two basic categories: *dynamic crack propagation*, and *dynamic loading of bodies with stationary cracks*. Often a mixture of these two kinds of processes appears, for example when dynamic loading on a body which contains a stationary crack causes dynamic crack propagation, or when dynamic crack propagation generates waves, which after reflection at an outer boundary of the body, impact on the crack.

Because an additional dimension, the time, enters when going from a static to a corresponding dynamic case, the mathematical models and the analysis are, of course, more difficult and complex. From the experimental point of view, the time dependence requires that many accurate sequential measurements of quantities of interest must be made in an extremely short time period such that there is no interference with the process being observed.

Elasto-dynamic analysis of crack problems indicates that stresses and displacements caused by dynamic loading can differ greatly from those associated with the corresponding static loading. At some locations in the structure the dynamic stresses are higher than the corresponding static one. This result may be explained by the intersection of the elastic waves with the crack faces and other characteristic boundaries of the structure [2].

Dynamic loads give rise to high stress levels near cracks and fracture takes place so rapidly that there is insufficient time for yielding to develop. Energy is therefore released within a short time, leading to rapid crack propagation; this explains the experimental observation that dynamic loads generally promote brittle fractures [2].

Dynamic analysis of composite shells has attracted much attention to the researchers. A quick and accurate prediction of dynamic behavior of such composite shells is of very much interest to designers and experimentalists alike. This normally requires a comprehensive development of a physical and mathematical model. Due to the complexity of engineering characteristics of composite shell type structures, analytical solutions cannot be obtained in a straight forward manner. The differential quadrature method (DQM) is an efficient numerical technique which transforms governing equations of dynamic equilibrium to a matrix form by using weighted matrices.

In dynamic analysis problems, the inertial characteristic of the problem is very important but its analysis is complicated. One of the first contributions in this area is due to Yoffe, who considered that cracks grow by propagating in a perpendicular direction to the maximum main stress. Also, when its speed reaches 60% of the transversal wave speed, cracks change their propagation direction and if such speed increases the cracks branches out. Broberg studied the case of stationary and running cracks loaded by a stress wave for the case of transversal wave propagation. For running cracks, he found that they grow from an initial length with constant opposite velocities at the two crack tips. His research has had considerable impact in the field of dynamic fracture mechanics in stating that the resistance must be proportional to the crack length in order to comply with the motion.

Numerical methods have been developed for the solution of problems in fracture dynamics such as those related to the interaction of waves in cracked media. Such techniques have been efficient in simulating cracked components under various loads and boundary conditions. Among those numerical methods, the Finite Difference Method has been applied in solving wave propagation problems in cracked media. Chen [18] studied the case of a central cracked plate under an impulsive load using the Finite Difference Method. He found that the stress field in the plate, and particularly at the crack tip, is controlled by the interaction of the stress waves generated by the impulsive load. Variations of the DSIF versus time were found, and it was stated that interaction of elastic waves participate in this variation.

Alastair F. Johnson [15] presents materials modeling and numerical simulation of the impact and crash response of fiber reinforced composite structures. The work is based on the application of explicit finite element (FE) analysis codes to composite aircraft

structures under both low velocity crash and high velocity impact conditions. He also presented the crash response of helicopter sub floor box structures using a strain based damage and failure criterion for fabric reinforced composites. He discussed also improved models for predicting delamination and a novel approach has been presented in which a composite laminate is modeled numerically by stacked shell elements with contact interfaces whose delamination is controlled by fracture mechanics criteria. The result showed that the measured impact response is agreed with the simulation result.

Elasto-dynamic crack problems, in a linear elastic material, can be solved efficiently with alternative boundary element formulations. J. C. F Telles and C. A. R Vera-Tudela[16] introduces an approach that involves the Numerical Green's Function (NGF) and the Operational Quadrature Method (OQM). The Numerical Green's Function, in the Laplace domain, is used as a fundamental solution in which element discretization of actual crack surfaces is no longer required. In the adopted OQM technique the convolution integral is substituted by a quadrature formula, whose weights are computed using the fundamental solution in the Laplace domain, producing the direct solution to the problem in the time domain. They get the result that basic function works for kinked cracks is also used for branched cracks.

The objective of dynamic fracture mechanics is to describe the behavior of a body with crack under dynamic loading. Thereby a crack is a partial (microscopic) or complete macroscopic separation of a body. Pre-existing cracks are very common and virtually impossible to avoid in large structures. An important question is whether a pre-existing crack will grow for a given loading or not.

Cracks are also frequently formed during manufacturing of the material or as the result of mechanical processes during manufacturing structural parts and during service. Modeling of fracture processes in structures and its simulations are challenging problems in mechanics as well as in mathematics. Its understanding is important for the construction of thin structures and the development of new materials.

Typically the mathematical model consists of an idealized description of the geometrical configuration of the deformable body, an empirical relationship between internal stress and deformation, and a corresponding balance law of physics dealing with mechanical quantities.

1.2 Airplane loads

Aircrafts are subjected to a range of static and dynamic loads resulting from flight maneuvers, ground maneuvers and gust/turbulence encounters. These load case are responsible for the critical design loads over the aircraft structure and hence influence the structural design. Determination of such loads involves consideration of aerodynamic, elastic and inertia effects and requires the solution of the dynamic responses.

The structure of an airplane is required to support two distinct classes of loads: the first termed, *ground loads* include all loads encountered by the airplane during movement or transportation on the ground such as taxiing and landing loads, towing and hoisting loads; while the second; *air loads* comprise loads imposed on the structure during flight by maneuvering and gusts. In addition, aircraft designed for a particular role encounter loads peculiar to their sphere of operation. Conventional aircraft usually consists of fuselage, wing and tail plane. The fuselage designed to hold crew and payload, the wings provide the lift and the tail plane is the main contributor to the directional control and stability. Ground loads encountered in landing and taxiing subject the aircraft to concentrated shock loads through the undercarriage system. The basic functions of airplane structural parts are to transmit and resist the applied loads; to provide an aerodynamic shape and to protect passengers, payload systems, etc from the environmental conditions encountered in flight. These requirements, in most aircraft, result in thin shell structures where the outer surface or skin of the shell is usually supported by longitudinal stiffening members and transverse frames to enable it to resist bending, compressive and torsional loads without buckling.

Types of fuselage

There are three types of fuselage structure in modern aircraft construction: these are

(i) Longeron or reinforced fuselage

(ii) Stringer or semi-monocoque fuselage

(iii) Skin or shell (pure monocoque) fuselage

The load bearing and constructional features of each type fuselage varies depending on the purpose of airplane. But in this research, shell type fuselage is considered for the analysis.

When the aircraft touches the ground by the wheels during landing (Fig 1.2), it has vertical component υ_y in addition to the horizontal component of speed υ_{land}. Speed υ_{land} is gradually decreased at landing run. Vertical component υ_y would be damped instantaneously if no shock absorbing devices were provided. This would lead to the considerable loads were applied to the structural members.

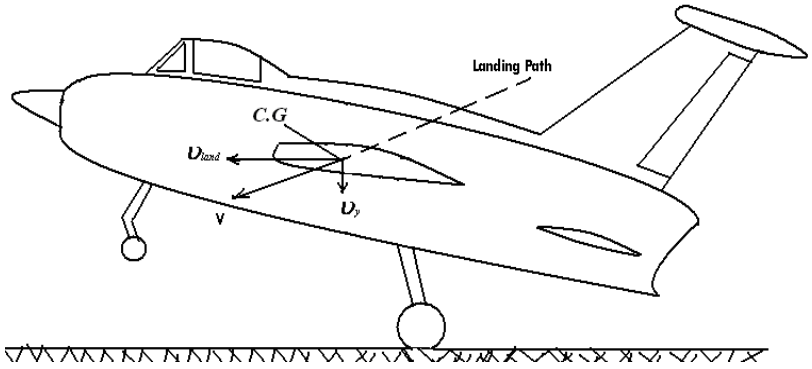

Figure 1.1Airplane at touch down speed. [11]

Actually, at landing the landing gear experiences reaction forces R_M (Fig.1.2) which balance aircraft weight W, lift force L, and inertia force N.

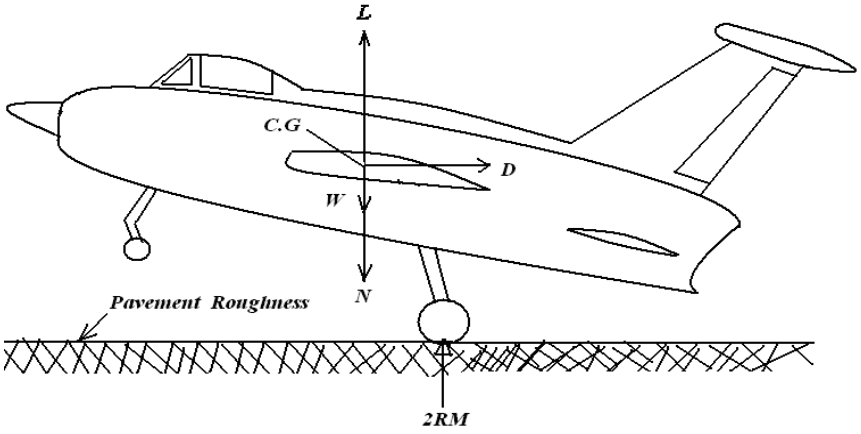

Figure 1.2Forces *acting on aircraft at landing* [11]

where $N = m a_y$

m = mass of aircraft

a_y =vertical acceleration in the center of gravity

Equation of motion along the vertical direction gives:

$$\sum \vec{F} = -m\vec{a}$$

$$2\vec{R}_M + \vec{L} - \vec{W} = -m\vec{a}$$

It may be assumed that at touchdown $L = W$, then

$$2R_M = -m a_y = N .$$

Thus, the higher is the absolute value of vertical acceleration a_y, the higher are the loads R_M on the landing gear and inertia loads acting on all the members of the aircraft structures.

The vertical considerable acceleration may appear at crossing airfield irregularities with a high speed. The vertical acceleration may be decreased by increasing the time of damping speed v_y. This is achieved by the shock absorbing devices which smoothly change their length under the action of a load thus increasing the track and the time of lowering of the aircraft c.g. position, and, hence, decreasing the absolute value of the vertical accelerations. Thus, the landing gear shock absorbing devices are designed to ease loads propagated to all the moments of the aircraft structure during landing and during movement along the airfield irregular surface.

The landing gear shock absorbing devices include wheel tires and shock absorbers. Depending on the inflation pressure, the wheel tire takes up 15-25% of the entire energy of the impact but dissipates only a small part of it. The shock absorber takes up the major part of the kinetic energy and dissipates it in to heat.

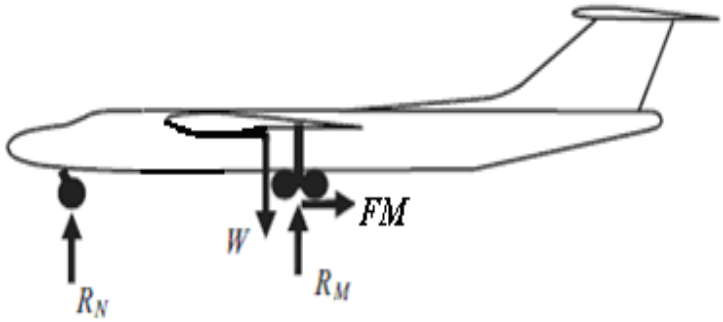

Figure1.3 ***Principal loads on aircraft during ground roll*** **[1]**

During service, any aircraft is subjected to loads that cause stresses, vibrations and noise in the different components of its structure. This requires appropriate strength, stiffness and fatigue properties of the components to be able to withstand these loads. On top of that, quality of an airplane, as a system, which include efficient energy consumption, safety, and provision of comfort to the passenger are highly desired.

Forces and moments generated by tires at the ground are significant in controlling motion of the aircraft during movement on the ground. The responses of the structures to these loads are dealt with in ground maneuvers. The responses of a structure are defined in terms of deflections, stresses and strains, natural frequencies, random response functions, fatigue life and so on.

1.3 Cracks [2]

At the crack tip the stress field can be broken up into three components, called Mode I, Mode II and Mode III, as sketched in figure 1.5.

Mode I: The forces are perpendicular to the crack; causing the crack to open orthogonal to the local fracture surface and results in tension or compressive stresses in the x2 direction (see fig 1.4).

Mode II: The forces are parallel to the crack; causing the crack surfaces to slide relative to each other in the x1 direction (see fig 1.4).

Mode III: The forces are perpendicular to the crack (the crack is in front back direction, the forces are pulling left and right) causing the crack surface to slide relative to each other in the x3 direction (see fig 1.4).

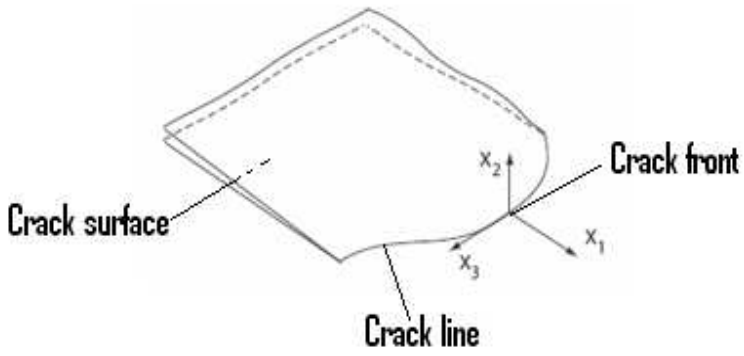

Figure 1.4*Crack front for an arbitrarily shaped crack surface in a solid [16]*

At any point along the crack line a local coordinate system may be defined as shown in the fig 1.4. Think of this as representing the state of stress for a cube of material surrounding part of a crack tip. The actual crack may have a mix of Mode-I, II, III loadings and this mix may vary along the crack front.

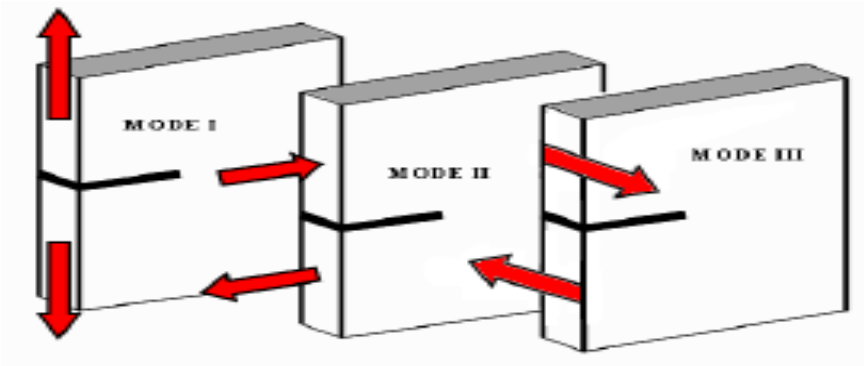

Figure1.5*Three loading modes of fracture. In plane cases: Mode I, II,*
Out-of- plane case: Mode III

1.3.1 Debonds

Debonds are types of fracture in composite materials where the bonding between the material molecules are vulnerable to breakage. These occur in weak strength materials more often. These are due to mould defects during manufacturing.

1.3.2 Delaminations

One of the most commonly observed failure modes in composite materials is delamination, a separation of the fiber reinforced layers that are stacked together to form laminates. The most common sources of delamination are the material and structural discontinuities shown in the figure 1.6. Delamination occur at stress free edges due to the mismatch in properties of the individual layers, at ply drops where thickness must be reduced, and at regions subjected to out of plane loading such as bending of curved beams.

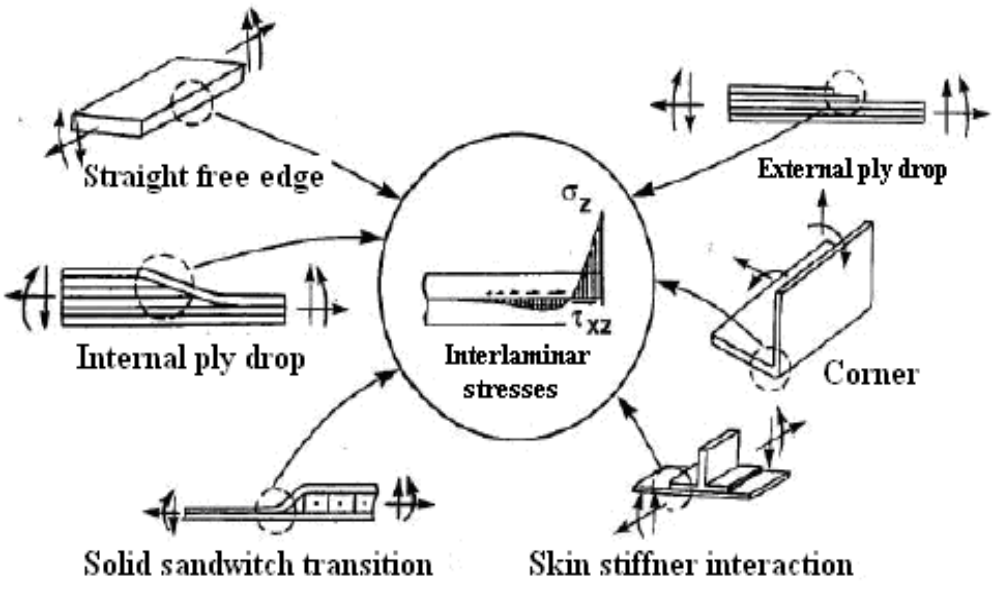

Figure 1.6*Forms of delaminations* [14]

1.4 Linear Elastic Fracture Mechanics

Linear Elastic Fracture Mechanics applies when the non-linear deformation of the material is confined to a small region near the crack tip. For the analysis it is assumes that:

a) The material is homogeneous isotropic continuum; its behavior is linear elastic, strains and displacements are small and crack surfaces are smooth,

b) The material is free from large scale self-equilibrating internal stresses and from body forces (gravity),

c) The analyzed domain has a constant thickness,

d) The initial crack is large (i.e. longer than 1 mm),

e) Loads are applied dynamically and randomly; and

f) The growth of a single dominant crack leads to failure.

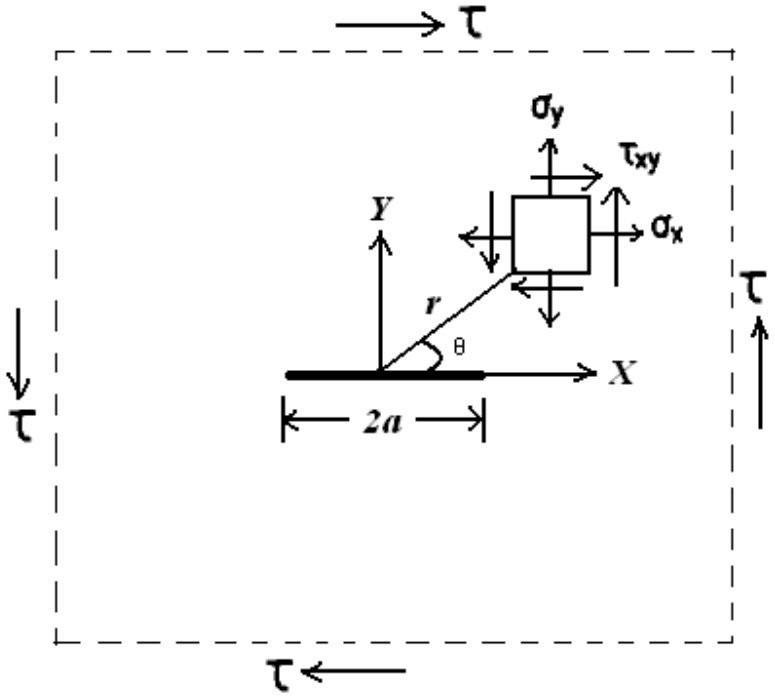

Figure 1.7 ***A*** *crack* ***of length 2a in an infinite plate subjected*** *to* ***uniform*** *in-plane shear stresses* τ *at infinity* [2].

The governing equation for the expressions of the singular polar components of stress and displacement for static loading may be given by

$$\sigma_r = \frac{K_1}{\sqrt{2\pi r}}\left(\frac{5}{4}\cos\frac{\theta}{2} - \frac{1}{4}\cos\frac{3\theta}{2}\right) \quad \text{.....1.1}$$

$$\sigma_\theta = \frac{K_1}{\sqrt{2\pi r}}\left(\frac{3}{4}\cos\frac{\theta}{2} + \frac{1}{4}\cos\frac{3\theta}{2}\right) \quad \text{.....1.2}$$

$$\tau_{r\theta} = \frac{K_1}{\sqrt{2\pi r}}\left(\frac{1}{4}\sin\frac{\theta}{2} + \frac{1}{4}\sin\frac{3\theta}{2}\right) \quad \text{.....1.3}$$

and

$$u_r = \frac{K_1}{4\mu}\sqrt{\frac{r}{2\pi}}\left[(2k-1)\cos\frac{\theta}{2} - \cos\frac{3\theta}{2}\right] \text{.....1.4}$$

$$u_\theta = \frac{K_1}{4\mu}\sqrt{\frac{r}{2\pi}}\left[(-2k-1)\sin\frac{\theta}{2} + \sin\frac{3\theta}{2}\right] \text{.....1.5}$$

and for the principal singular stresses

$$\sigma_1 = \frac{K_1}{\sqrt{2\pi r}}\cos\frac{\theta}{2}\left(1+\sin\frac{\theta}{2}\right) \text{.....1.6}$$

$$\sigma_2 = \frac{K_1}{\sqrt{2\pi r}}\cos\frac{\theta}{2}\left(1-\sin\frac{\theta}{2}\right) \text{.....1.7}$$

1.5 Dynamic fracture mechanics analysis

When cracks propagate in homogenous and brittle solids, they can only do so under locally mode-I conditions and at sub-Rayleigh wave speeds typically below the crack branching speed. Even if the applied loading is asymmetric, the dynamically growing crack will curve and follow the path that will result in locally opening (mode-I) conditions. The situation is entirely different if a crack is constrained to propagate along a weak preferred path in an otherwise homogenous solid. In this case and depending on the bond strength, the weak crack path or bond often traps the crack, suppresses any tendency of branching or kinking out of the weak plane and permits very fast crack growth much beyond the speeds observable in monolithic solids. Indeed, when mode-I cracks propagate in both isotropic and orthotropic solids containing weak crack paths, they can reach speeds as high as the Rayleigh wave speed of the solid. On the other hand, when mode-II cracks are made to propagate along such weak paths, they tend to go at even faster speeds that are clearly within the intersonic regime of the solid. Although the extreme mode-I and mode-II cases have recently been studied experimentally and theoretically, very little is known about the dynamic mixed-mode crack growth along weak paths, a situation that has only recently been analyzed by Geubelle and Kubair about the transition of an incident dynamic mode-I crack into a mixed-mode crack as it

encounters a weak plane or interface. Recently, Xu et al. examined the incidence of dynamically growing cracks at inclined interfaces of various strengths. Interesting phenomena on mixed-mode crack growth along an interface were observed. They tested weakly bonded systems composed of identical constituents so that the resulting material remains constitutively homogenous. However, the existence of a weak bond (bond of lower fracture toughness) made this material inhomogeneous regarding its fracture resistance behavior. Therefore, the complication of the stiffness property and wave speed mismatch across the interface was avoided while retaining the essential properties of a weak interface or bond whose strength could be experimentally varied and analytically modeled.

In dynamic fracture mechanics problems, the most important parameter is the DSIF, which represents the stress singularity of $r^{1/2}$ near the crack tip or the crack center for a central crack; *r* is the normal distance to the crack tip. The DSIF is a function of time t, and the way to evaluate it is by knowing the displacements at the crack surfaces in a local coordinate system for full models.

1.5.1 Stress field around the tip of a dynamically propagating Mode-I crack

Williams characterized mathematically the distribution of the stresses, σ_{ij} near the crack tip in the *LEFM* domain by means of an expansion series with the contracted form in equation

$$\sigma_{ij} = \frac{1}{\sqrt{2\pi r}}\left[K_I f_{ij}^{I}(\varphi) + K_{II} f_{ij}^{II}(\varphi) + K_{III} f_{ij}^{III}(\varphi) + T\delta_{il}\delta_{li} + O(l) \right] \text{.....1.8}$$

Where $K_I, K_{II}, and\ K_{III}$, are the stress intensity factors (*SIF*) for *Mode I, II* and *III* respectively; *r* is the distance from the crack tip; σ_{ij} are the stresses defined near the crack tip; φ is the polar coordinate angle. $f_{ij}^{I}(\varphi)$, $f_{ij}^{II}(\varphi)$, and $f_{ij}^{III}(\varphi)$ are functions dependent on crack length and geometry, which for a large number of two dimensional (*2D*) crack cases are available on form of diagrams, tables and interpolation formula.

These functions are also called the beta or the geometric factors. $O(l)$ represents the contribution of higher order terms on the stress field and T, called the *T*-stress, is a uniform non-singular stress, normal to the crack line and dependent on the type of loading and specimen geometry [14].

Neglecting the contributions of higher order terms, the developed form of equation 1.8, for a *3D* cracked body under pure *Mode I* loading, can be written as [2]:

$$\begin{bmatrix} \sigma_{xx} & \sigma_{xy} & \sigma_{xz} \\ \sigma_{yx} & \sigma_{yy} & \sigma_{yz} \\ \sigma_{zx} & \sigma_{zy} & \sigma_{zz} \end{bmatrix} = \frac{K_I}{\sqrt{2\pi r}} \begin{bmatrix} f^I_{xx}(\varphi) & f^I_{xy}(\varphi) & f^I_{xz}(\varphi) \\ f^I_{yx}(\varphi) & f^I_{yy}(\varphi) & f^I_{yz}(\varphi) \\ f^I_{zx}(\varphi) & f^I_{zy}(\varphi) & f^I_{zz}(\varphi) \end{bmatrix} + \begin{bmatrix} T & 0 & T_{xz} \\ 0 & 0 & 0 \\ T_{zx} & 0 & T_{zz} \end{bmatrix} \text{.....1.9}$$

Stress field of a steady mode-I crack is given for dynamic loading by a well-known form

$$\sigma^I_{ij} = \frac{K_I(t)}{\sqrt{2\pi r}} \sum^I_{ij}(\theta, \upsilon) + T\,\delta_{il}\,\delta_{jl} + O(l) \qquad (i, j = 1,2) \text{.....1.10}$$

where *KI(t)* is the dynamic stress intensity factor of the mode-I crack as a function of time *t*; *T* is a non-singular term, which is called ''the *T-stress*''; *O(1)* represents higher order terms; the functions $\sum^I_{ij}(\theta, \upsilon)$ that represent the angular variation of stress components for an instantaneous crack tip speed υ.

1.5.2 Stress field around the tip of a dynamically propagating mixed-mode crack

Similarly, the asymptotic stress field of a steady mode-II crack can be expressed by

$$\sigma^{II}_{ij} = \frac{K_{II}(t)}{\sqrt{2\pi r}} \sum^{II}_{ij}(\theta, \upsilon) + O(l) \quad (i, j = 1,2) \text{.....1.11}$$

where $K_{II}(t)$ is the dynamic stress intensity factor of the mode-II crack as a function of time *t*. There is no *T-stress* involved in a pure mode-II crack stress expression. The functions $\sum^{II}_{ij}(\theta, \upsilon)$ that represent the angular variation of stress components for an instantaneous crack tip speed υ.

Based on Esq. (1.10) and (1.11), the stress field of a mixed-mode crack can be obtained using linear superposition principle:

$$\sigma_{ij} = \sigma_{ij}^{I} + \sigma_{ij}^{II} = \frac{K_I(t)}{\sqrt{2\pi r}} \sum_{ij}^{I}(\theta, \upsilon) + T\,\delta_{il}\delta_{jl} + \frac{K_{II}(t)}{\sqrt{2\pi r}} \sum_{ij}^{II}(\theta, \upsilon) + O(l)\ (i, j=1,2) \quad \textbf{.....1.12}$$

1.6 Objectives of the problem

The objective of this thesis is to analyze the effect of crack length on the stresses, strain and their distribution near the crack tips in an all composite made fuselage shell by using finite element software. This will be done through modeling and simulating the cracked shell and applying the loads which exist in the fuselage at landing; such as, ground induced excitation due to pavement irregularities.

Basically, the problem consists in the evaluation of stress and displacement response and behaviors of an all composite made shell having *a stationary crack* due to dynamic loading. In this research the dynamic loading represents, random vibration loading induced by the different types of surface irregularities; such as smooth runway (Class A road type), pasture (class G runway) and plowed field(class H runway) propagated in to the shell, particularly to the skin. By “stationary crack” it means that crack length is constant and crack tips remain permanently fixed in a finite medium.

1.7 Methodology

To fulfill the objectives of the study the following are used.

i. ***Literature Review*:** Survey of books, journal articles, proceedings of international conferences, aircraft manufacturer catalogues, and other relevant literatures are done.

ii. ***Data Collection*:** data used for this research are collected from internet. The data include dimensions of the thin structure, material used to construct the structure, loads acting on the structure. Pavement roughness data of the different types of runways and roads are obtained from books and journals.

iii. ***Modeling and Analysis:*** The finite element model development as well as the corresponding dynamic analysis is performed using ANSYS software.

iv. ***Conclusions and Recommendations.***

1.8 Thesis Layout

This thesis document details the theoretical background, modeling and analysis of the shell type thin structures and algorithms required to perform the analysis on the software used. It has been divided into five separate chapters. The first chapter discusses thesis background and previous research works carried in the field of dynamic fracture mechanics on composite shells. The second chapter deals with the basic concepts of physical modeling and mathematical formulation of random vibration loadings, representing of a typical pavement roughness model, tire and wheel assembly model, and using the above physical and mathematical models arrive at a reasonably mathematical formulations used as an input for the dynamic fracture problem. Chapter three presents finite element mathematical modeling and geometric descritaization of the shell structure. It discusses elasticity of structural matrix derivation, modeling of spring and damper combination used to represent the shock absorbing mechanism for the complete airplane sketch, crack modeling as a semi elliptical shape. Chapter four covers all the numerical results and discussion of results obtained in the ANSYS. Finally, chapter five gives principal conclusions and propositions for areas of future works.

Chapter Two

Physical modeling and mathematical formulations

2.1 Introduction

This chapter deals with random vibration loading due to different types pavement roughness excitations.

2.1.1 Random variable loadings

In determining aircraft responses for gusts and maneuvers [1], the aircraft response to a number of different types of forcing functions needs to be considered. These tend to divide into three categories:

1. *Harmonic excitation* is primarily concerned with excitation at a single frequency (for engine or rotor out-of-balance and as a constituent part of continuous turbulence analysis).
2. *Non-harmonic deterministic excitation* includes the '1-cosine' input (for discrete gusts or runway bumps) and various shaped inputs (for flight maneuvers); such forcing functions often have clearly defined analytical forms and tend to be of short duration, often called transient.
3. *Random excitation* includes continuous turbulence and runway profiles. Random excitation can be specified using a time or frequency domain description [1].

2.1.2 Analytical Fourier Transform

In practice the definition of the FRF may be extended to cover a more general excitation by employing the Fourier transform (FT), so that [1]

$$H(\omega)=\frac{X(\omega)}{F(\omega)}= \quad \text{.....2.1 (a)}$$

Where $X(\omega)$ is Fourier transform of response $x(t)$

$F(\omega)$ is Fourier transform of excitation $f(t)$

$H(\omega)$ is the frequency response or transfer function.

2.1.3 Frequency Domain Response

It may be seen that rearranging Equation (2.1, a) leads to

$$X(\omega) = H(\omega)F(\omega) \quad \text{……..……2.1 (b)}$$

There are two cases in aircraft loads where response to a random-type excitation is required: flying through continuous turbulence and taxiing on a runway with a non-smooth profile. For continuous turbulence, it is normal practice to use a spectral approach based on a linear-zed model (lumped mass, that means the landing gear and the fuselage shell are connected by flexible/elastic /force elements) of the aircraft [1]. When the effect of significant nonlinearity is to be explored, a time domain computation would need to be used. However, for taxiing [1], the solution would be carried out in the time domain using numerical integration of the equations of motion, as they are highly nonlinear due to the presence of the landing gear.

When a random excitation is considered, then a statistical approach is normally employed by defining the so-called power spectral density (PSD) of the excitation and response [4].

The PSD of response *x* (*t*) is defined by [1]:

$$S_{xx}(\omega) = \frac{T}{2\pi} X(\omega)^* X(\omega) = \frac{T}{2\pi} \left| X(\omega)^2 \right| \quad \text{……...2.2}$$

Thus the PSD is essentially proportional to the modulus squared of the Fourier amplitude at each frequency and it is a measure of how the 'power' in *x* (*t*) is distributed over the frequency range of interest.

Multiplying equation (2.1, b) on both sides by its complex conjugate then

$$X(\omega)X^*(\omega) = H(\omega)F(\omega)H^*(\omega)F^*(\omega) = |H(\omega)|^2 F(\omega)F^*(\omega) \quad \text{……...……...2.3}$$

and if the relevant scalar factors present in Equation (2.2) are accounted for, then equation (2.3) becomes

$$S_{xx}(\omega) = |H(\omega)|^2 S_{FF}(\omega) \quad \text{…..……...……...……..2.4}$$

Thus, knowing the definition of the excitation PSD S_{FF} (ω), the response PSD $S_{xx}(\omega)$ may be determined given the FRF for the system. It may be seen from Equation (2.4) that

the spectral shape of the excitation is carried through to the response, but is filtered by the system dynamic characteristics.
The aircraft dynamics responses are sometimes nonlinear i.e. doubling the input does not double the response, which complicates the solution process, but in this research only the linear landing gear case is considered. Using frequency domain approaches, the determination of the response near crack tips to random excitation for continuous runway profiles will be analyzed. Moreover 2DoF of the system is considered.

2.2 Airplane ground maneuver dynamics

Vehicle motion on the take-off and landing strip which includes landing, take off, braking, and turning is response of the system to loads imposed on the aircraft from the ground reaction, gravity, and aerodynamic loads. In addition, stresses, deflections, vibration induced in the components of the airplane are also responses of the vehicle. Ride is associated with dynamic response of the shell structure and other parts to excitations produced by different sources. The main sources of these excitations include road roughness, wheel run out, engine and driveline vibrations and aerodynamic loads. Of these, road roughness causes significant amount of the shell structural vibration [1].

Determination of dynamic responses specially crack tip stress and strains of the thin shell necessitates development of models representing the shell. Appropriate physical and mathematical models are necessary to arrive at reasonable results. Equations of motions, the solution of which gives the response of the system, and which govern the system at hand are formulated based on the mathematical model. Closed form solutions are attainable for models of less complication which happen to approximate the problem reality to a lesser extent. The better the reality is modeled the complicated the model becomes and this calls for advanced solution methods the implementation of which is possible using highly capable computers and computer software's. In this respect, finite element modeling and software analysis is worth mentioning.

Airplane parts such as fuselages, wings and other airframe parts are modeled as thin shells for simulation purpose. In this topic, the definition of some of the physical

quantities used to define motion and loads, the physical and mathematical modeling of the problem are presented.

2.2.1 Coordinate systems

Flight vehicle motion and the response of the vehicle to excitations are described using quantities which do represent some reality with respect to the motion and response of the vehicle. To define the different motion quantities and loads associated with flight vehicle motion and simulations regarding the motion, different axes systems are in use. Two coordinate systems are used in flight vehicle simulations. These are the body fixed coordinate system and the earth fixed coordinate system (Fig 2.1). The body fixed coordinate system; x-y-z has its origin at the center of gravity of the vehicle and travels with the moving vehicle. The longitudinal(x) axis extends from nose to tail of the fuselage; lateral (y) axis extends from wing tip to wing tip. The normal (z) axis drops perpendicular to the line joining longitudinal and the lateral axis.

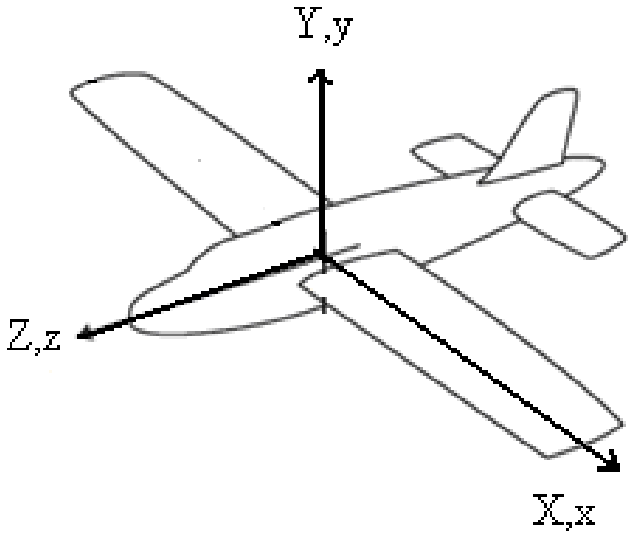

Figure 2. 1 ***Notation for body fixed and earth fixed axes***

The Earth fixed coordinate system, X-Y-Z is selected to coincide with the vehicle coordinate system at the start of maneuver which from then on remains fixed on the earth. The absolute motion quantities are defined with respect to this coordinate system and the components of these quantities are defined along the axes of the vehicle fixed coordinate system.

2.2.2. Motion and forces with reference to aircraft ground maneuvers

The motion of aerospace vehicle is defined by three translational and three rotational (angular) components. Using the vehicle fixed coordinate system introduced in the previous article the linear velocity and acceleration of the vehicle are decomposed along the three axes producing the longitudinal, lateral and vertical components. Roll, pitch, and yaw correspond to the rotational motion about the x-, y- and z- axes of the aircraft fixed coordinate system. Forces and moments are the causes for state and trajectory that a vehicle attains during the course of motion. The loads include aerodynamic, gravity and loads generated at the tire ground contact. The primary forces with which the motion of the aerospace vehicle is controlled are developed at the tire ground contact. Figure 1.3 shows the most significant forces on the vehicle in the x-z plane.

2.3. Road roughness model

Road roughness, as outlined in the introduction, is the major source of excitation. It stands for the irregularities in the road profile. Sine waves, step functions, and triangular waves can serve as models to represent road roughness. Nonetheless, random function modeling more realistically defines road profiles.

Random processes are defined using power spectral density (PSD) functions. Mathematically, PSD function of a random variable/process represents the Fourier transform of the autocorrelation function of the random process. Autocorrelation or correlation of a function with itself indicates how the value of a random variable a time t is related to the value at time $t+\tau$ [4, 15]. The autocorrelation function is dependent on the period τ and not on the specific time, t. In addition, other parameters like expected (mean) value, root mean squared value, variance, and standard deviation are used to describe random variables and processes. Based on this, a random function representing a random variable is said to be stationary, if the expected value of the function at time t is the same as the expected value at time $t+\tau$. A random road profile is stationary as long as

a contour representing portion of the road repeats itself after time, τ. In this study, stationary conditions are considered. PSD measure of road roughness is one of the internationally recognized methods to describe road roughness. The road elevation profile is decomposed into series of trigonometric waves varying in their amplitude and frequency. The plot of density of the mean square values of amplitudes versus the spatial frequency gives the PSD function corresponding to the signal. Spatial frequency Ω represents the number of cycles corresponding to specific amplitude per unit length and it is the inverse of wave length.

Various road rough nesses ranging from that of smooth runway to off-road ground could be modeled as random signals which are defined with PSD functions. Accordingly, the relationship between power spectral density $S_g(\Omega)$ and the spatial frequency Ω can be approximated by [8]:

$$S_g(\Omega) = C_{sp}(\Omega)^{-N} \quad \text{.....2.5}$$

In equation 2.5, $S_g(\Omega)$ is the power spectral density of the road roughness elevation profile, and C_{sp} and N are constants whose values for the different road profiles are given in Table 2.1. The values of the constants differ depending on different conditions. The area under the $S_g - \Omega$ curve shows the variance of the function. The higher the area is the higher the level of roughness.

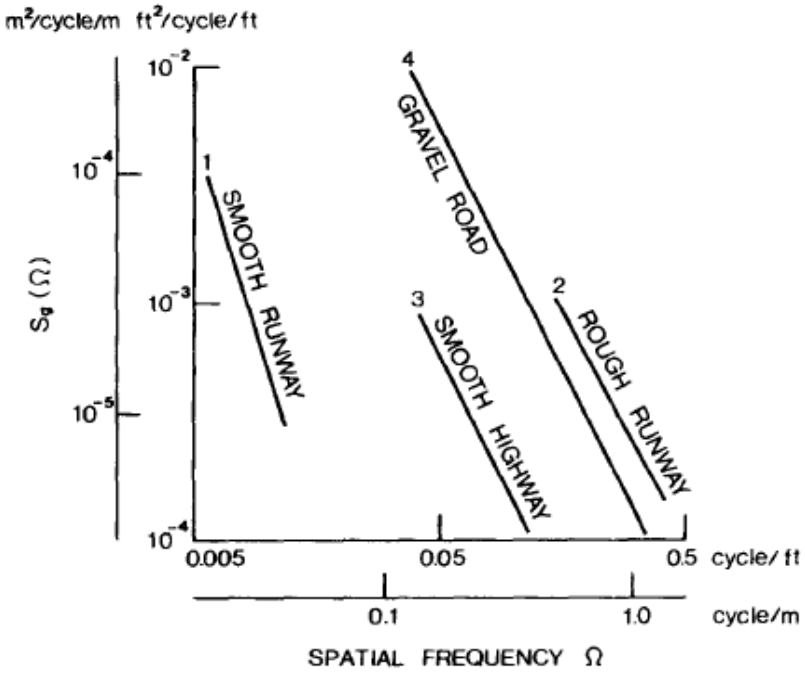

Figure 2. 2 ***Power spectral densities as function of spatial frequency*** *for various types of road and runway [8]*

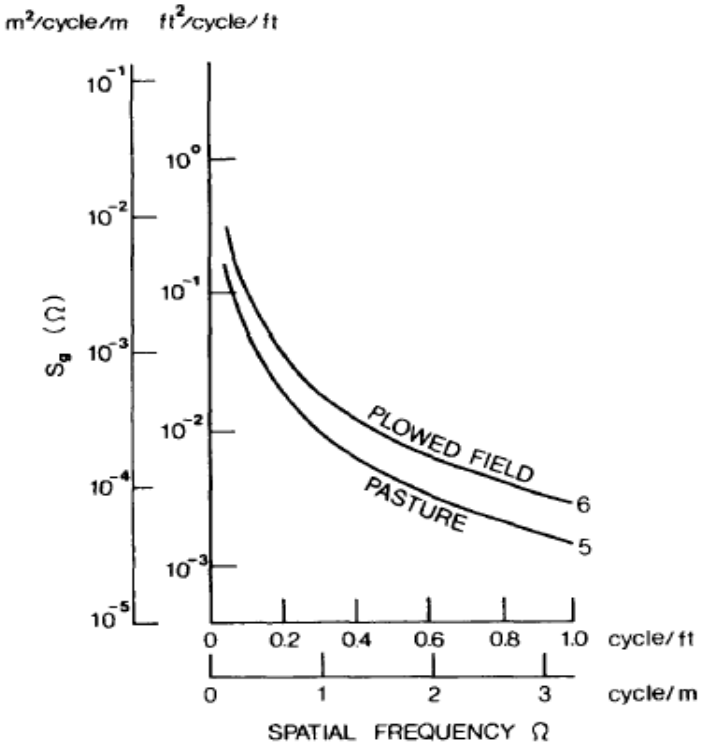

Figure 2. 3 ***Power spectral densities as a function of special frequency*** *for two types of un-prepared terrain [8]*

No	*Description*	*N*	C_{sp}
1	**Smooth runway**	**3.5**	$4.3*10^{-11}$
2	**Rough run way**	**2.1**	$8.1*10^{-6}$
3	**Smooth highway**	**2.1**	$4.8*10^{-7}$
4	**Highway with gravel**	**2.1**	$4.4*10^{-6}$
5	**Pasture**	**1.6**	$3.0*10^{-4}$
6	***Plowed field***	***1.6***	$6.5*10^{-4}$

Table 2.1 ***Values of C_{sp} and N for Power Spectral Density Functions*** *for various Surfaces[8].*

On the other hand, the International organization for Standardization (ISO) classifies road surface roughness into eight classes (classes A-H) based on power spectral density [8]. Accordingly, the relationship between the power spectral density and the spatial frequency for different classes of road profile may be approximated by two straight lines with different slopes (Fig 2.4).

The corresponding relationships are [8]:

For $\Omega \le \Omega_0$

$$S_g(\Omega) = S_g(\Omega_0)\left(\Omega / \Omega_0\right)^{-N1} \quad \text{; and} \quad \textbf{…….....….2.6(a)}$$

For $\Omega > \Omega_0$

$$S_g(\Omega) = S_g(\Omega_0)\left(\Omega / \Omega_0\right)^{-N2} \quad \textbf{……...….2.6(b)}$$

In the above equations, $S_g(\Omega)$ and Ω, as discussed earlier, represent the power spectral density and the spatial frequency. The term Ω_0 corresponds to the value of the spatial frequency which is equal to $1/2\pi$ cycles/m or wavelength equal to 2π. The values of *N1* and *N2*, respectively, are 2 and 1.5.

Table 2.2 gives the range of spectral density at Ω_0 for each class of road roughness.

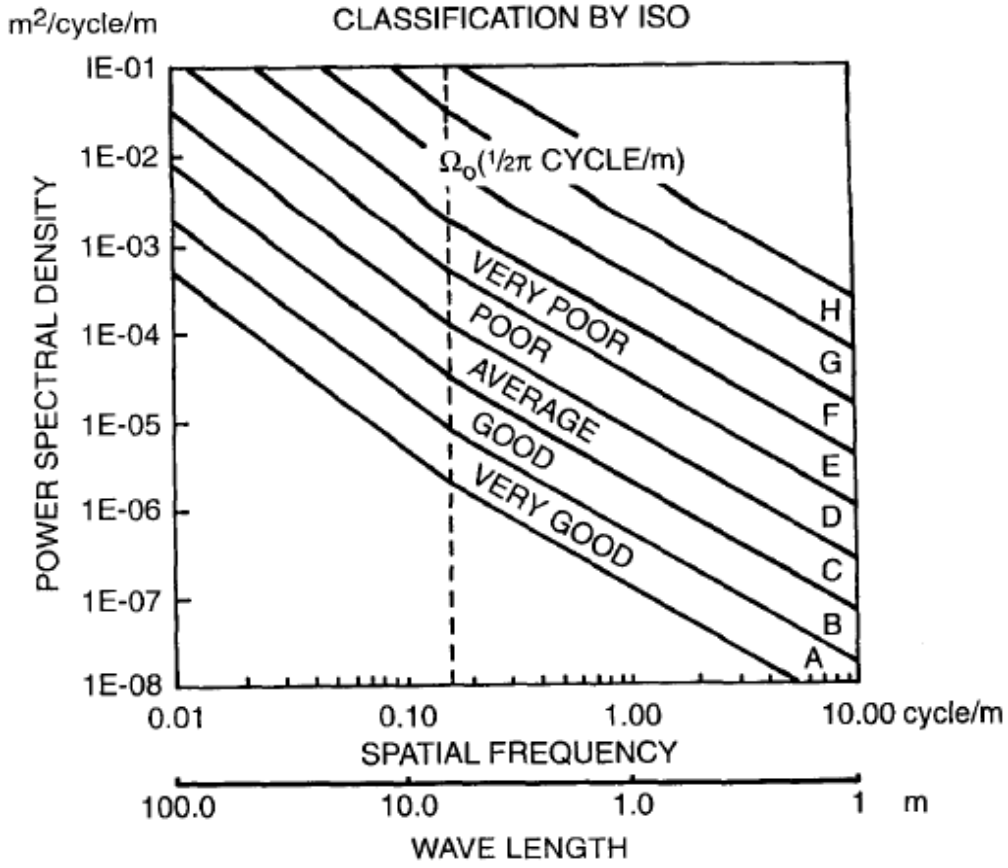

Figure 2. 4 ***Classification of Road Surface Roughness by ISO [8].***

Road class	Degree of roughness, $S_g(\Omega_0)\left(*10^{-6}\ m^2/cycles/m\right)$	
	Range	**Geometric mean**
A(VERY GOOD)	**<8**	**4**
B(GOOD)	**8-32**	**16**
C(AVERAGE)	**32-128**	**64**
D(POOR)	**128-512**	**256**
E(VERY POOR)	**512-2048**	**1024**
F	**2048-8192**	**4096**
G	**8192-32768**	**4096**
H	**>32768**	**16384**

Table 2.2 ***Classification of Road Roughness by ISO [8]***

The International Roughness Index (IRI) to evaluate road roughness of roads in service and under construction. IRI stands for total accumulated vertical movement of a vehicle divided by the distance traveled by the vehicle during motion. It is given in meters per kilometer. There exists relationship between PSD values or, particularly, the area under $S_g - \Omega$ curve and the IRI, i.e. as the roughness increases, both the area and IRI increase.

In this research, for the purpose of fracture analysis of an all composite made fuselage, roads of three different roughness classes are taken into account. In the first case, the condition in which the airplane lands and traverses over class A (smooth runway) surface profile type; in the second case landing on class G (pastured) rough strip or off-road; and finally, landing on class H (plowed field) are considered. The analysis of road type G and H are considered for the worst case landing pavement conditions.

By considering the mean values of road roughness, the following PSD vs Spatial frequency graphs are generated.

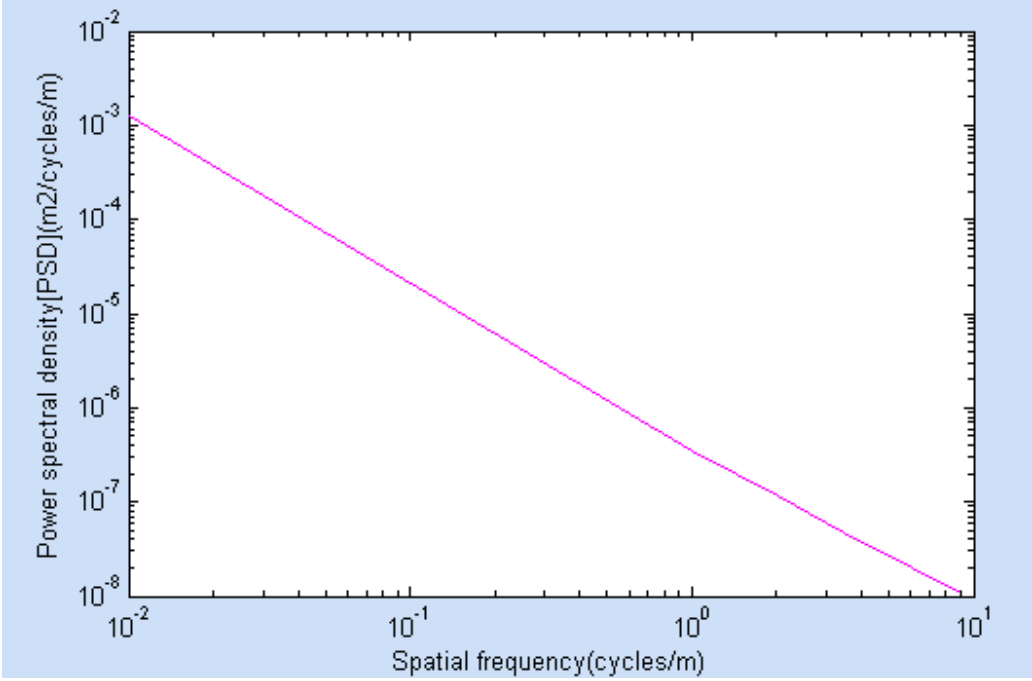

Figure 2. 5 ***Power Spectral Density verses Special Frequency for class-A road***

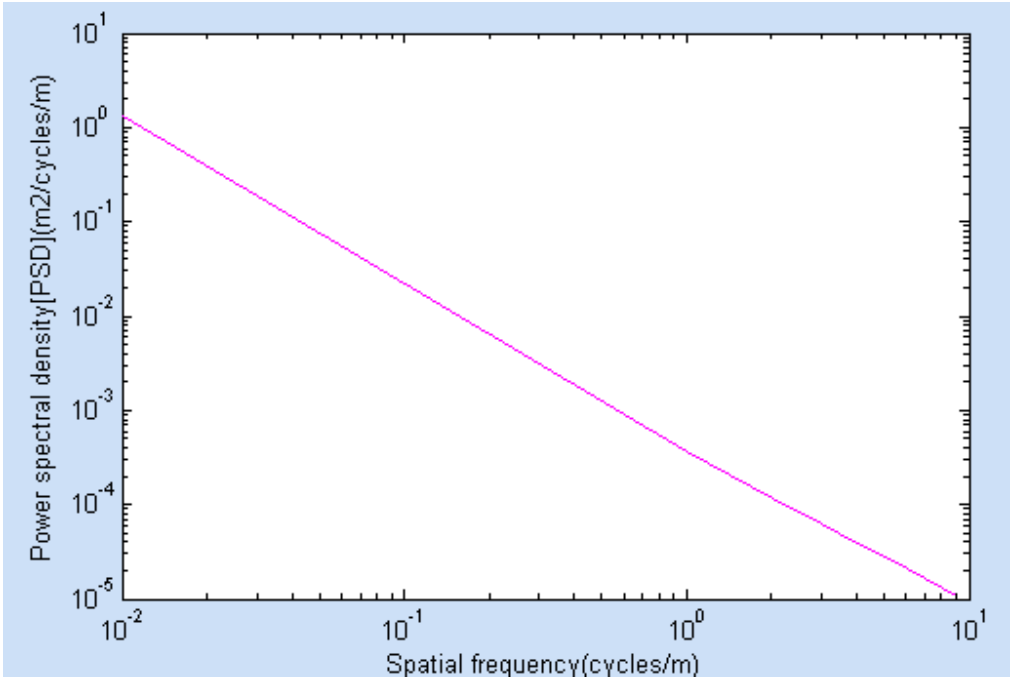

Figure 2. 6 ***Power Spectral Density verses Spatial Frequency for pastured***

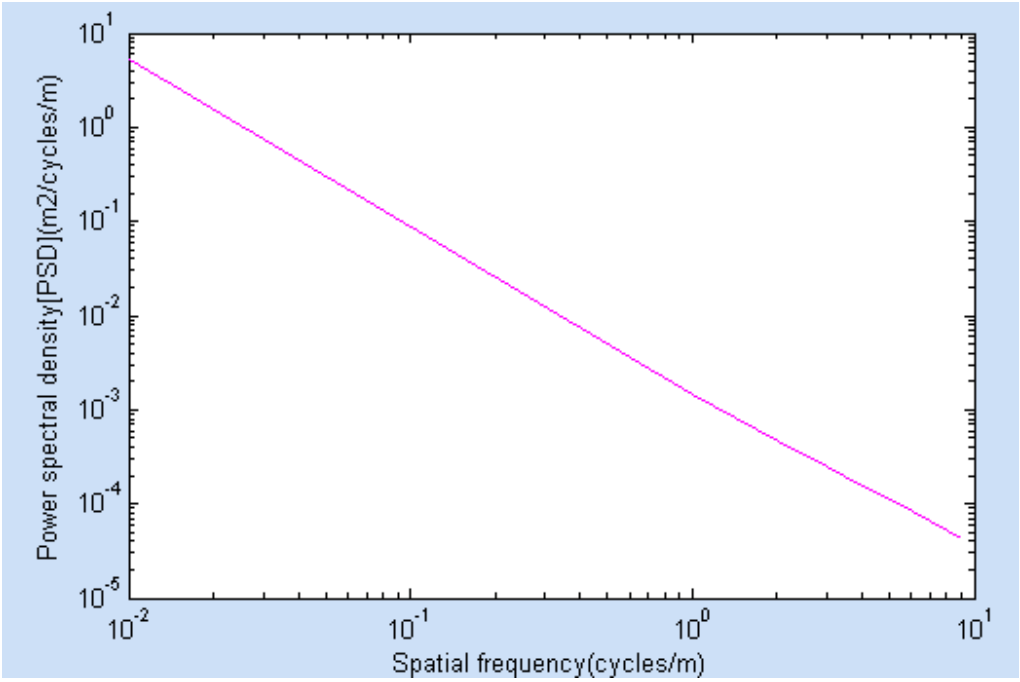

Figure 2. 7 ***Power Spectral Density verses Spatial Frequency for plowed field***

For flight vehicle ground induced vibration analysis, it is more convenient to express the power spectral density of surface profiles in terms of the temporal frequency in cycles/sec rather than in terms of the spatial frequency in cycles/m, since vehicle vibration is a function of time.

The transformation of the spatial frequency **Ω** in cycles/m to the temporal frequency *f* in cycles/sec is that of the landing speed of the airplane υ_{land} :

$$f(Hz) = \Omega(cycles/m) * \upsilon_{land}(m/s) \quad \text{.....2.7}$$

For an airplane moving with velocity, υ_{land} on the ground the power spectral density in terms of temporal frequency, ω (number of cycles per second,) $S_g(\omega)$ can be determined as [8]:

$$S_g(\omega) = \frac{S_g(\Omega)}{\upsilon_{land}} \text{.....2.8}$$

Using *Flight data's for B-787 passenger airliner* [23], assuming a landing velocity of 150m/sec the corresponding graphs in terms of temporal values are shown below.

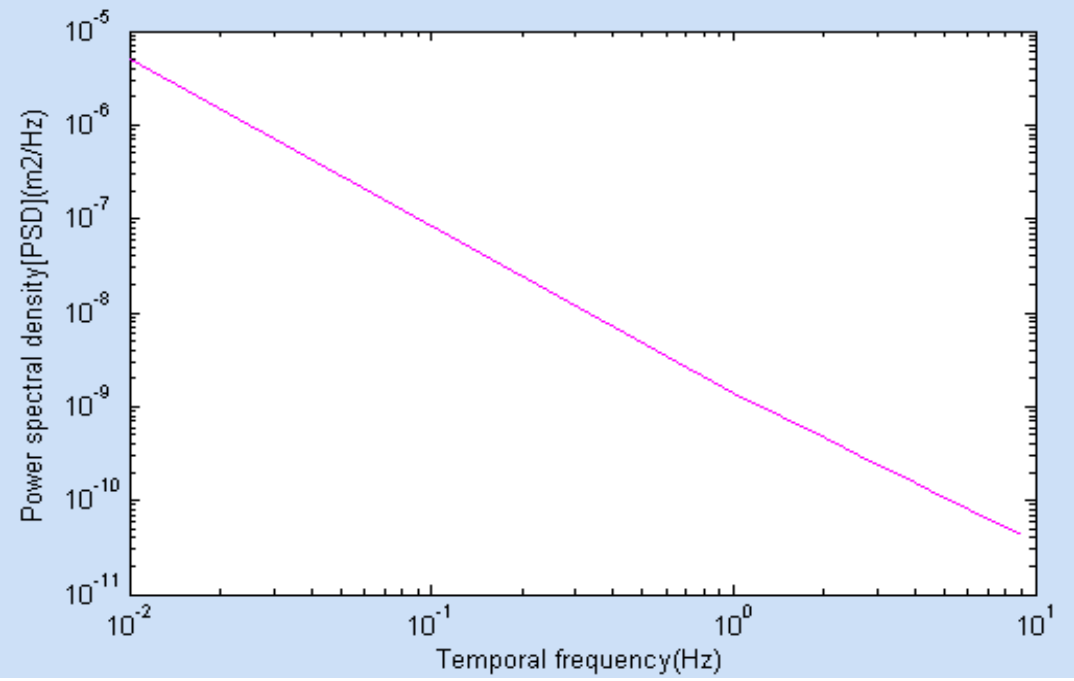

Figure 2. 8 ***Power Spectral Density verses Temporal Frequency for class-A road***

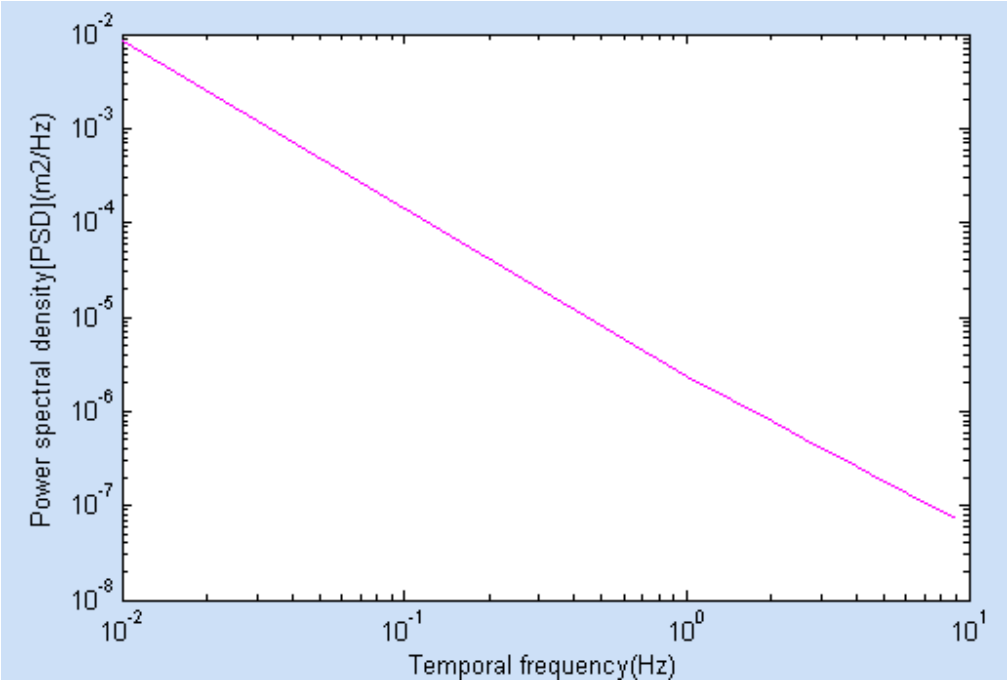

Figure 2. 9 ***Power Spectral Density verses Temporal Frequency for pastured***

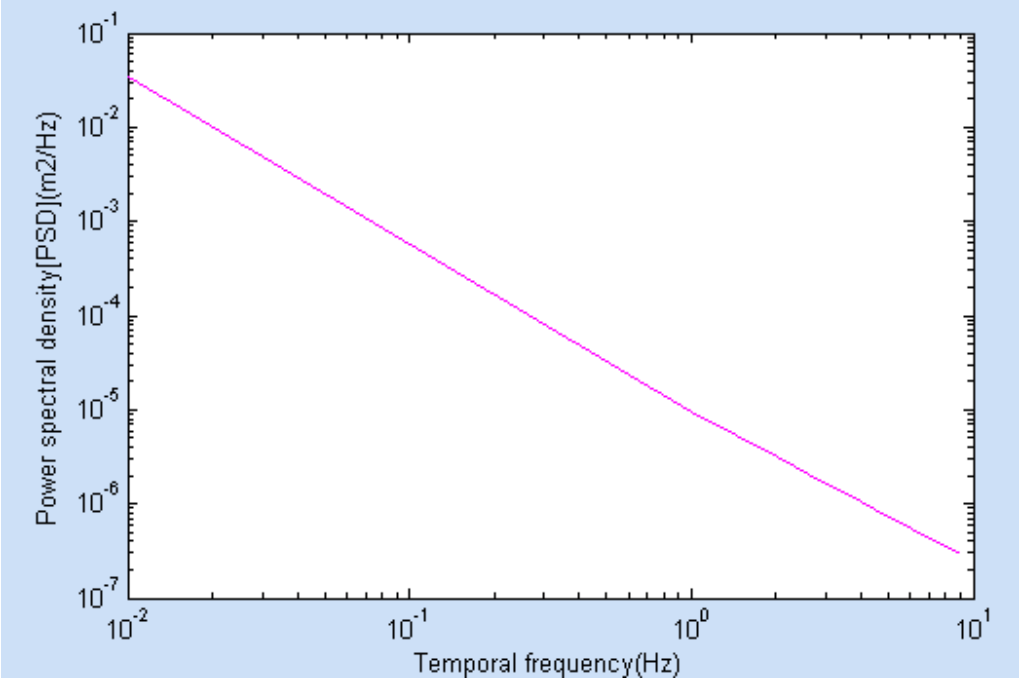

Figure 2. 10 ***Power Spectral Density verses Temporal Frequency for plowed field***

2.3.1 Runway Profile

To calculate the aircraft dynamic response during ground maneuvering, the runway profile over which the aircraft is operating must be specified. Every runway in the world has a different profile. However, it is not possible to consider them all in the design process so only representative runways are considered [1]. The profile $h(\chi_r)$ of a runway is defined relative to a flat datum as shown in figure 2.11, a) and b) where the distance along the runway χ_r is measured with respect to a convenient origin. The profile is taken as downwards positive, to be consistent with downwards positive displacements on the aircraft. An assumption is taken that there is no variation of profile across the runway.

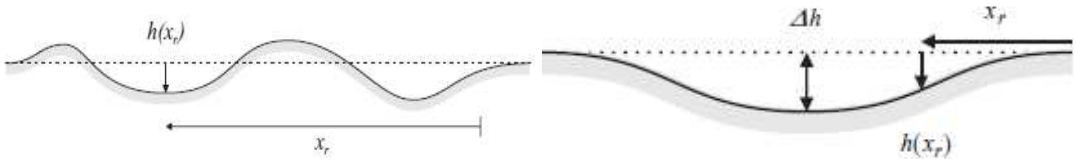

a) b)

Figure 2. 11 *a), b)* ***Model of a representative runway profile [2]***

For a '1-cosine' dip of depth Δh_r and total length of runways, L_r as shown in figure 2.11 would have a runway profile [1]:

$$h(\chi_r) = \frac{\Delta h_r}{2}\left(1 - \cos\frac{2\pi\chi_r}{L_r}\right) \quad \text{.....2.9}$$

The aircraft nose and main gears would pass over the 'dip' at different times, so causing both heave and pitch motions of the aircraft.

When the equations are set up, both $h(t)$ and $\dot{h}(t)$ i.e. the runway profile and rate of change with time of the profile, as seen by each gear, are required; thus a temporal definition must be obtained from the spatial profile. The value of $h(t)$ is equal to the value of $h(\chi_r)$ at the current location of the aircraft during the taxiing process. The time rate of change of the profile $\dot{h}(t)$ depends upon the local runway slope and the aircraft velocity. Noting that the aircraft forward velocity is υ_{land} at the instant of time considered.

Then, using the chain rule, the rate of change of profile with time is given by [1]

$$\dot{h} = \frac{dh}{dt} = \frac{dh}{dx_r}\frac{dx_r}{dt} = \upsilon_{land}\frac{dh}{dx_r} \quad \text{.....2.10}$$

where the runway slope may be estimated from the profile values near to the point of interest.

2.3.2 Airplane Multi-body Model: Mathematical Formulation

Consider a rigid aircraft supported on linear spring/damper gears as shown in figure 2.12. Multi-body models are used to determine displacement, stress responses of airplane. In such model, stiffness, mass and damping properties of the tire and shock absorbing device are considered such that the appropriate combination of these gives the mathematical model based on which equations governing the model are formulated. The model can vary from the simple and most common two degree of freedom model to a model having higher degree of freedom. But for the sake of simplicity two degree of freedom will be considered.

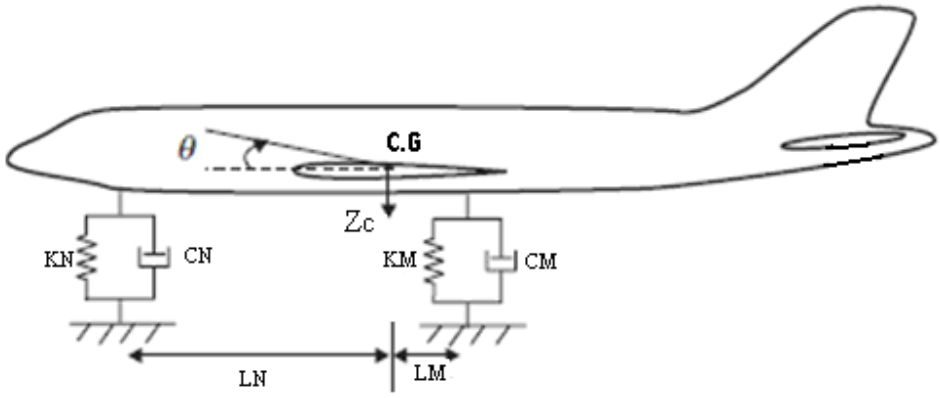

Figure 2. 12 ***Two degree of freedom*** *rigid* ***aircraft in heave/pitch***
supported on landing gear[1]

The aircraft response is represented by the centre of mass, subscript C; heave z_C and pitch θ, relative to any horizontal datum; zero motion corresponds to the aircraft at rest in its static equilibrium position on the datum runway. Thus responses are actually calculated *relative to* this datum state and so are incremental. The aircraft has mass *m*, pitch moment of inertia about the centre of mass I_y, nose (subscript N) and main

(subscript M) gear stiffness K_N, K_M and viscous damping C_N, C_M; clearly the main gears on both sides of the aircraft have been combined into one unit.

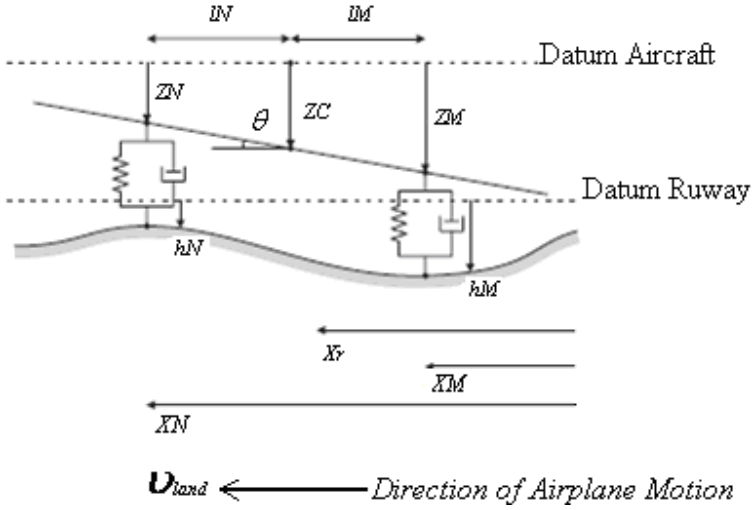

Figure 2. 13 ***Rigid aircraft with a linear landing gear during landing[1]***

Consider the aircraft position at any instant, being defined with the centre of mass at distance x_r from the runway origin, the nose gear at x_N and the main gear at x_M as shown in the figure 3.13. The profile values at the gear positions are then [1]

$$h_N = h(x_N) = h(x_r + l_N) \quad \textbf{.....2.11(a)}$$

$$h_M = h(x_M) = h(x_r - l_M) \quad \textbf{.....2.11(b)}$$

The energy dissipation and work done functions depend upon expressions for compression and the rate of compression of the landing gear springs and dampers, and these values will depend on the runway profile and rate of change of the profile. Thus, the compression and rate of compression of the nose gear are [1]:

$$\Delta_N = z_N - h_N = z_C - l_N\theta - h_N, \quad \dot{\Delta}_N = \dot{z}_C - l_N\dot{\theta} - \dot{h}_N \quad \textbf{..... .....2.12}$$

And the compression and rate of compression of the main gears are [1]:

$$\Delta_M = z_M - h_M = z_C + l_M\theta - h_M \quad , \dot{\Delta}_M = \dot{z}_C + l_M\dot{\theta} - \dot{h}_M \quad \textbf{.....2.13}$$

The kinetic energy is given by [1]:

$$T = \frac{1}{2}m\dot{z}_C^2 + \frac{1}{2}I_y\dot{\theta}^2 \quad \textbf{.....2.14}$$

The potential or strain energy is V [1]:

$$V = \frac{1}{2} K_N \Delta_N^2 + \frac{1}{2} K_M \Delta_M^2 \quad \text{.....2.15}$$

And the energy of dissipation is given by [1]:

$$\Xi = \frac{1}{2} C_N \dot{\Delta}_N^2 + \frac{1}{2} C_M \dot{\Delta}_M^2 \quad \text{.....2.16}$$

The effect of the forces is included in Lagrange's equation by considering the incremental work done δW obtained due to the ground reaction forces transferred through the supports at the ground to structure contact points incremental displacements δz_N, δz_M, namely

$$\delta W = \delta z_N R_N + 2\delta z_M R_M \quad \text{.....2.17}$$

Then, applying Lagrange's equations with generalized coordinates (z_C, θ), it may be shown that the equations of motion for the aircraft landing on the runway are

$$L = T - V - \Xi \quad \text{.....2.18}$$

Substituting the values of the kinetic energy, potential energy, and damping energy, the equation of motion will become [1]:

$$\frac{d}{dt}\left(\frac{\partial T}{\partial \dot{q}_j}\right) - \frac{\partial T}{\partial q_j} + \frac{\partial V}{\partial q_j} + \frac{\partial \Xi}{\partial \dot{q}_j} = Q_j = \frac{\partial(\delta W)}{\partial(\delta q_j)} \qquad \text{for } j = 1,2,3,\ldots,N.$$

For $N = 2$, the equation of motion becomes;

$$\begin{bmatrix} m & 0 \\ 0 & I_y \end{bmatrix} \begin{Bmatrix} \ddot{z}_C \\ \ddot{\theta} \end{Bmatrix} + \begin{bmatrix} c_N + c_M & -l_N c_N + l_M c_M \\ -l_N c_N + l_M c_M & l_N^2 c_N + l_M^2 c_M \end{bmatrix} \begin{Bmatrix} \dot{z}_C \\ \dot{\theta} \end{Bmatrix}$$

$$+ \begin{bmatrix} K_N + K_M & -l_N K_N + l_M K_M \\ -l_N K_N + l_M K_M & l_N^2 K_N + l_M^2 K_M \end{bmatrix} \begin{Bmatrix} z_C \\ \theta \end{Bmatrix}$$

$$= \begin{bmatrix} c_N & c_M \\ -l_N c_N & l_M c_M \end{bmatrix} \begin{Bmatrix} \dot{h}_N \\ \dot{h}_M \end{Bmatrix} + \begin{bmatrix} K_N & K_M \\ -l_N K_N & l_M K_M \end{bmatrix} \begin{Bmatrix} h_N \\ h_M \end{Bmatrix} \quad \text{.....2.19}$$

A right-hand side excitation term is present due to the variation in the runway profile.

To determine the transfer function matrix, harmonic inputs h_N, h_M are assumed for such that:

$$\begin{bmatrix} h_N \\ h_M \end{bmatrix} = \begin{bmatrix} h'_N \\ h'_M \end{bmatrix} e^{i\omega t} \quad \text{.....2.20}$$

where h'_N is the amplitude input excitations at the nose gear.

h'_M is the amplitude input excitations at the main landing gear.

The assumed harmonic output will be of the form

$$\begin{bmatrix} z_C \\ \theta \end{bmatrix} = \begin{bmatrix} z'_C \\ \theta' \end{bmatrix} e^{i\omega t} \quad \text{.....2.21}$$

where z'_C - Amplitudes of the translational response of the aircraft at the center of gravity.

θ' - Amplitudes of the pitch response of the aircraft at the center of gravity.

Substituting these equations in the equation of motion:

$$\begin{aligned} &\left[-\omega^2 \begin{bmatrix} m & 0 \\ 0 & I_y \end{bmatrix} + (i\omega) \begin{bmatrix} c_N + c_M & -l_N c_N + l_M c_M \\ -l_N c_N + l_M c_M & l_N^2 c_N + l_M^2 c_M \end{bmatrix} \right] \begin{bmatrix} z'_C \\ \theta' \end{bmatrix} e^{i\omega t} \\ &\quad + \begin{bmatrix} K_N + K_M & -l_N K_N + l_M K_M \\ -l_N K_N + l_M K_M & l_N^2 K_N + l_M^2 K_M \end{bmatrix} \begin{Bmatrix} z'_C \\ \theta' \end{Bmatrix} e^{i\omega t} \\ &\quad = \left[(i\omega) \begin{bmatrix} c_N & c_M \\ -l_N c_N & l_M c_M \end{bmatrix} + \begin{bmatrix} K_N & K_M \\ -l_N K_N & l_M K_M \end{bmatrix} \right] \begin{Bmatrix} h'_N \\ h'_M \end{Bmatrix} e^{i\omega t} \quad \text{.....2.22} \end{aligned}$$

In this research, the dynamic analysis is carried out for two degree of freedom, i.e., bounce and pitch, cases. The same PSD input is applied at three points (nodes) in the finite element model which correspond to the nose and main gears. The analysis is carried out by applying one PSD input for one type of pavement at the three points (nodes) corresponding to the three legs.

The PSD input to be applied at the points corresponding to the legs are not exactly equal to the excitation at the tire ground contact point. Since damping occurs due to tire and shock absorber, the excitation at the points will be different. To determine the excitations at these points, one gear leg model of the vehicle, discussed in the next section is used.

2.4. Tire model

Tires are components of an airplane which provide the necessary adhesion for the vehicle to advance over take off and landing strips. Tires are characterized by their stiffness and damping properties. To model the mechanism of dissipation energy for a turning tire, we assume there are many small dampers and springs in the tire structure. Pairs of parallel dampers and springs are installed radially and circumstantially [10]. Figures 2.14 a) and b) illustrate the damping and spring structure of a tire [10].

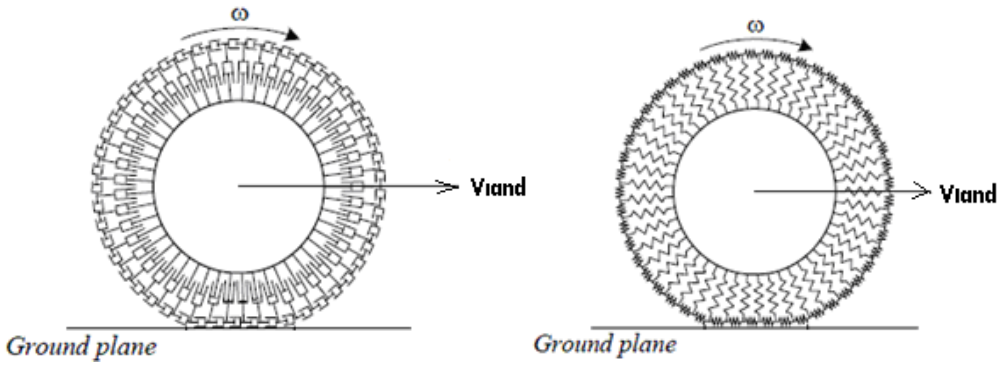

a) Damping structure of a tire. *b) Spring structure of a tire.*

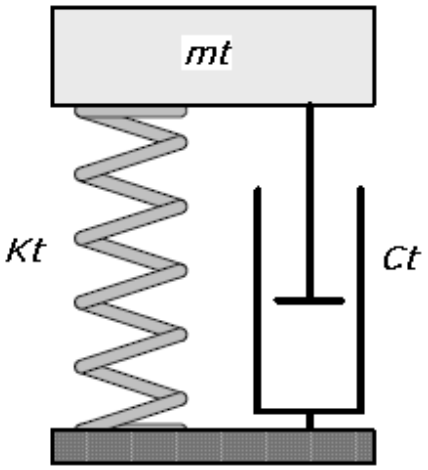

c) Linear model of tire.

Figure 2. 14 ***Tire structure (Spring-Damper combination) [10]***

In studies regarding dynamic response of tires, a linear single degree of freedom model consisting of a spring and damper element is used (Figure 2.14(c)). *Mt*, *Kt* and *Ct* stand for mass, stiffness, and damping of the tire.

The stiffness characteristics; tire damping and tire stiffness depend much on the inflation pressure. Some of the important properties of tires are given in table 2.3.

Tire	Inflation pressure(kPa)	Load(kN)	Static stiffness(kN/m)	Average nonrolling dynamic stiffness(kN/m)	Damping coefficient(N/m/s)
11-36(4 ply)	82.7	6.67	357.5	379.4	2.4
		8	357.5	394	2.6
		9.34		423.2	3.4
	110.3	6.67	379.4	394	2.1
		8	386.7	437.8	2.5
		9.34	394	423.2	2.5
7.5-16(6 ply)	138	3.56	175.1	218.9	0.58
		4.45	175.1	233.5	0.66
		4.89	182.4	248.1	0.88
	193	3.56	218.9	233.5	0.36
		4.45	226.2	262.7	0.66
		4.89	255.4	277.3	0.73

Table 2. 3 ***Stiffness and Damping Properties of tires [8]***

2.4.1 Wheel and Tire Assembly

A landing gear has two major dynamic elements in series, namely the shock absorber and the wheel/tire assembly. The dynamic behavior of this assembly is complex and has an impact upon ground maneuvering such as taxiing, braking, turning, etc. The assembly also influences the landing in that when tire deformations are included, the required shock absorber stroke reduces somewhat. It is important for the accurate estimation of the landing gear internal loads and the loads at the airframe attachment points such that the system is modeled adequately.

A very simple representation that includes tire characteristics is the two DoF model is shown in Figure 2.16(a), (b), (c) and (d). Where the un-sprung mass consists of the sliding tube, axle and wheel/tire/brake; a linear, un-damped tire model is used for the simple calculations involving vertical motion. In practice, the tire model is nonlinear,

complex, particularly when representing lateral forces and depends upon material properties, pressure, temperature, tire wall flexibility, etc.

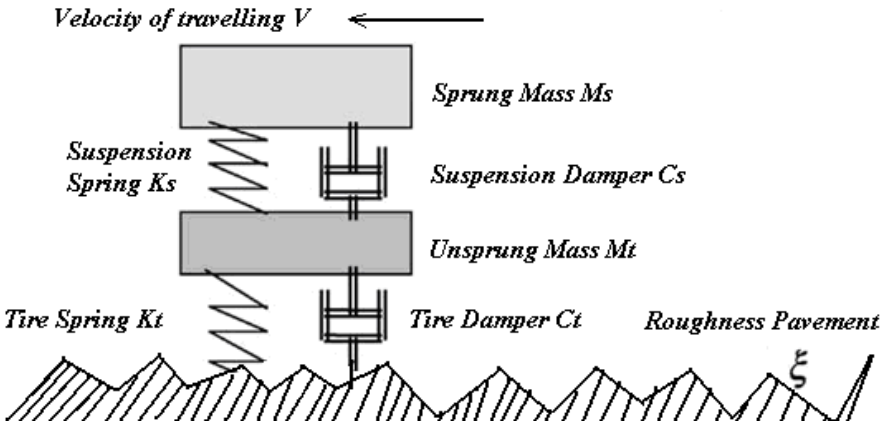

Figure 2. 15 ***One gear leg of airplane shock absorbing system***

A one third airplane model with two degrees of freedom on a rough pavement is shown in figure 2.15. The model is applicable for both nose and main landing gear of the airplane.

Assumptions taken during analysis are:

- Determinate landing gear layout.
- Linear model of the airplane landing gear.
- Rigid airplane landing.

The power spectral densities, PSD of χ_U and χ_S of the un-sprung and sprung masses, in each case, are determined through the introduction of the transfer function matrix $H(\omega)$, the determination of which is detailed below.

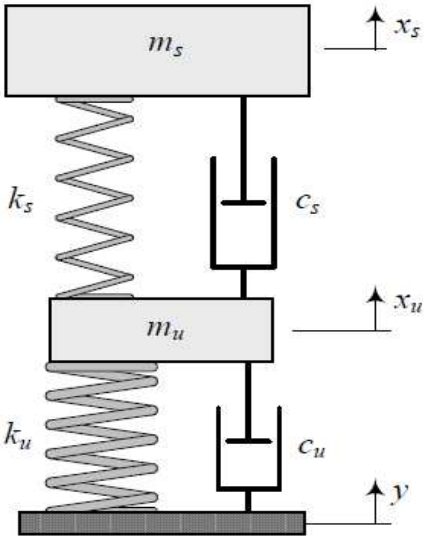

a) Physical model

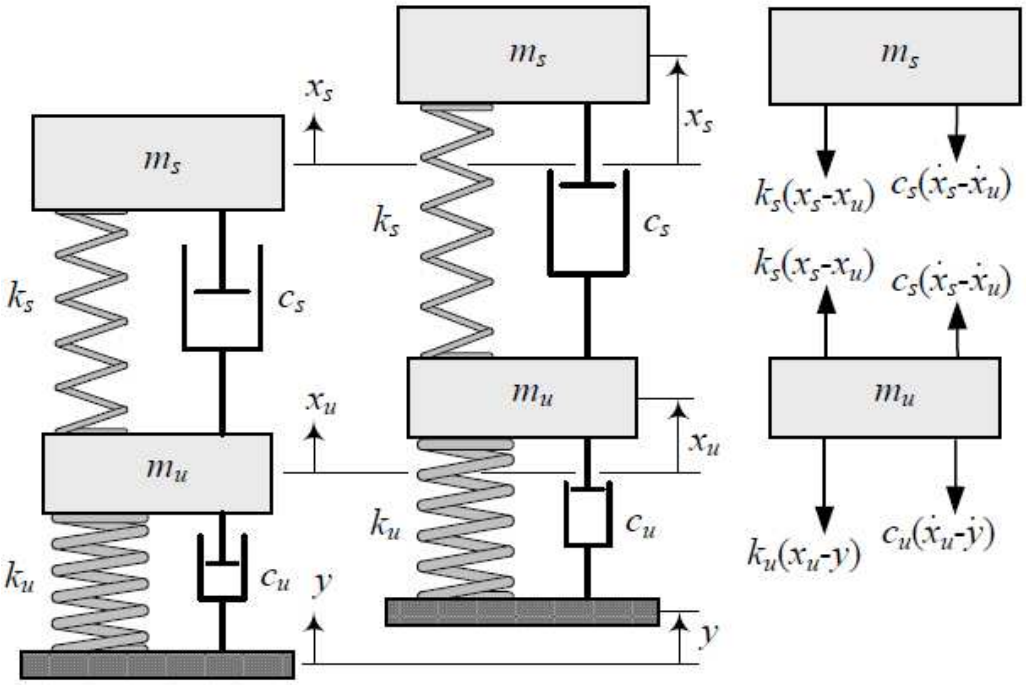

b) Equilibrium *c) Motion* *d) Free body diagram*

Figure 2. 16 ***Landing gear shock absorbing device model[10]***

Applying Newton's method provides two equations of motion and assuming that

$$x_S > x_U > y$$

$$m_S \ddot{x}_S = -K_S(x_S - x_U) - C_S(\dot{x}_S - \dot{x}_U) \quad \text{.....2.23}$$

$$m_U \ddot{x}_U = K_S(x_S - x_U) + C_S(\dot{x}_S - \dot{x}_U) - K_U(x_U - y) - C_U(\dot{x}_U - \dot{y}) \quad \text{.....2.24}$$

We usually rearrange the equations of motion for a linear system in a matrix form

$$[M]\{\ddot{X}\} + [C]\{\dot{X}\} + [K]\{X\} = \{F\} \quad \text{.....2.25}$$

Take advantage of matrix calculus, rearrangement of Equations (2.23) and (2.24) results in the following set of equations:

$$\begin{bmatrix} m_S & 0 \\ 0 & m_U \end{bmatrix}\begin{Bmatrix} \ddot{x}_S \\ \ddot{x}_U \end{Bmatrix} + \begin{bmatrix} C_S & -C_S \\ -C_S & c_S + c_U \end{bmatrix}\begin{Bmatrix} \dot{x}_S \\ \dot{x}_U \end{Bmatrix} + \begin{bmatrix} K_S & -K_S \\ -K_S & K_S + K_U \end{bmatrix}\begin{Bmatrix} x_S \\ x_U \end{Bmatrix} = \begin{bmatrix} 0 \\ K_U y + C_U \dot{y} \end{bmatrix} \quad \text{.....2.26}$$

The term $K_U + C_U \dot{y}$ refers to the force transmitted to the un-sprung masses due to the displacement ***y*** excitation.

To determine the transfer function matrix, a harmonic input is assumed for ***y*** such that:

$$y = y' e^{i\omega t}$$

where y' is the amplitude input excitations.

The assumed harmonic output will be of the form

$$\begin{bmatrix} x_S \\ x_U \end{bmatrix} = \begin{bmatrix} x'_S \\ x'_U \end{bmatrix} e^{i\omega t} \quad \text{.....2.27}$$

where x'_U, x'_S amplitudes of the responses of the un-sprung and sprung masses.

Substituting these equations in the equation of motion:

$$\left[-\omega^2\begin{bmatrix} m_S & 0 \\ 0 & m_U \end{bmatrix} + (i\omega)\begin{bmatrix} C_S & -C_S \\ -C_S & c_S + c_U \end{bmatrix} + \begin{bmatrix} K_S & -K_S \\ -K_S & K_S + K_U \end{bmatrix}\right]\begin{Bmatrix} x'_S \\ x'_U \end{Bmatrix} e^{i\omega t} = \begin{Bmatrix} 0 \\ K_U y' + (i\omega) C_U \end{Bmatrix}\begin{Bmatrix} 0 \\ y' \end{Bmatrix} e^{i\omega t} \quad \text{.....2.28}$$

The transfer function matrix relates the output to the input such that:

$$\begin{bmatrix} x'_S \\ x'_U \end{bmatrix} = H(\omega)\begin{bmatrix} 0 \\ K_U y' + (i\omega)C_U \end{bmatrix} \quad \text{……..…2.29}$$

This gives,

$$H(\omega) = \left[-\omega^2 \begin{bmatrix} m_S & 0 \\ 0 & m_U \end{bmatrix} + (i\omega)\begin{bmatrix} C_S & -C_S \\ -C_S & c_S + c_U \end{bmatrix} + \begin{bmatrix} K_S & -K_S \\ -K_S & K_S + K_U \end{bmatrix}\right]^{-1}$$

$$= \begin{bmatrix} -\omega^2 m_S + (i\omega)C_S + K_S & -(i\omega)C_S - K_S \\ (i\omega)C_S - K_S & -\omega^2 m_U + (i\omega)C_S + (i\omega)C_U + K_S + K_U \end{bmatrix}^{-1} \quad \text{……..2.30}$$

$$= \frac{1}{g(\omega)}\begin{bmatrix} -\omega^2 m_U + (i\omega)(C_S + C_U) + K_S + K_U & (i\omega)C_S + K_S \\ -i\omega C_S + K_S & -\omega^2 m_s + (i\omega)C_S + K_S \end{bmatrix}$$

where $g(\omega) = m_S\left(\omega^4 m_U - i\omega^3(c_S + c_U) - \omega^2(K_S + K_U)\right)$

$$+ C_S\left((i\omega^3)m_U - 2\omega^2 C_S - \omega^2 C_U + i\omega(2K_S + K_U)\right)$$

$$+ K_S\left(-\omega^2 m_U - i\omega\, C_U + K_U\right)$$

In multi-degree of freedom system (MDoF), the power spectral density function of the response is given by [4]

$$[S_Z(\omega)] = [H(\omega)]\,[S_F(\omega)]\,[H^*(\omega)]^T \quad \text{……..……..2.31}$$

where $[S_F(\omega)]$ is the Spectral density function matrix of a load or excitation,

$[S_Z(\omega)]$ is the Spectral density function matrix of the responses.

and $[H^*(\omega)]$ is the complex conjugate of the transfer function.

Denoting the spectral density function of *y*, by $S_g(\omega)$, the spectral density function matrix of the load for the one aircraft shock absorbing device model becomes [15]:

$$[S_Z(\omega)] = [S_g(\omega)]K_t^2 \quad \text{……..……..2.32}$$

Thus, substituting the variables in to equation 2.32, we have the following;

$$[S_Z(\omega)] = \frac{K_t^2}{g(\omega)g^*(\omega)} \begin{bmatrix} -\omega^2 m_U + (i\omega)(C_S + C_U) + K_S + K_U & (i\omega)C_S + K_S \\ -i\omega C_S + K_S & -\omega^2 m_S + (i\omega)C_S + K_S \end{bmatrix}$$

$$\begin{bmatrix} S_g(\omega) & 0 \\ 0 & 0 \end{bmatrix} \begin{bmatrix} -\omega^2 m_U + (i\omega)(C_S + C_U) + K_S + K_U & -(i\omega)C_S + K_S \\ (i\omega)C_S + K_S & -\omega^2 m_S + (i\omega)C_S + K_S \end{bmatrix}$$

……...…. ……...…….2.33

$$[S_Z(\omega)] = \frac{K_t^2}{g(\omega)g^*(\omega)} \begin{bmatrix} X_{Z11} & X_{Z12} \\ X_{Z21} & X_{Z22} \end{bmatrix}$$

where $X_{Z11} = S_g(\omega)\left(-\omega^2 m_U + i\omega\,(c_S + c_U) + K_S + K_U\right)^2$

$$X_{Z12} = S_g(\omega)\left(-\omega^2 m_U + i\omega\,(c_S + c_U) + K_S + K_U\right)\left((-i\omega)C_S + K_S\right)$$

$$X_{Z21} = S_g(\omega)\left((-i\omega)C_S + K_S\right)\left(-\omega^2 m_U + i\omega\,(c_S + c_U) + K_S + K_U\right)$$

$$X_{Z22} = S_g(\omega)\left((-i\omega)C_S + K_S\right)\left((-i\omega)C_S + K_S\right)$$

and $g^*(\omega) = m_S\left(\omega^4 m_U + i\omega^3(c_S + c_U) - \omega^2(K_S + K_U)\right)$

$$+C_S\left((-i\omega^3)m_U - 2\omega^2 C_S - \omega^2 C_U - i\omega(2K_S + K_U)\right)$$

$$+K_S\left(-\omega^2 m_U + i\omega\, C_U + K_U\right)$$

In the above equations, the diagonals of the spectral density functions matrix of the responses X_{Z11} and X_{Z22} represent the power spectral density functions of χ_S and χ_U respectively. The PSD function, $X_{Z11}(\Omega)$, is used as input for the FE analysis, while $X_{Z22}(\Omega)$ would be the response of the structure [15].

Similarly, in terms of the spatial frequency term Ω, the response of the model is defined by the formula [4]:

$$[S_Z(\Omega)] = \upsilon_{land}[S_Z(\omega)] \text{……..2.34}$$

The inputs for the finite element analysis are taken as combination of data from the above equations and figures.

The ANSYS program is used to simulate the airplane dynamic near crack tip responses. A representative airplane geometrical data is taken from Boeing-787 (B-787). Stress and displacement response when landing on different types of pavement roughness with a landing velocity of 150m/sec is going to be simulated. A symmetrical longitudinal pavement profile will be assumed because the pavement roughness along the longitudinal direction is the most important concern. This means that the profiles for the left and right main landing gears and the nose gear is simplified as one profile, and thus, roll can not occur in the aircraft motions.

Chapter Three

Finite Element mathematical formulations

3.1 Introductions

The finite element method (FEM) is a powerful numerical solution of a wide range of engineering problems, such as the deformation and stress analysis of aircraft, automotive, buildings, bridges and dam structures to field analysis of heat flux, fluid flow, magnetic flux, seepage, and other flow problems.

With the advances in computer technology and CAD systems, complex problems can be modeled with relative ease, and several alternative configurations can be tried out on a computer before the first prototype is built.

In this method of analysis, a complex region defining a continuum is dissected into simple geometric shapes called *finite elements*. The material properties and the governing relationships are considered over these elements and expressed in terms of unknown values at element corners. An assembly process, duly considering the loading and constraints, results in a set of equations. Solution of these equations gives us the approximate behavior of the continuum.

3.1.1 Basic concepts of engineering analysis

The analysis of an engineering system requires:

- Idealization of system.
- Formulation of equilibrium equations.
- Solution of equation.
- Interpretation of the result.

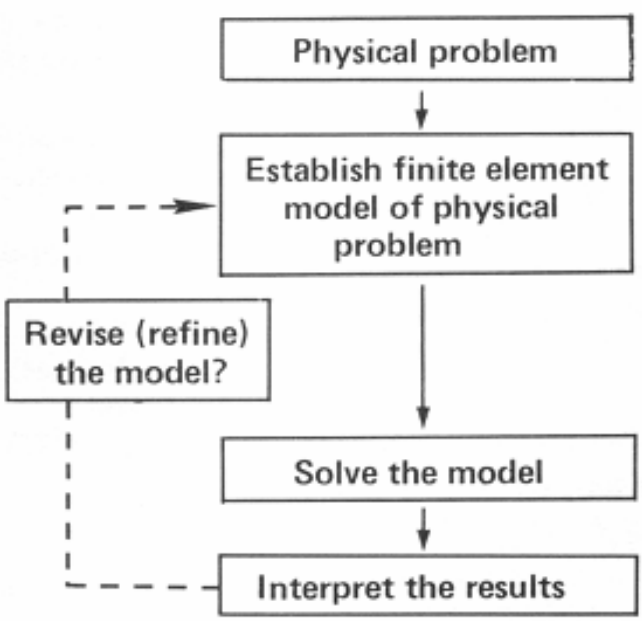

Figure 3. 1 ***Algorithm for Finite element solution process***

3.1.2 Structural analysis

Structural analysis is probably the most common application of the finite element method. Composite materials are those containing more than one bonded material, each with different structural properties. Composites used for typical engineering applications are advanced fiber or laminated composites, such as fiberglass, glass epoxy, graphite epoxy, boron epoxy and so on.

ANSYS allows us to model composite materials with specialized elements called *layered elements*. Once we build our model using these elements, we can do any structural analysis.

3.1.3 Modal analysis

Modal analysis to determine the vibration characteristics (natural frequencies and mode shapes) of a structure while it is being designed. It also can be a starting point for a spectrum analysis.

3.2 Random Vibration analysis

A Random Vibration Analysis is a form of Spectrum Analysis. The spectrum is a graph of spectral value versus frequency that captures the intensity and frequency content of time-history loads. Random vibration analysis is probabilistic in nature, because both input and output quantities represent only the probability that they take on certain values. Random Vibration Analysis uses Power spectral density to quantify the loading. (PSD) is a statistical measure defined as the limiting mean-square value of a random variable. It is used in random vibration analyses in which the instantaneous magnitudes of the response can be specified only by probability distribution functions that show the probability of the magnitude taking a particular value. In addition, 1 sigma displacement and 1 sigma stresses are used to characterize the responses. The implication of 1 sigma stresses is that, say, for a component, if the 1 sigma stress is specified to have value K, then during motion of the vehicle, 68.22% of the time, the stress level is at or below K, 27.2% of the time between K and 2K, and 4.3% of the time, between 2k and 3k.

3.3 Spectrum analysis

A spectrum analysis is one in which the results of a modal analysis are used with a known *spectrum* to calculate displacements and stresses in the model and around the crack tip. It is mainly used in place of a time-history analysis to determine the response of structures to random or time-dependent loading conditions such as earthquakes, wind loads (turbulence), ocean wave loads, jet engine thrust, rocket motor vibrations, and ground induced excitation.

Three types of spectra are available for a spectrum analysis: these are

- Response Spectrum
    - Single-point Response Spectrum (SPRS)
    - Multi-point Response Spectrum (MPRS)
- Dynamic Design Analysis Method (DDAM)
- Power Spectral Density (PSD)

3.3.1 Response Spectrum

A response spectrum represents the response of single-DOF systems to a time-history loading function. It is a graph of response versus frequency, where the response might be displacement, velocity, acceleration, force. Two types of response spectrum analysis are possible: Single-point response spectrum and multi-point response spectrum.

3.3.2 Single-Point Response Spectrum (SPRS)

In a single-point response spectrum (SPRS) analysis, you specify one response spectrum curve (or a family of curves) at a set of points in the model, such as at all supports, as shown in Figure 3.2(a)

3.3.3 Multi-Point Response Spectrum (MPRS)

In a multi-point response spectrum (MPRS) analysis, we specify different spectrum curves at different sets of points, as shown in Figure 3.2(b)

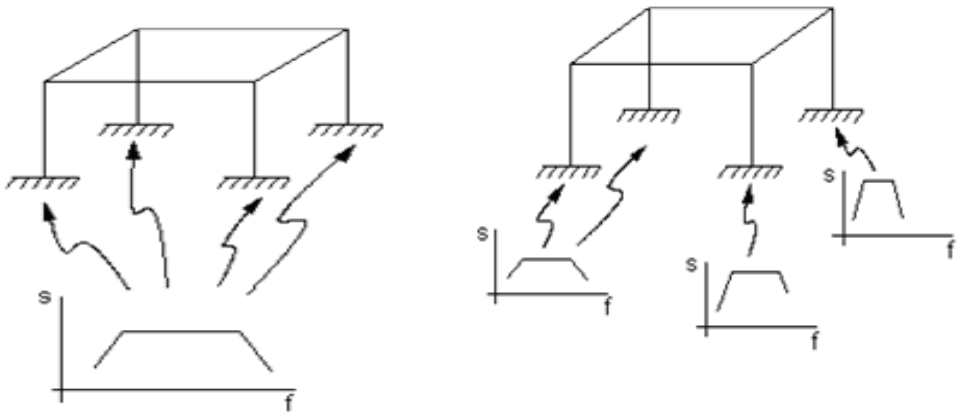

a) *b)*

Figure 3. 2 ***Response spectrums***

3.3.4 Dynamic Design Analysis Method (DDAM)

The Dynamic Design Analysis Method (DDAM) is a technique used to evaluate the shock resistance of equipments. The technique is essentially a response spectrum analysis in which the spectrum is obtained from a series of empirical equations.

3.4 Power Spectral Density

Power spectral density (PSD) is a statistical measure defined as the limiting mean-square value of a random variable. It is used in random vibration analyses in which the instantaneous magnitudes of the response can be specified only by probability distribution functions that show the probability of the magnitude taking a particular value. A PSD is a statistical measure of the response of a structure to random dynamic loading conditions. It is a graph of the PSD value versus frequency, where the PSD may be a displacement PSD, velocity PSD, acceleration PSD, or force PSD. Mathematically, the area under a PSD-versus-frequency curve is equal to the variance (square of the standard deviation of the response).

Similar to response spectrum analysis, a random vibration analysis may be single-point or multi-point. In a single point random vibration analysis, we specify one PSD spectrum at a set of points in the model. In a multi-point random vibration analysis, we specify different PSD spectra at different points in the model.

3.5 Derivation of structural matrix

In the theory of finite element structural analysis, Lagrange's principle is used in the dynamic analysis equation formulation for rigid aircraft.

The Lagrange's principle states

$$\frac{d}{dt}\left(\frac{\partial T}{\partial \dot{\phi}}\right) - \frac{\partial T}{\partial \phi} + \frac{\partial \Pi}{\partial \phi} = 0 \quad \text{.....3.1}$$

In this case, the Lagrangian's, L is defined as:

$$L = T - \Pi \quad \text{.....3.2}$$

Where, T is kinetic energy, and Π is the potential energy.

The potential energy of a linear elastic body is given by

$$\Pi = U - W_E \quad \text{.....3.3}$$

Where, U is the internal/strain energy; and

W_E is the external energy which is work done by external loads.

The internal energy is the strain energy caused by deformation of the body, and can be written as

$$U = \frac{1}{2}\iiint_V \{\sigma\}^T \{\varepsilon\} dV \quad \text{.....3.4}$$

Where $\{\sigma\} = \{\sigma_x, \sigma_y, \tau_{xy}\}^T$ is the stress vector and

$\{\varepsilon\} = \{\varepsilon_x, \varepsilon_y, \gamma_{xy}\}^T$ is the strain.

The strain vector is related to the stress vector by the equation:

$$\{\sigma\} = [D]\{\varepsilon\} \quad \text{.....3.5}$$

where [D] is the constitutive matrix.

Substituting equation (3.5) in to equation (3.4) yields

$$U = \frac{1}{2}\iiint_V \{\varepsilon\}^T [D]\{\varepsilon\} dV \quad \text{.....3.6}$$

The external energy is the work done by the external loads, and can be given by

$$W_E = \iiint_V \{u\}^T \{f\} dV + \iint_S \{u\}^T \{\overline{\Phi}\} dS \quad \text{.....3.7}$$

Where $\{u\} = \{u_x, u_y, u_z\}$ is displacement vector for the element

$\{f\} = \{f_x, f_y, f_z\}$ is body force vector

$\{\overline{\Phi}\} = \{\overline{\Phi}_x, \overline{\Phi}_y\}$ is surface load vector

Substituting equations (3.6) and equations (3.7) in to equations (3.3) and discretization of the domain in to a number of finite element domains yields:

$$\Pi = \frac{1}{2}\iiint_V \{\varepsilon\}^T [D]\{\varepsilon\} dV - \iiint_V \{u\}^T \{f\} dV - \iint_S \{u\}^T \{\overline{\Phi}\} dS \quad \text{.....3.8}$$

The kinetic energy term, T, can be given by

$$T = \frac{1}{2}\iiint_V \rho\{\dot{u}\}^T \{\dot{u}\} dV \quad \text{.....3.9}$$

Displacement vector, $\{u\}$ can be expresses in terms on the nodal displacement vector as:

$$\{u\} = [N]\{\phi\} \quad \text{.....3.10}$$

where [N] is the displacement transformation matrix

$\{\phi\}$ is the nodal displacement vector

Substituting the vector $\{u\}$ in to the kinetic energy equation (3.9):

$$T = \frac{1}{2}\iiint_V \rho[N]^T \{\dot{\phi}\}^T [N]\{\dot{\phi}\}dV$$

$$T = \frac{1}{2}\{\dot{\phi}\}^T (\iiint_V \rho[N]^T \ [N]dV)\{\dot{\phi}\}$$

$$T = \frac{1}{2}\{\dot{\phi}\}^T [M_e]\{\dot{\phi}\} \text{.....3.11}$$

$[M_e] = \iiint_V \rho[N]^T \ [N]dV$ = is element mass matrix.

The strain and displacement vectors are related by the matrix, [B] such that

$$\{\varepsilon\} = [B]\{\phi\} \text{.....3.12}$$

$[B]$ is strain displacement matrix.

Using equations (3.12), equations (3.6), can be re-written as

$$U = \frac{1}{2}\iiint_V \{B\}^T \{\phi\}^T [D][B]\{\phi\}dV$$

$$U = \frac{1}{2}\phi^T (\iiint_V \{B\}^T [D][B]dV)\{\phi\}$$

$$U = \frac{1}{2}\{\phi\}^T [K_e]\{\phi\} \text{.....3.13}$$

where $[K_e]$ is element stiffness matrix.

Substituting the vector $\{u\}$ in to the external energy

$$W_E = \iiint_V [N]^T \{\phi\}^T \{f\}dV + \iint_S [N]^T \{\phi\}^T \{\overline{\Phi}\}dS \text{.....3.14}$$

Substituting equations 3.13 and 3.14, in to equation 3.3, then the potential energy is

$$\Pi = \frac{1}{2}\{\phi\}^T [K_e]\{\phi\} - \iiint_V [N]^T \{\phi\}^T \{f\}dV - \iint_S [N]^T \{\phi\}^T \{\overline{\Phi}\}dS \text{.....3.15}$$

Substituting equations 3.11 and 3.15, in to equation 3.1, the governing equation of motion for general vibration of composite shell becomes:

$$[M]\{\ddot{\phi}\} + [K]\{\phi\} = \{F^B\} + \{F^S\} \text{.....3.16}$$

where F^B is body force vector

F^S is surface load vector

The equation of motion for free vibration of the shell becomes;

$$[M]\{\ddot{\phi}\} + [K]\{\phi\} = 0 \text{.....3.17}$$

Reducing in to Eigen-value of the problem is:

$$\left([K]-\varpi^2[M]\right)\{\phi\}=0 \text{ ……..……3.18}$$

The natural frequency ϖ_i, mode shapes and other parameters can be obtained by using the equation 3.18.

Equation (3.16) is the governing equation for an element. Substituting the appropriate displacement transformation matrices, strain displacement matrices, and constitutive matrices, the stiffness and mass matrices can be determined.

I) Four node shell element

Four node shell elements (fig 3.3) are used to model the shell structure of the vehicle. The element has four nodes with each having six degrees of freedom. For the model 4 node element 63 is used.

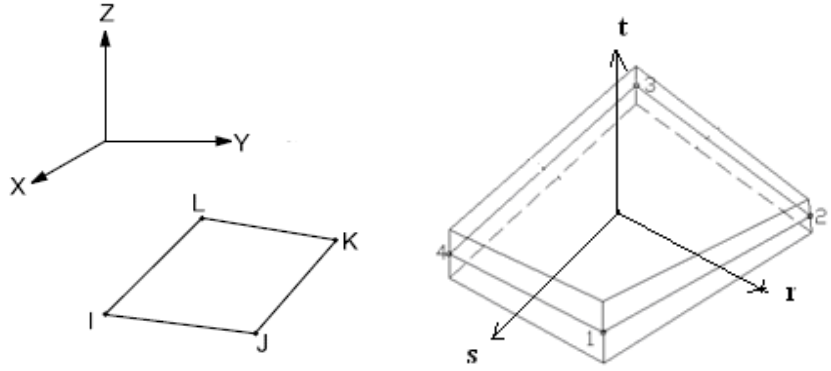

Figure 3. 3 ***Four node shell element***

II) Spring-Damper Element

Spring-Damper finite elements are used to model the shock absorber and the tire of the flying vehicle. Generally, the element is used to model the shock absorbing mechanism.

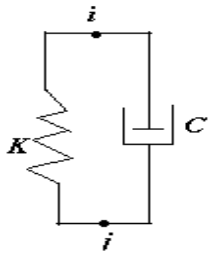

Figure 3. 4 ***Spring-Damper Element***

III) Crack description

As seen in figure 3.5 a semi-elliptic crack is generated by removing out an elliptical volume having a crack length 2a=200mm, a depth of c =27.5mm, and a narrow width of W=12mm. The surface crack in this case is oriented longitudinally and circumferentially on the outer top most surface of the shell as shown in figure 3.5.

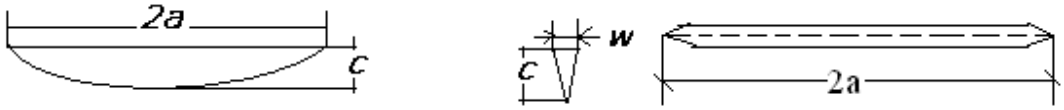

a) *Semi-elliptical Crack geometry viewed from the thickness and on top of the shell*

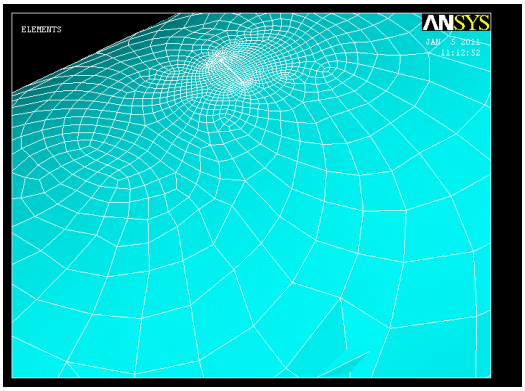

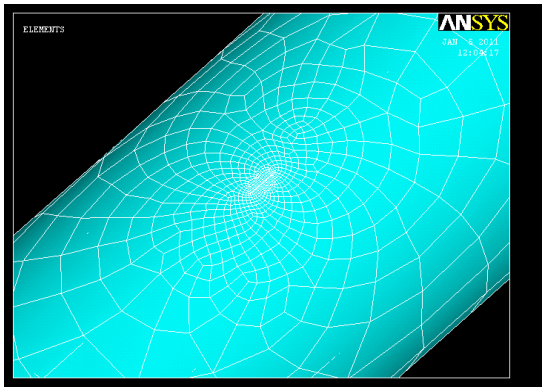

b) Circumferential surface crack orientation *c) Longitudinal surface crack orientation*

Figure 3. 5 ***Semi-elliptical surface crack model and meshes***

IV) Meshing the Model

The model is meshed with automatic mesh generation command "Auto Mesh Generation". As can be seen from figure 3.5, the model is meshed with more refined elements in the vicinity of the crack and coarsely meshed in areas away from the crack to economize the computation time.

V) Geometric parameters of the model

The parameters are taken from Boeing 767-series of the airplane [23].

Outer radius of shell = 2900mm K_N = 80 000 N/m

Thickness of the shell = 27.5mm C_N = 3200 N s/m

Layer thickness = 2.5mm C_M = 19 200 N s/m

Length of the fuselage shell =18000mm K_M = 240 000 N/m

VI) Material of the laminate:

Carbon Fiber Reinforced Plastic (CFRP)

The material of the laminate is made of linear elastic orthotropic material that is taken from reference [11] with the following properties:

E_x =181Gpa, $G_{xy} = 7.0$Gpa

E_y =10.3Gpa $\gamma_x = 0.28$

E_{xy} =10.3Gpa $\gamma_y = 0.60$

$G_x = 7.17$Gpa $\gamma_{xy} = 0.27$

$G_y = 3.0$Gpa $\rho =$ Density =1550

VII) Layup sequence: symmetric: [45/0/-45/90/0/-45/0/90/-45/0/45] °

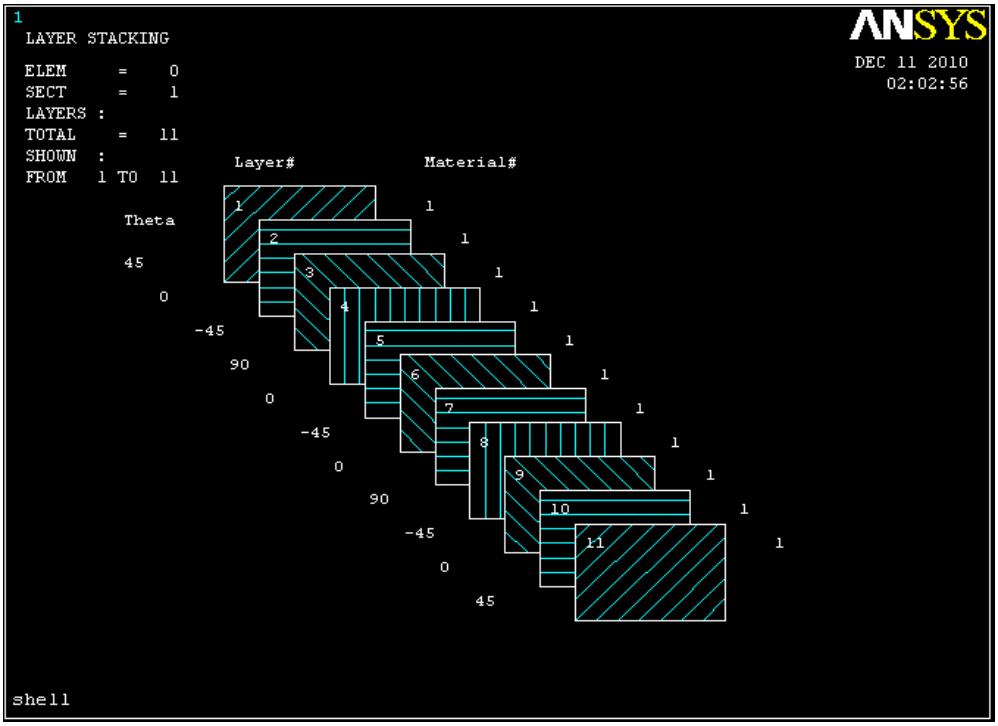

Figure 3. 6 ***Layer stacking sequence of composite shell***

VIII) Loading and Boundary conditions

Boundary conditions: The fuselage shell is constrained in both rotary and linear displacement in the x and z directions, and free to excite linearly and constrained to rotate in the y direction as shown in figure 3.8. The model is done with the absence of longitudinal and transversal stiffening members.

Loading: The applied load, which is the power spectral density (PSD) input at the three points of the node that the landing gear fuselage attachment points in the direction of excitation(y axis) are applied for the analysis.

Figure 3. 7 ***Aircraft Sketch***

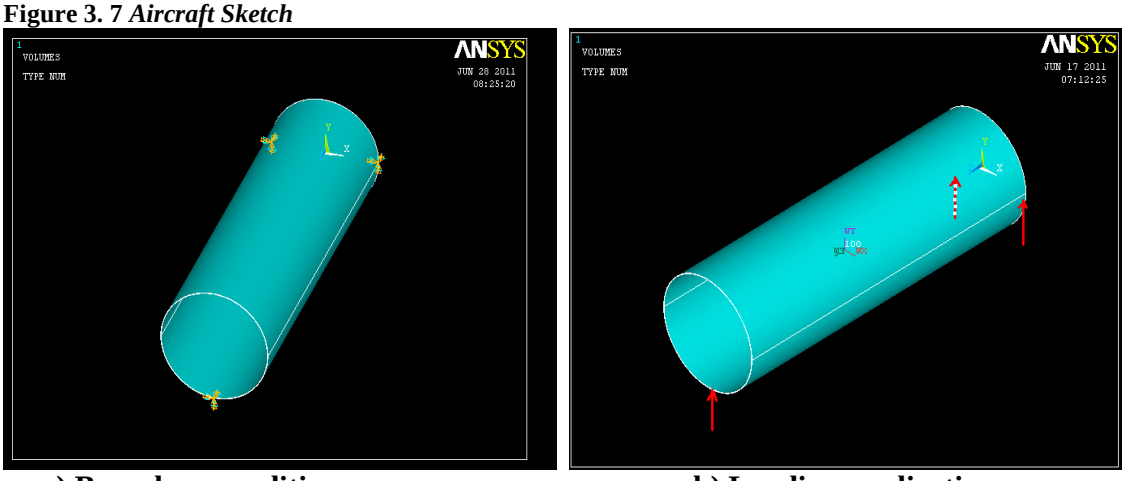

a) **Boundary conditions** **b) Loading application**

Figure 3. 8 *Finite Element* ***model of all composite shell,***
loading and boundary conditions

Chapter Four

4.1 Finite Element software results and discussions

The analysis carried out using the finite element model consists of modal analysis, and spectrum analysis. The same finite element model is used for all the analyses. The difference among the cases considered lies in the type of application of loads, variation of crack length and crack orientation. The solution procedure followed for the analysis is shown in the figure 4.1 below.

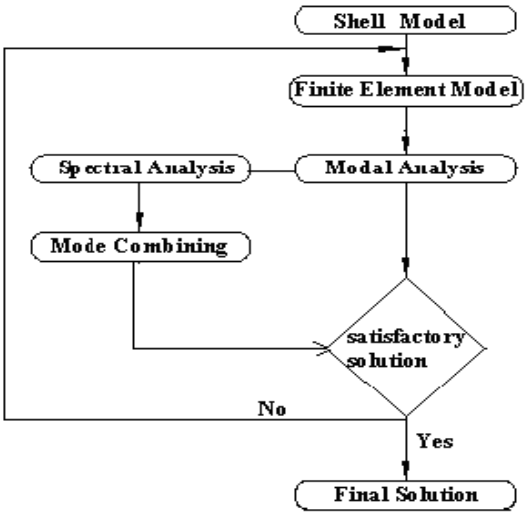

Figure 4. 1 ***Flow diagram of solution procedure***

4.2 Modal analysis

Modal analysis provides results which indicate the natural vibration characteristics of a structure. It involves determination of the natural frequencies and modes of vibration. In addition to studying vibration characteristics, the results obtained from modal analysis are used for spectrum analysis.

4.3 Random vibration analysis

Random vibration analysis deals with response of a structure to random dynamic loads. The responses are defined using power spectral density functions. As explained in chapter four, 1σ displacementes and stresses, 2σ displacementes and stress, and 3σ displacementes and stress are used to characterize the responses.

4.4 Finite element Software results

Here the analysis is done for the initial crack length of given parameters as explained in section 3.4.

4.4.1 Class A runways types, longitudinal crack orientation

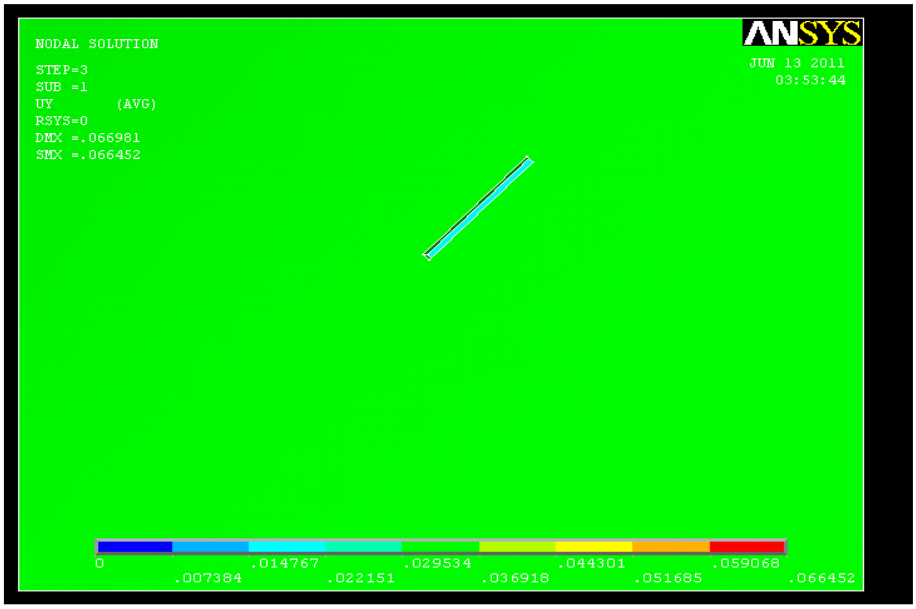

Figure 4.2. 1 ***Y-displacement response for initial crack length =200mm***

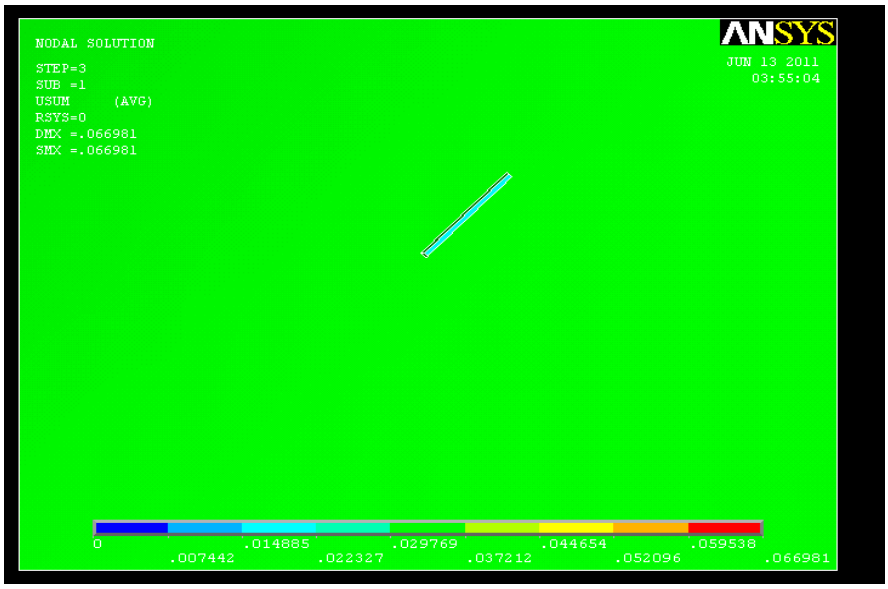

Figure 4.2. 2 ***Total displacement response for initial crack length=200mm***

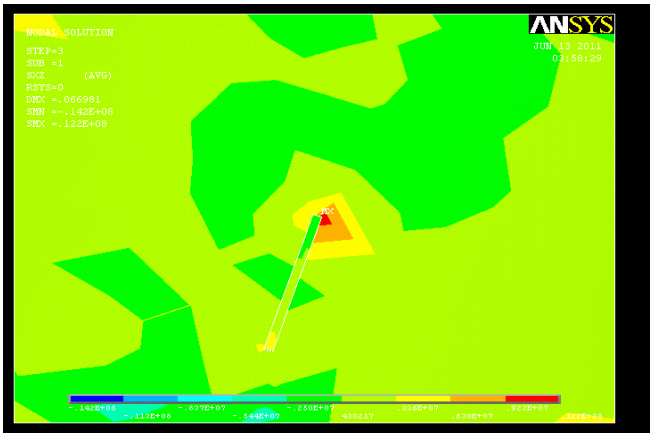

Figure 4.2. 3 ***Nodal shear stress for initial crack length=200mm***

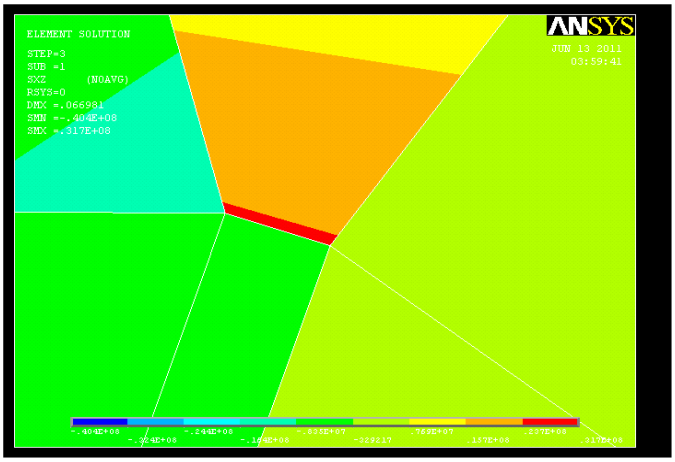

Figure 4.2. 4 ***Element shear stress for initial crack length=200mm***

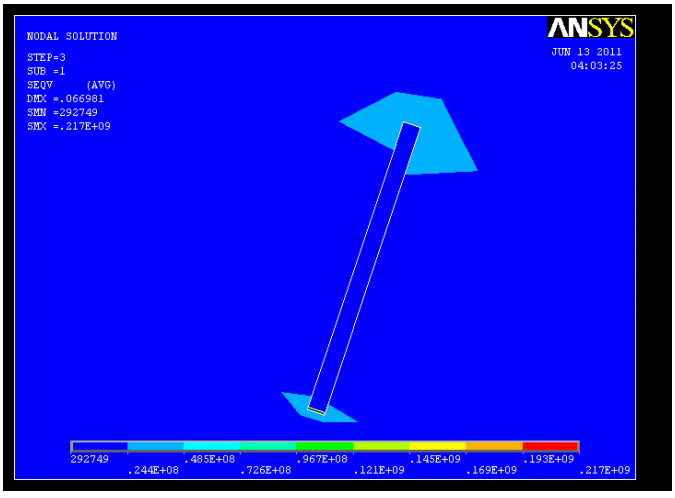

Figure 4.2. 5 ***Von misses stress for initial crack length=200mm***

4.4.2 Class A pavement types circumferential crack orientation

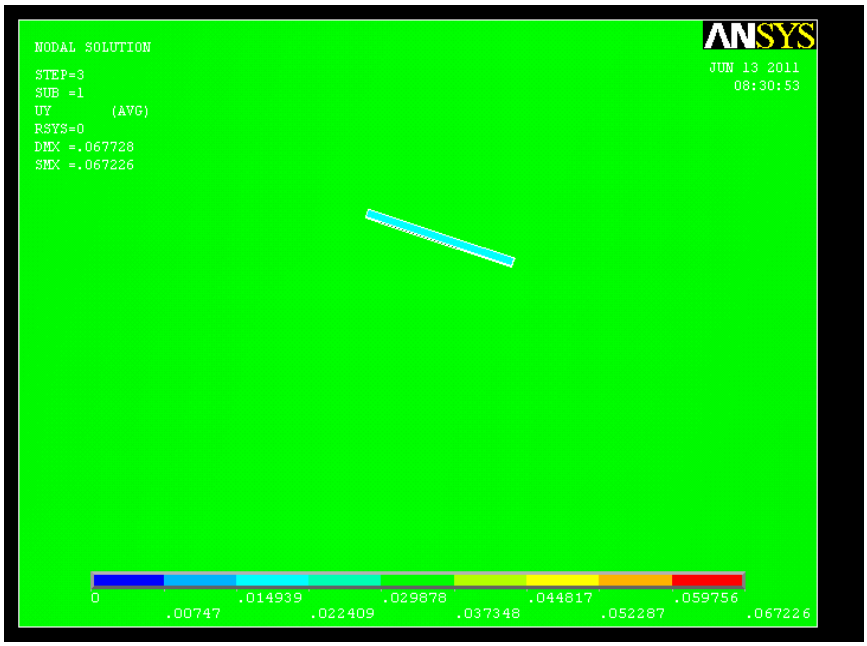

Figure 4.2. 6 ***Y-displacement response for initial crack length =200mm***

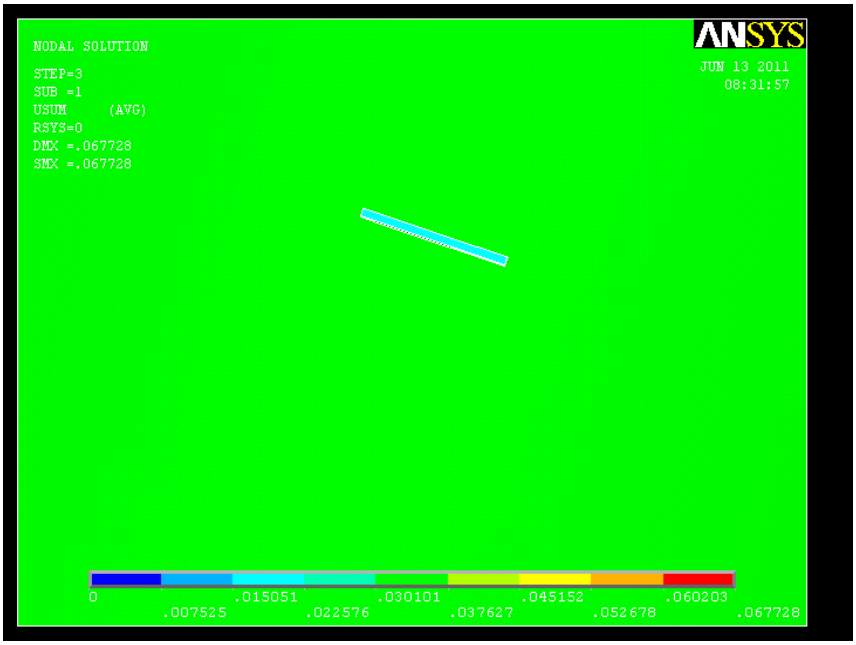

Figure 4.2. 7 ***Total displacement response for initial crack length=200mm***

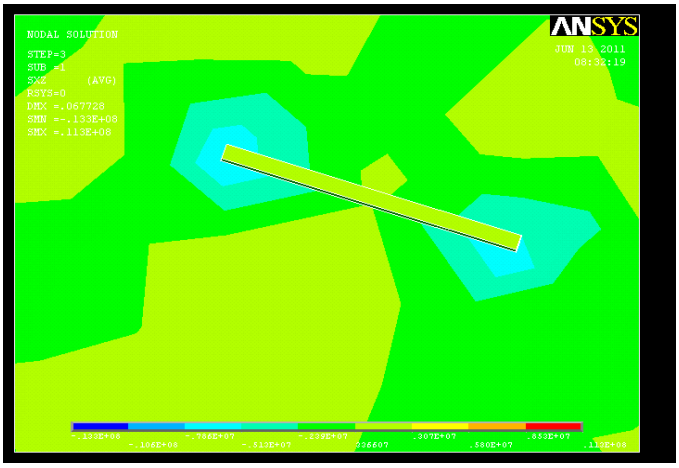

Figure 4.2. 8 ***Nodal shear stress for initial crack length=200mm***

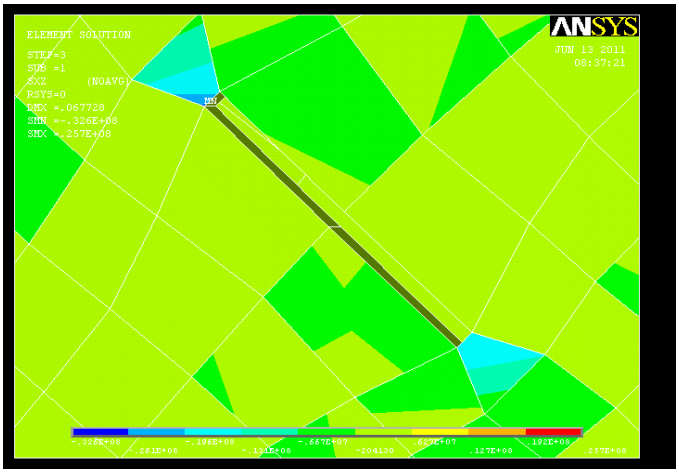

Figure 4.2. 9 ***Element shear stress for initial crack length=200mm***

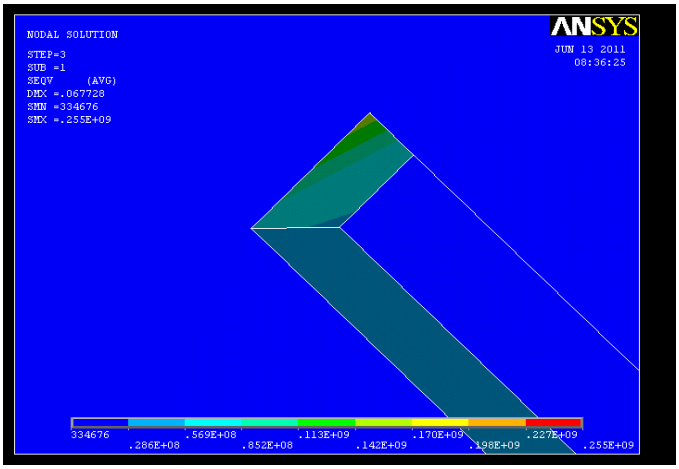

Figure 4.2. 10 ***Von misses stress for initial crack length=200mm***

Table 4. 1 Simulation results: Class A runways.

The analysis is done on a 20%, 40%, 60%, 80% and 100% increase of crack length with the same type of loadings, crack orientation, and model.

Initial crack length =200mm					
S/N	Type of result	Parameter	Longitudinal crack Orientation	Circumferential crack Orientation	% Remark
1	Nodal solution	Uy=y-Displacement (mm)	0.066452	0.067226	
2		Usum=Total displacement (mm)	0.066981	0.067728	
3		Sxz= Shear stresses(Mpa)	12.2	11.3	
4		SEQV=Equivalent stresses (Mpa)	217	255	
5	Element solution	Sxz=Shear stresses(Mpa)	31.7	25.7	
20% Increase of crack length =240mm					
1	Nodal solution	Uy=y-Displacement (mm)	0.0718042	0.0917676	
2		Usum=Total displacement (mm)	0.0723732	0.0924494	
3		Sxz= Shear stresses(Mpa)	16.16	15.9	
4		SEQV=Equivalent stresses (Mpa)	234.4	349.2	
5	Element solution	Sxz=Shear stresses(Mpa)	37.16	40.18	
40% Increase of crack length =280mm					
1	Nodal solution	Uy=y-Displacement (mm)	0.0771564	0.1163092	
2		Usum=Total displacement (mm)	0.0777654	0.1171708	
3		Sxz= Shear stresses(Mpa)	20.12	20.5	
4		SEQV=Equivalent stresses(Mpa)	251.8	443.4	
5	Element solution	Sxz=Shear stresses(Mpa)	42.62	54.66	
60% Increase of crack length =320mm					
1	Nodal solution	Uy=y-Displacement (mm)	0.0825086	0.1408508	
2		Usum=Total displacement (mm)	0.0831576	0.1418922	
3		Sxz=Shear stresses(Mpa)	24.08	25.1	
4		SEQV=Equivalent stresses(Mpa)	269.2	537.6	
5	Element solution	Sxz=Shear stresses(Mpa)	48.08	69.14	
80% Increase of crack length =360mm					
1	Nodal solution	Uy=y-Displacement (mm)	0.0878608	0.1653924	
2		Usum=Total displacement (mm)	0.0885498	0.1666136	
3		Sxz= Shear stresses(Mpa)	28.04	29.7	
4		SEQV=Equivalent stresses(Mpa)	286.6	631.8	
5	Element solution	Sxz=Shear stresses(Mpa)	53.54	83.62	
100% Increase of crack length =400mm					
1	Nodal solution	Uy=y-Displacement (mm)	0.093213	0.189934	
2		Usum=Total displacement (mm)	0.093942	0.191335	
3		Sxz= Shear stresses(Mpa)	32	34.3	
4		SEQV=Equivalent stresses(Mpa)	304	726	
5	Element solution	Sxz=Shear stresses(Mpa)	59	98.1	

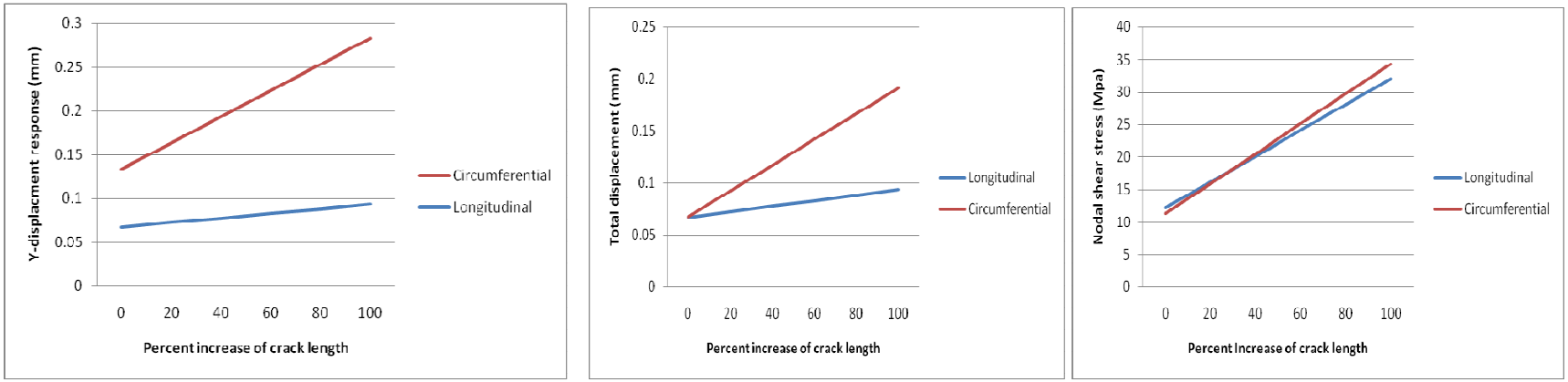

a)

b)

c)

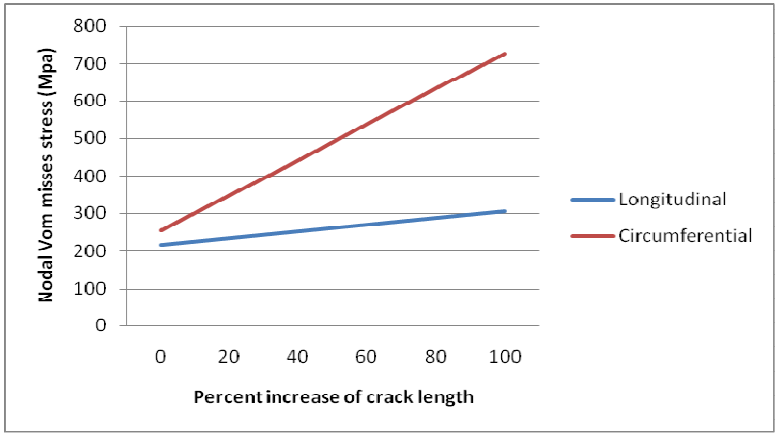

d)

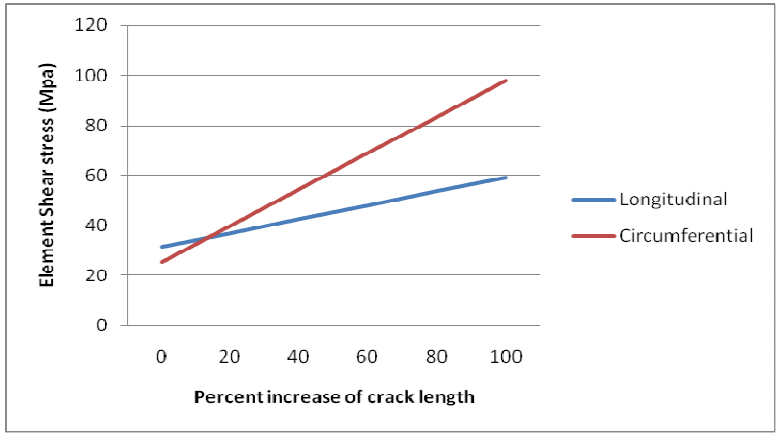

e)

Figure 4.2. 11 ***Percentage of crack length versus some parameters***

Result and Discussion for Class-A runway excitations

One sigma and three sigma results:

- One sigma corner stress for the longitudinal crack orientation is 217 Mpa, and 68.2% of time of vehicle motion the stress level is at or below this value. Three sigma corner stresses for the longitudinal crack orientation is 651 Mpa, and 4.3 % of time of vehicle motion the stress level reach this value.
- One sigma corner stress for the circumferential crack orientation is 255 Mpa, and 68.2% of time of vehicle motion the stress level is at or below this value. Three sigma corner stresses for the radial crack orientation is 765 Mpa, and 4.3% of time of vehicle motion the stress level reaches at this value.

Since the stress and strain response both in the longitudinal and circumferential orientation of the crack is less than the elastic limit of the material, the excitation severs less to the shell and causes less fatigue.

Figure 4.2.11 a) and figure 4.2.11 b) show the variation of *y-displacement and total displacement response* with percentage *increase of crack length* respectively, for the *longitudinal and circumferential* crack orientation, with Class-A input excitations.

And figure 4.2.11 c) and figure 4.2.11 e) show the variation of nodal *shear stress and element shear stress responses* with *percentage increase of crack length* respectively, for the *longitudinal and circumferential* orientation of the crack, with the same Class-A input excitations.

Moreover, figure 4.2.11 d) shows the variation of nodal *Von Misses stress response with percentage increase of crack length*, for the *longitudinal and circumferential* orientation of the crack, having similar Class-A runways input excitations.

From the curves we can also see that the shell is highly affected by the circumferential crack orientation for nodal displacement, total displacement, nodal shear stress, Von misses stresses and element shear stresses. The reason is propagation of transverse stress wave and crack arrangements are perpendicular to each other, so that the applied load causes the stress to maximize and the strains to excite more near the crack tips.

4.4.3 Class G runways types longitudinal crack orientation

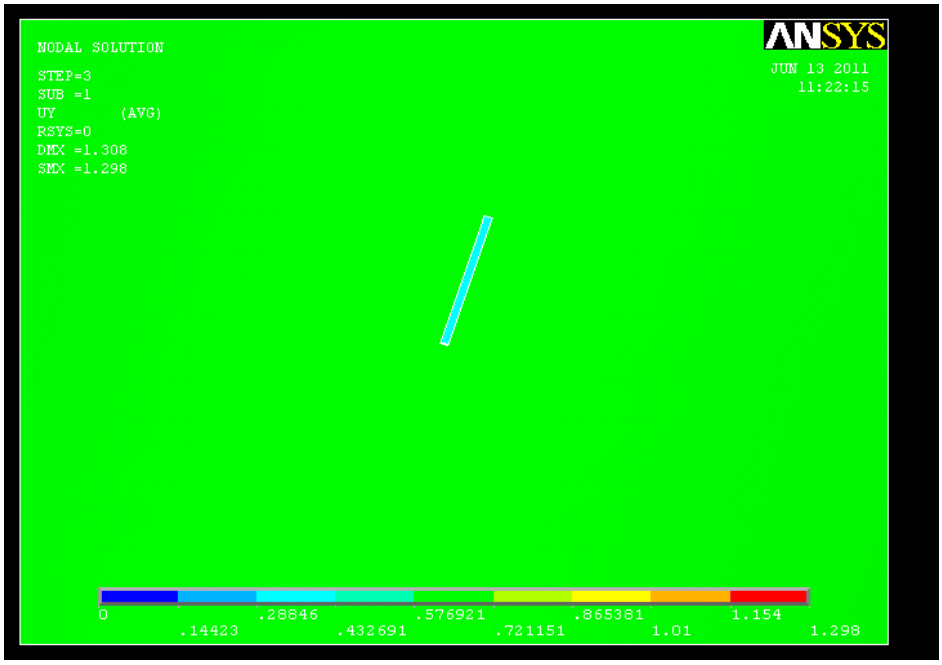

Figure 4.3. 1 ***Y-displacement response for initial crack length =200mm***

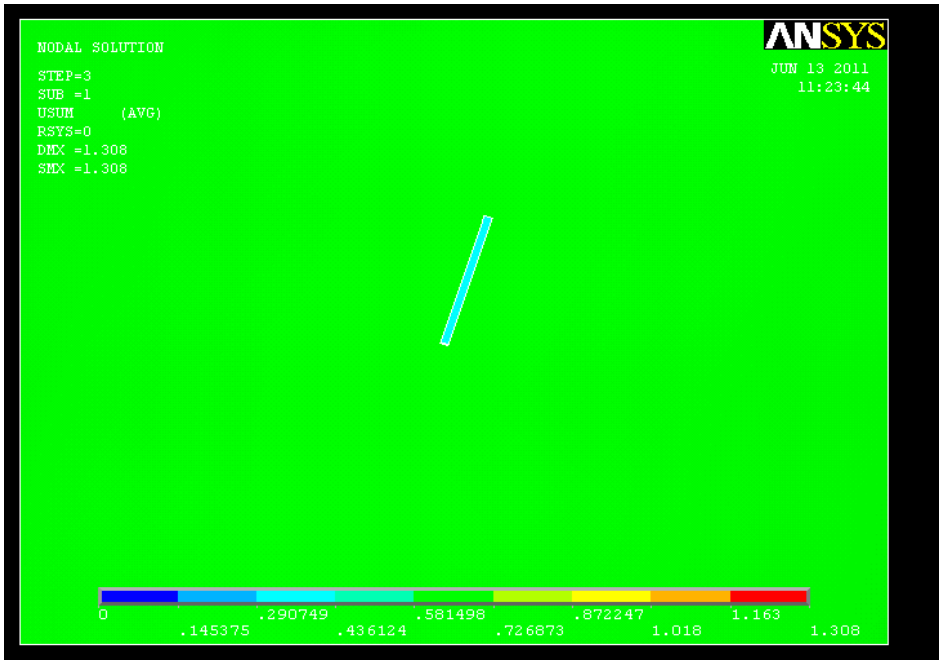

Figure 4.3. 2 ***Total displacement response for initial crack length =200mm***

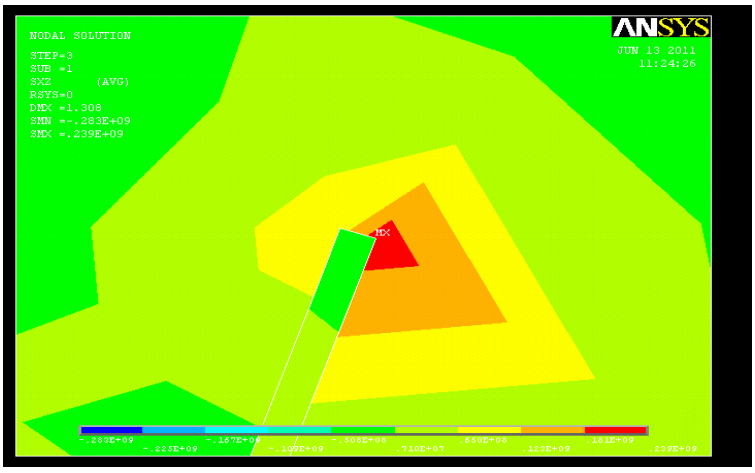

Figure 4.3. 3 ***Nodal shear stress for initial crack length=200mm***

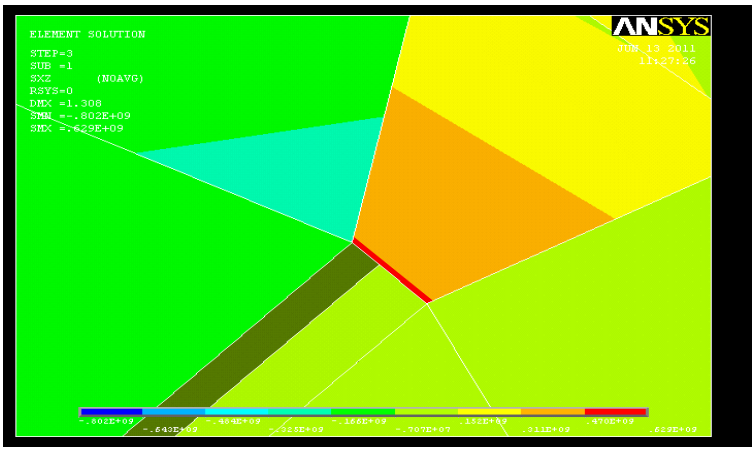

Figure 4.3. 4 ***Element shear stress for initial crack length=200mm***

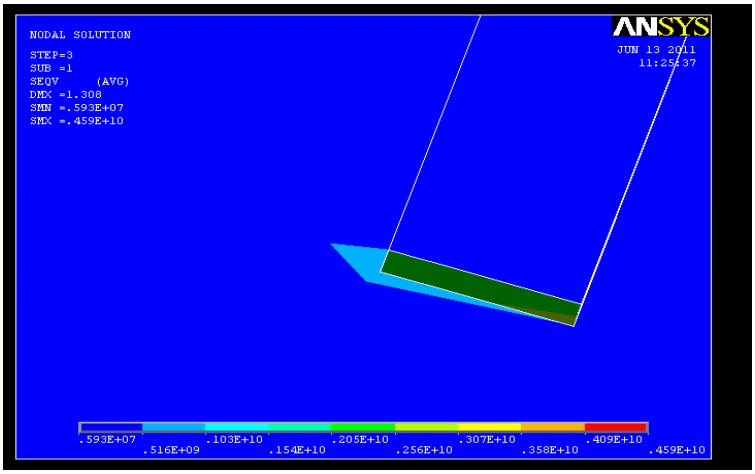

Figure 4.3. 5 ***Von misses stress for initial crack length=200mm***

4.4.4 Class G runways types circumferential crack orientation

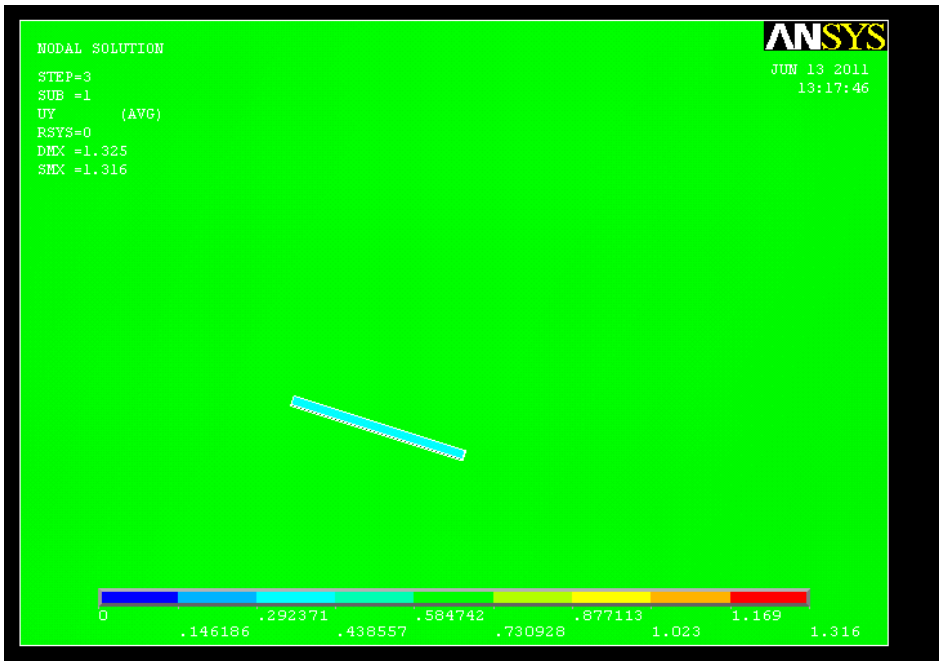

Figure 4.3. 6 ***Y-displacement response for initial crack length =200mm***

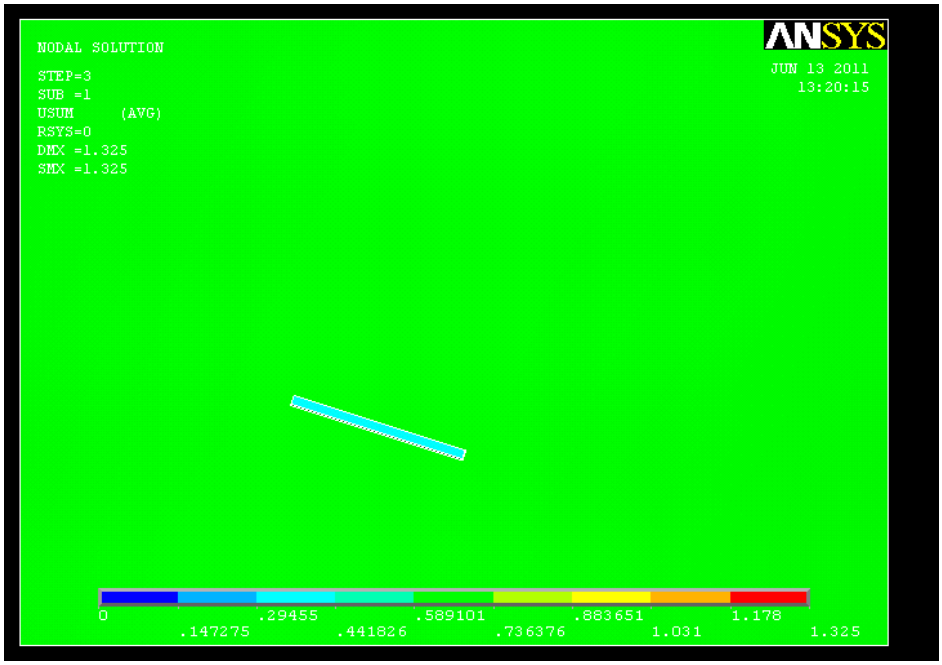

Figure 4.3. 7 ***Total displacement response for initial crack length =200mm***

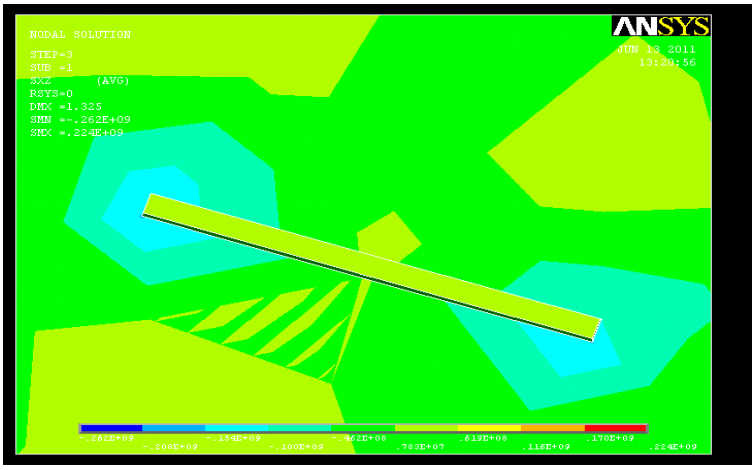

Figure 4.3. 8 ***Nodal shear stress for initial crack length=200mm***

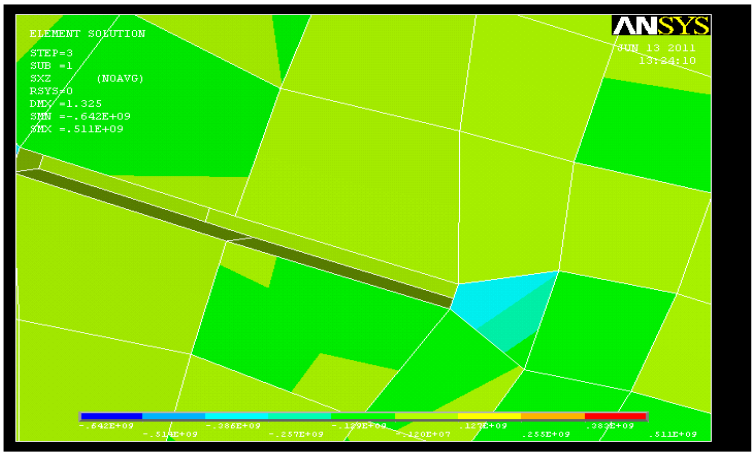

Figure 4.3. 9 ***Element shear stress for initial crack length=200mm***

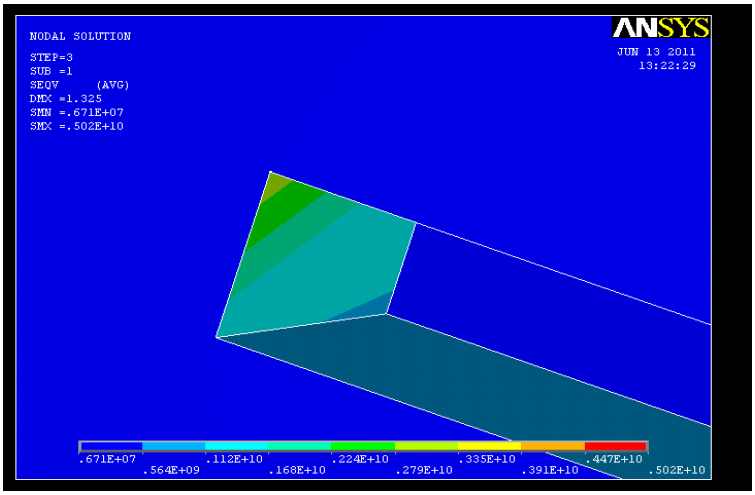

Figure 4.3. 10 ***Von misses stress for initial crack length=200mm***

Table 4. 2. Simulation results: Class G runways.

The analysis is done on a 20%, 40%, 60%, 80% and 100% increase of crack length with the same type of loadings crack orientation and model.

Initial crack length =200mm					
S/N	Type of result	Parameter	Longitudinal crack Orientation	Circumferential crack Orientation	% Remark
1	Nodal solution	Uy=y-Displacement (mm)	1.298	1.316	
2		Usum=Total displacement (mm)	1.308	1.325	
3		Sxz= Shear stresses(Mpa)	239	224	
4		SEQV=Equivalent stresses (Mpa)	4590	5020	
5	Element solution	Sxz=Shear stresses(Mpa)	629	511	
20% Increase of crack length =240mm					
1	Nodal solution	Uy=y-Displacement (mm)	1.3004	1.3208	
2		Usum=Total displacement (mm)	1.3104	1.332	
3		Sxz= Shear stresses(Mpa)	279.8	277	
4		SEQV=Equivalent stresses (Mpa)	4692	5036	
5	Element solution	Sxz=Shear stresses(Mpa)	668.2	546.6	
40% Increase of crack length =280mm					
1	Nodal solution	Uy=y-Displacement (mm)	1.3028	1.3256	
2		Usum=Total displacement (mm)	1.3128	1.339	
3		Sxz= Shear stresses(Mpa)	320.6	330	
4		SEQV=Equivalent stresses(Mpa)	4794	5052	
5	Element solution	Sxz=Shear stresses(Mpa)	707.4	582.2	
60% Increase of crack length =320mm					
1	Nodal solution	Uy=y-Displacement (mm)	1.3052	1.3304	
2		Usum=Total displacement (mm)	1.3152	1.346	
3		Sxz=Shear stresses(Mpa)	361.4	370	
4		SEQV=Equivalent stresses(Mpa)	4896	5068	
5	Element solution	Sxz=Shear stresses(Mpa)	746.6	617.8	
80% Increase of crack length =360mm					
1	Nodal solution	Uy=y-Displacement (mm)	1.3076	1.3352	
2		Usum=Total displacement (mm)	1.3176	1.353	
3		Sxz= Shear stresses(Mpa)	402.2	410	
4		SEQV=Equivalent stresses(Mpa)	4998	5084	
5	Element solution	Sxz=Shear stresses(Mpa)	785.8	653.4	
100% Increase of crack length =400mm					
1	Nodal solution	Uy=y-Displacement (mm)	1.31	1.340	
2		Usum=Total displacement (mm)	1.32	1.360	
3		Sxz= Shear stresses(Mpa)	443	450.2	
4		SEQV=Equivalent stresses(Mpa)	5100	5100	
5	Element solution	Sxz=Shear stresses(Mpa)	825	689	

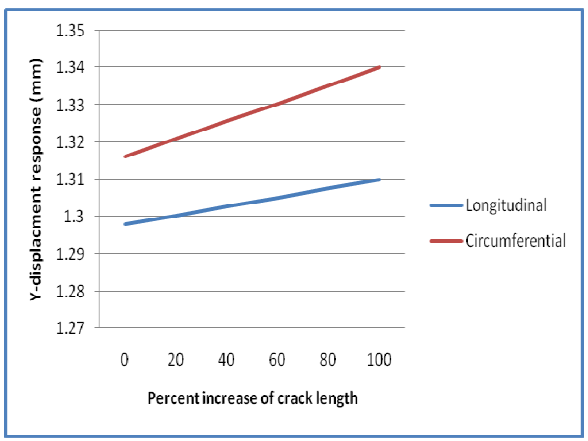

a)

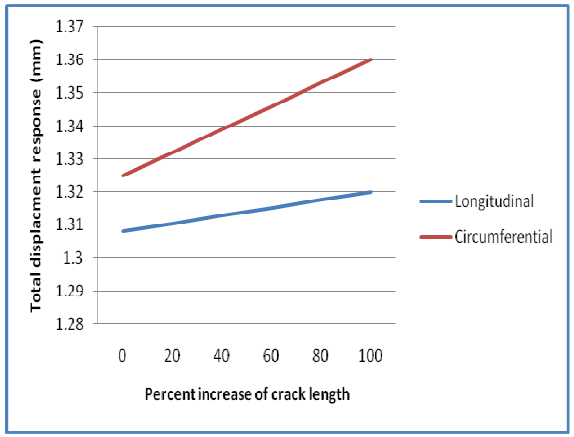

b)

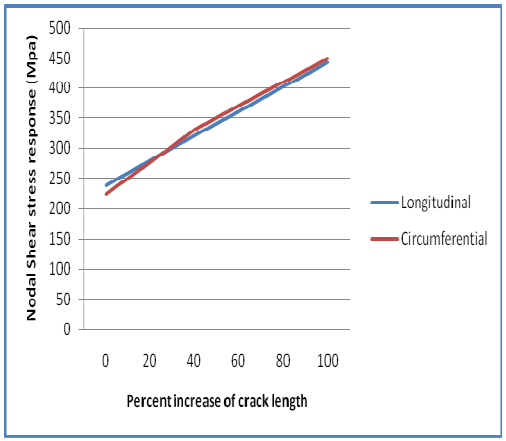

c)

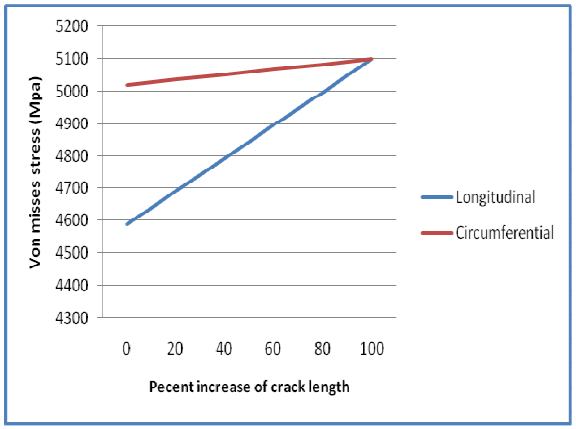

d)

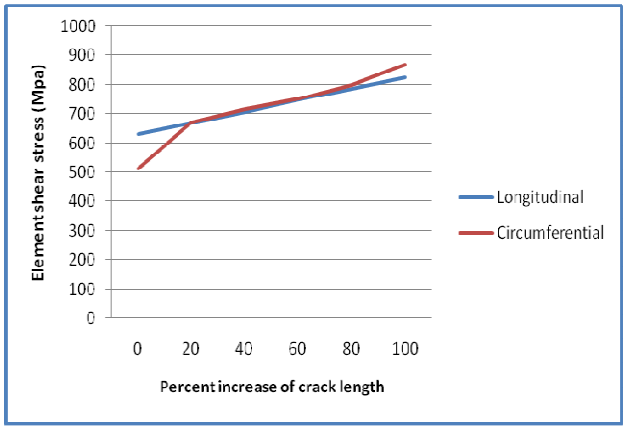

e)

Figure 4.3. 11 ***Percentage increase of crack length versus some parameters***

Result and Discussion for class G runways

One sigma and three sigma results:

- One sigma corner stress for the longitudinal crack orientation is 4.59GPa, and 68.2% of time of vehicle motion, the stress level is at or below this value. Three sigma corner stresses for the longitudinal crack orientation is 13.77GPa, and 4.3 % of time of vehicle motion, the stress level reach this value.
- One sigma corner stress for the circumferential crack orientation is 5.02GPa, and 68.2% of time of vehicle motion, the stress level is at or below this value. Three sigma corner stresses for the circumferential crack orientation is 15.06GPa, and 4.3% of time of vehicle motion, the stress level reaches at this value.

Here the sigma stress response in the longitudinal and circumferential orientation of the crack are greater than the fatigue strength of the material made and the excitation severs more the aerospace material and causes more fatigue as compared to smooth or Class-A runways.

Both figure 4.3.11 a) and figure 4.3.11 b) show the variation of *y-displacement* and *total displacement* response with *percentage increase of crack length* respectively, for the *longitudinal* and *circumferential* arrangement of the crack for pastured pavement excitations. Figure 4.3.11 c) and figure 4.3.11 e) respectively show the variation of *nodal shear stress* and *element shear stress responses* with *percentage increase of crack length*, for the *longitudinal* and *circumferential* orientation of the crack with the same pastured input loadings. Figure 4.3.11 d) shows the variation of *nodal Von Misses stress response* with *percentage increase of crack length*, for the *longitudinal* and *circumferential* crack orientation. Here again the excitation is pastured; that is Class-G input.

From the curves we can also see that the shell is highly affected by the circumferential crack orientation for nodal displacement, total displacement, nodal shear stress, Von misses stresses and element shear stresses. The reason is propagation of transverse stress wave and crack arrangements are perpendicular to each other, so that the applied load causes the stress to maximize and the strains to excite more near the crack tips.

4.4.5 Class H runways types longitudinal crack orientation

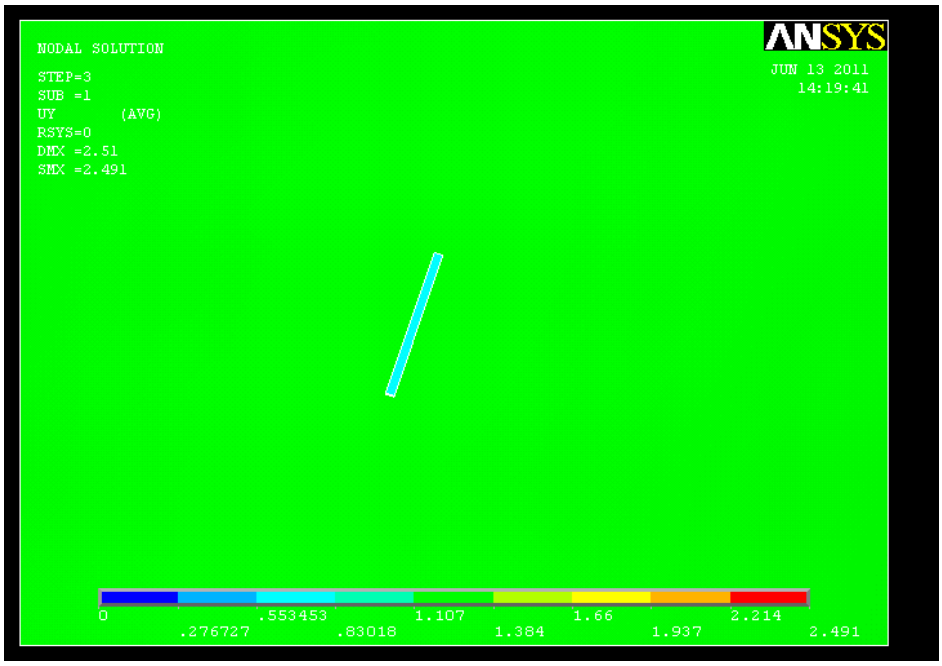

Figure 4.4. 1 ***Y-displacement response for initial crack length =200mm***

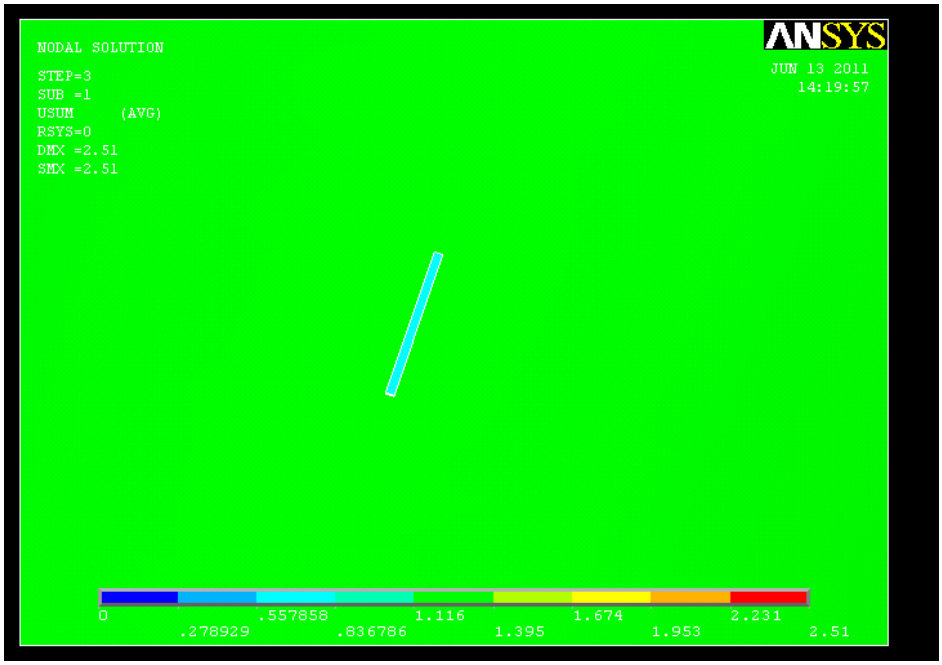

Figure 4.4. 2 ***Total displacement response for initial crack length =200mm***

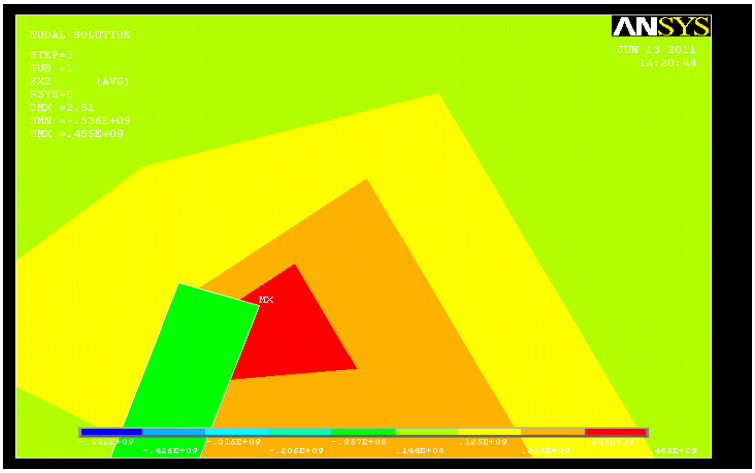

Figure 4.4. 3 ***Nodal shear stress for initial crack length=200mm***

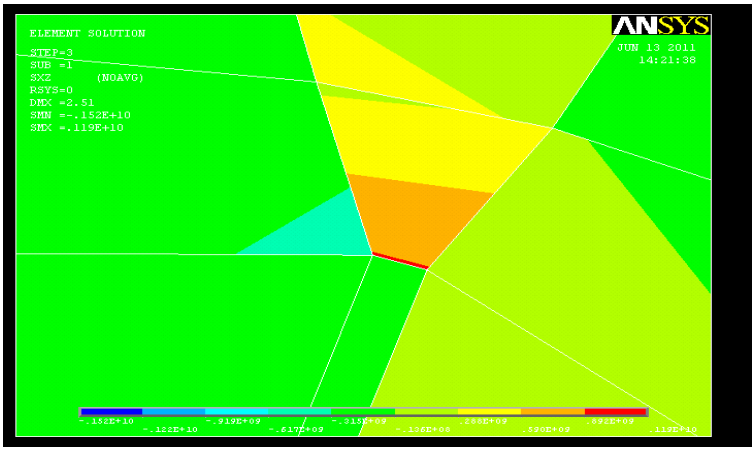

Figure 4.4. 4 ***Element shear stress for initial crack length=200mm***

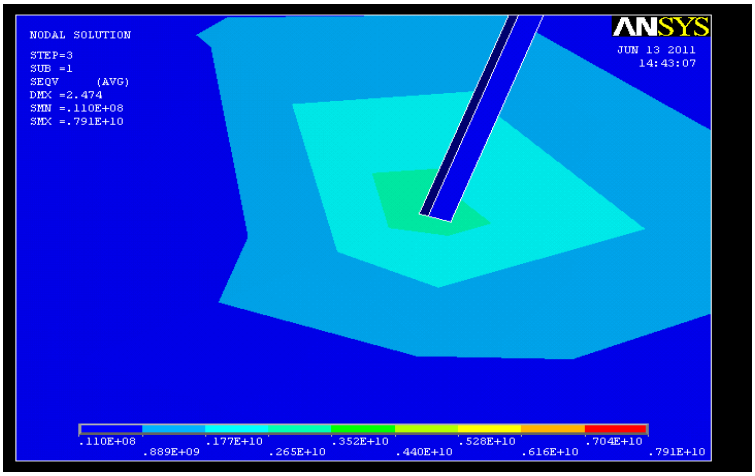

Figure 4.4. 5 ***Von misses stress for initial crack length=200mm***

4.4.6 Class H pavement, circumferential crack orientation

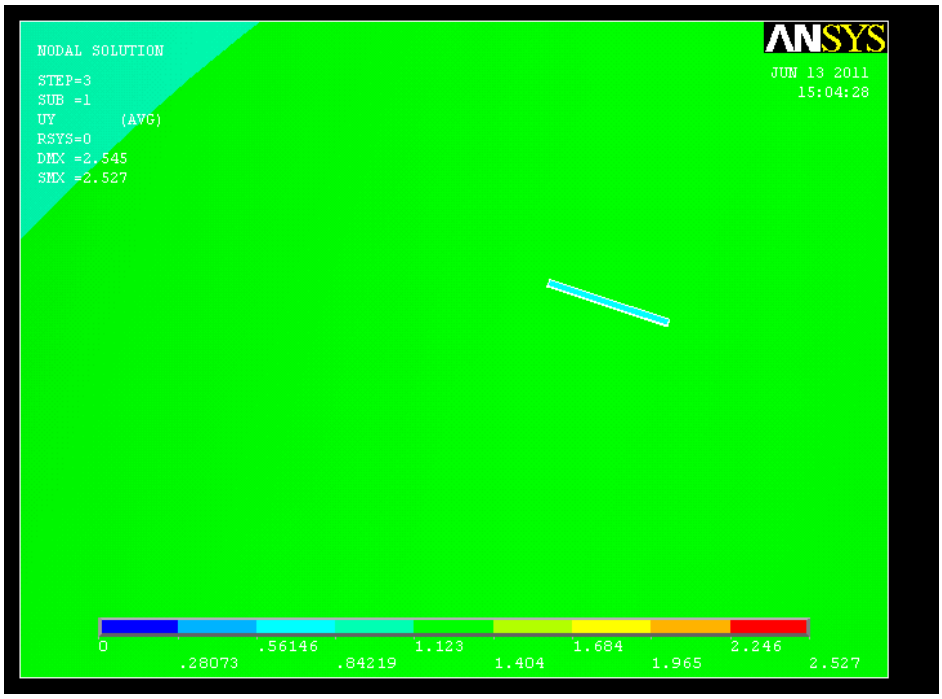

Figure 4.4. 6 ***Y-displacement response for initial crack length =200mm***

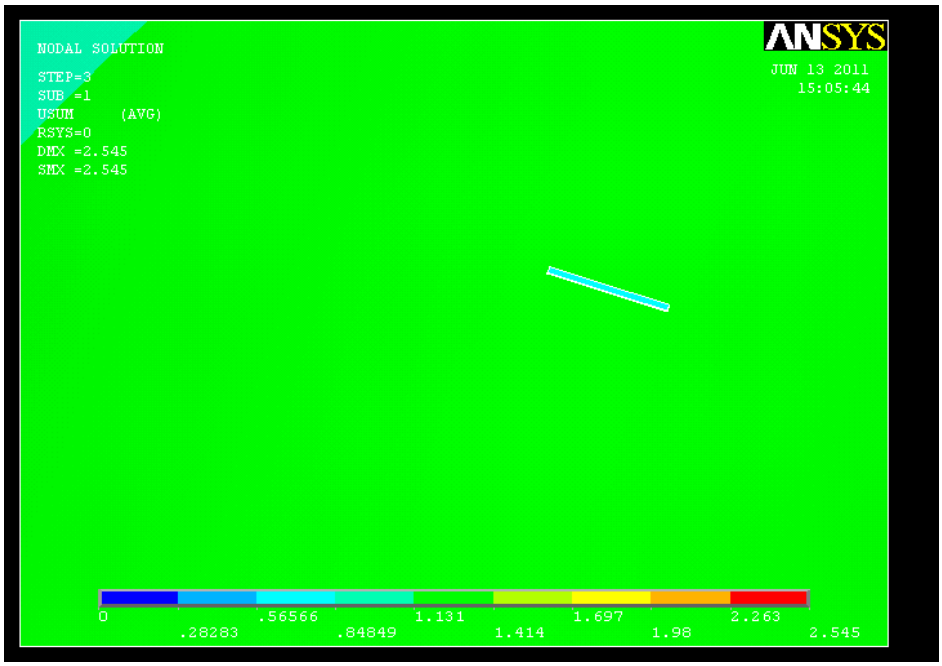

Figure 4.4. 7 ***Total displacement response for initial crack length =200mm***

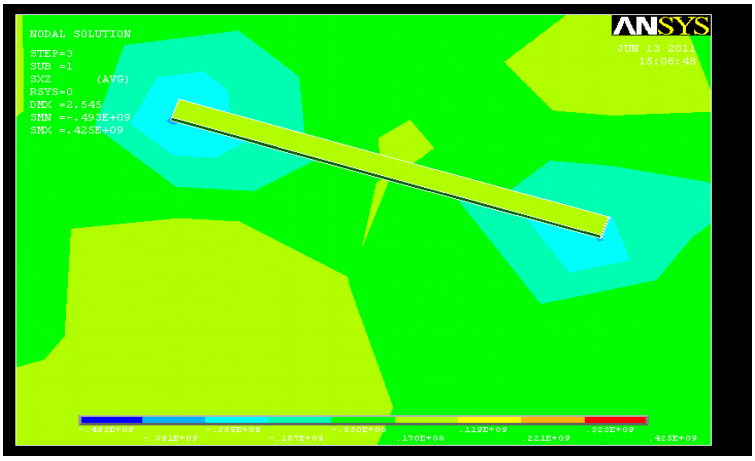

Figure 4.4. 8 ***Nodal shear stress for initial crack length=200mm***

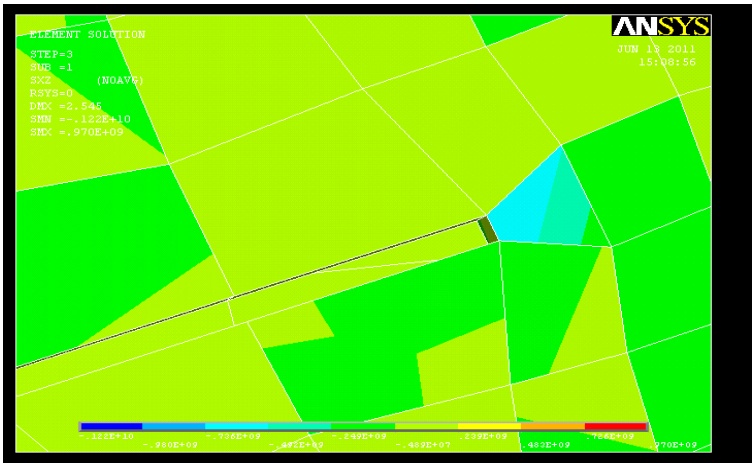

Figure 4.4. 9 ***Element shear stress for initial crack length=200mm***

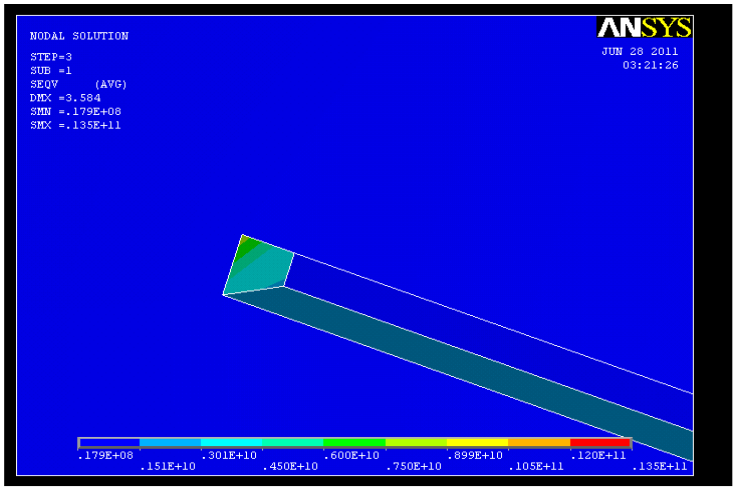

Figure 4.4. 10 ***Von misses stress for initial crack length=200mm***

Table 4. 3 Simulation results: Class H pavements.
The analysis is done on a 20%, 40%, 60%, 80% and 100% increase of crack length with the same type of loadings, crack orientation, and model.

Initial crack length =200mm					
S/N	Type of result	Parameter	Longitudinal crack Orientation	Circumferential crack Orientation	% Remark
1	Nodal solution	Uy=y-Displacement (mm)	2.491	2.527	
2		Usum=Total displacement (mm)	2.51	2.545	
3		Sxz= Shear stresses(Mpa)	455	425	
4		SEQV=Equivalent stresses (Mpa)	7910	13500	
5	Element solution	Sxz=Shear stresses(Mpa)	1190	970	
20% Increase of crack length =240mm					
1	Nodal solution	Uy=y-Displacement (mm)	2.4968	2.5476	
2		Usum=Total displacement (mm)	2.534	2.564	
3		Sxz= Shear stresses(Mpa)	532.2	431.2	
4		SEQV=Equivalent stresses (Mpa)	7968	13568.4	
5	Element solution	Sxz=Shear stresses(Mpa)	1264	1220	
40% Increase of crack length =280mm					
1	Nodal solution	Uy=y-Displacement (mm)	2.5026	2.5682	
2		Usum=Total displacement (mm)	2.558	2.583	
3		Sxz= Shear stresses(Mpa)	609.4	437.4	
4		SEQV=Equivalent stresses(Mpa)	8026	13636.8	
5	Element solution	Sxz=Shear stresses(Mpa)	1338	1340.5	
60% Increase of crack length =320mm					
1	Nodal solution	Uy=y-Displacement (mm)	2.5084	2.5888	
2		Usum=Total displacement (mm)	2.582	2.602	
3		Sxz=Shear stresses(Mpa)	686.6	443.6	
4		SEQV=Equivalent stresses(Mpa)	8084	13705.2	
5	Element solution	Sxz=Shear stresses(Mpa)	1412	1430	
80% Increase of crack length =360mm					
1	Nodal solution	Uy=y-Displacement (mm)	2.5142	2.6094	
2		Usum=Total displacement (mm)	2.606	2.621	
3		Sxz= Shear stresses(Mpa)	763.8	449.8	
4		SEQV=Equivalent stresses(Mpa)	8142	13773.6	
5	Element solution	Sxz=Shear stresses(Mpa)	1486	1500	
100% Increase of crack length =400mm					
1	Nodal solution	Uy=y-Displacement (mm)	2.52	2.63	
2		Usum=Total displacement (mm)	2.63	2.64	
3		Sxz= Shear stresses(Mpa)	841	456	
4		SEQV=Equivalent stresses(Mpa)	8200	13842	
5	Element solution	Sxz=Shear stresses(Mpa)	1560	1590	

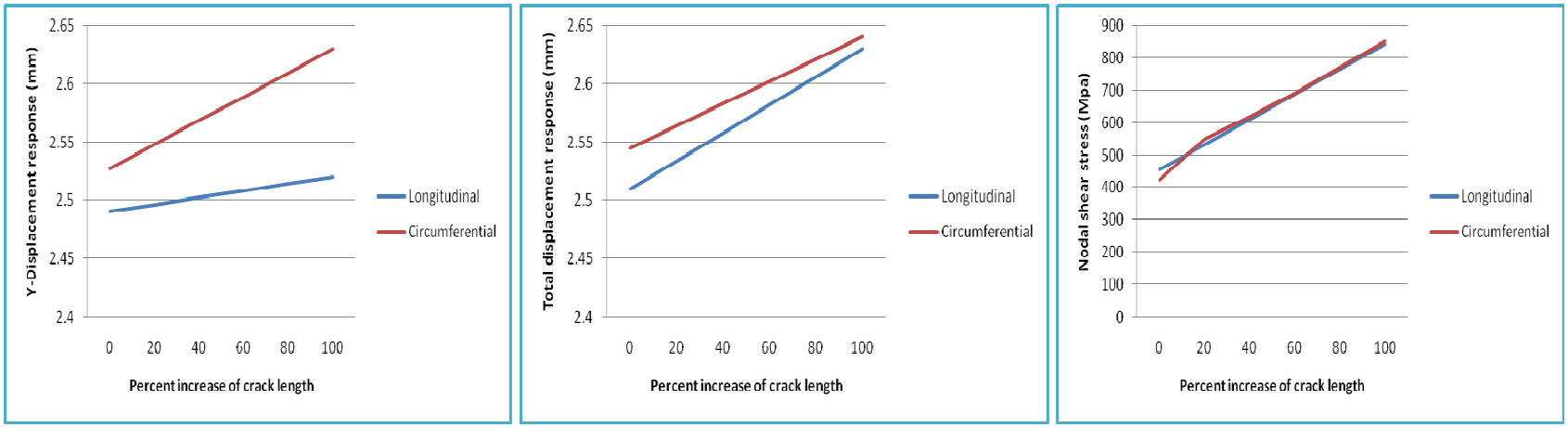

a)

b)

c)

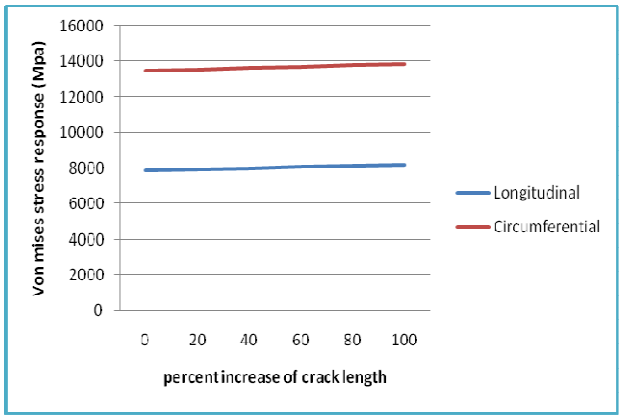

d)

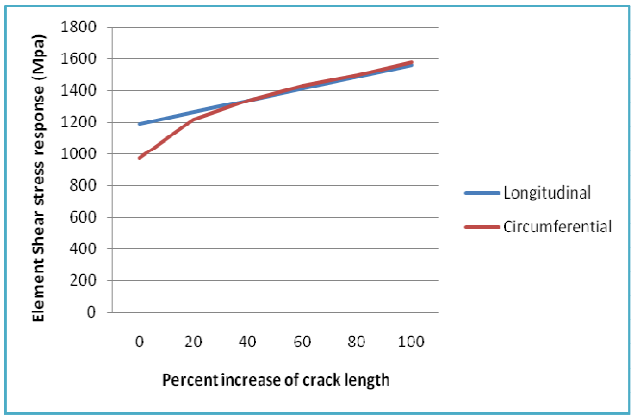

e)

Figure 4.4. 11 ***Percentage increase of crack length versus selected parameters***

Results and Discussion for class H runways

One Sigma and Three Sigma stress results:

- One sigma corner stress for the longitudinal crack orientation is 7.91GPa, and 68.2% of time of vehicle motion, the stress level is at or below this value. Three sigma corner stresses for the longitudinal crack orientation is 23.73GPa, and 4.3 % of time of vehicle motion, the stress level reach this value.
- One sigma corner stress for the circumferential crack orientation is 13.5GPa, and 68.2% of time of vehicle motion, the stress level is at or below this value. Three sigma corner stresses for the radial crack orientation is 40.05GPa, and 4.3% of time of vehicle motion, the stress level reaches at this value.

Here again, the sigma stress response both in the longitudinal and circumferential orientation of the crack is very high, which is much beyond the endurance limit of the shell, and the excitation severs the structure specially near crack tips and causes more fatigue as compared to smooth and pastured runway.

The curves on figures 4.4.11 a) and b) respectively show the variation of *y-displacement* and *total displacement responses* with percentage *increase of crack length*, for the *longitudinal and circumferential* crack orientation, for Class-H pavement input excitations. Figure 4.4.11 c) and figure 4.4.11 e) respectively show the variation of *nodal shear stress and element shear stress responses* with *percentage increase of crack length*, for the *longitudinal and circumferential* orientation of the crack, for the same Class-H pavement input excitations. And figure 4.4.11 d) shows the variation of *nodal Von Misses stress response* with *percentage increase of crack length*, for the *longitudinal and circumferential orientation of the crack* for similar type of pavement input excitations.

From the curves we can also see that the shell is highly damaged by the circumferential crack orientation for stresses and displacement/strain/ responses. The same reason can be applied for the stress response to maximize and the strains to excite more near the crack tips.

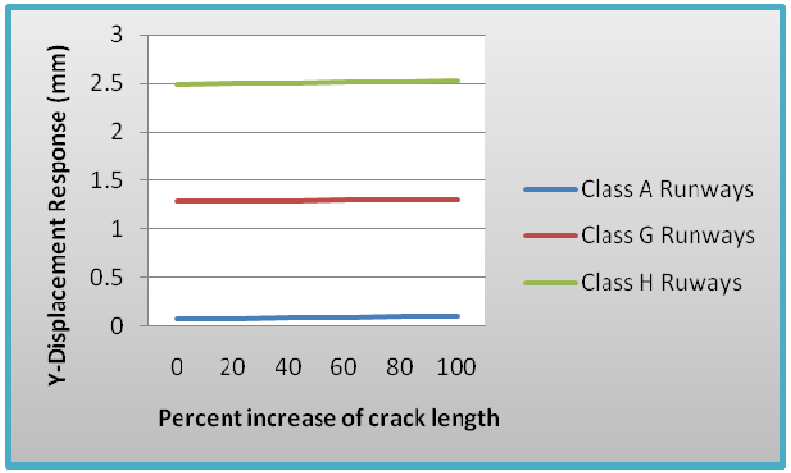

Figure 4.5. 1*Y-displacement response for longitudinal crack orientation*

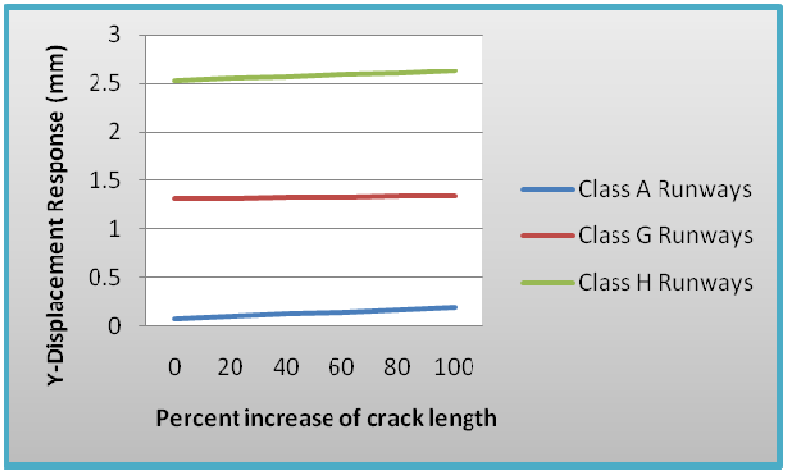

Figure 4.5. 2 *Y-displacement response f or circumferential crack orientation*

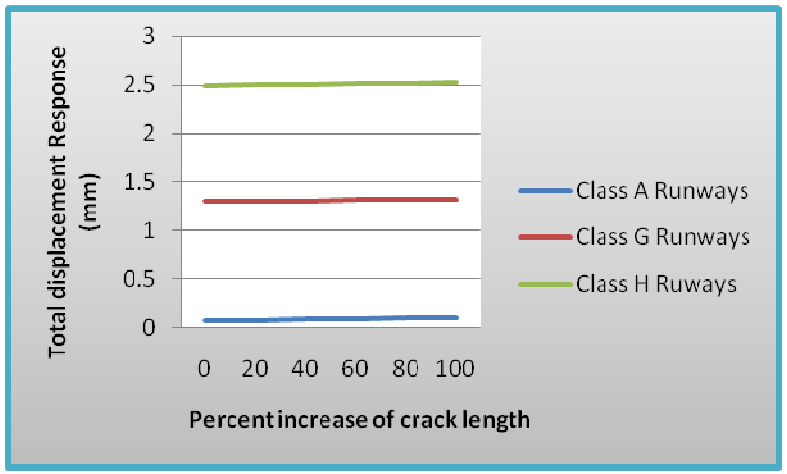

Figure 4.5. 3 *T*otal displacement response for longitudinal crack orientation

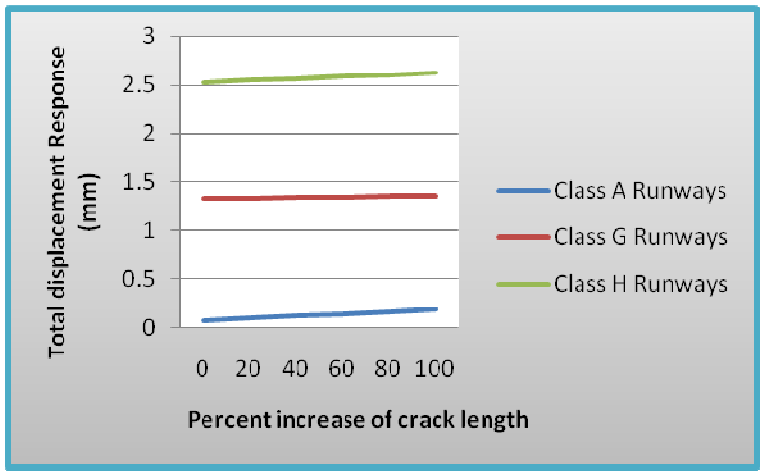

Figure 4.5. 4 *T*otal displacement response for *circumferential crack* orientation

Figure 4.5.5 and figure 4.5.6 respectively, represent *Y-displacement response with* percentage increase *of crack length* for *longitudinal* and *circumferential crack orientation,* for Class A, Class G and Class-H pavement input excitations.

Figure 4.5.3 and figure 4.5.4 represent *Total displacement response with* percentage increase *of crack length for longitudinal* and *circumferential crack orientation,* for Class A, Class G and Class-H pavement profiles.

All the curves are increasing as we go from smooth to plagued field. This is true that the smooth pavement is the least surface irregular as compared to pastured and plagued fields. The pastured excites more the shell especially near the crack tips due to its more random input in nature than next to smooth pavement and since, the plagued field is characterized by its highest nature of surface random, the stress and strain responses near crack zones are high.

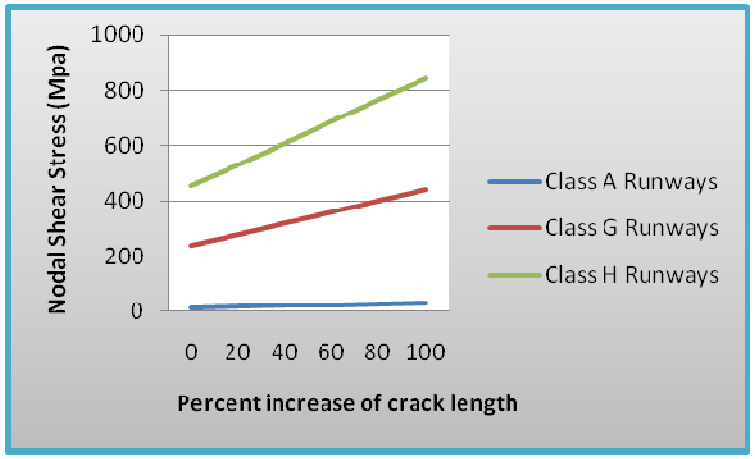

Figure 4.5. 7 *Nodal shear stress response for longitudinal crack*

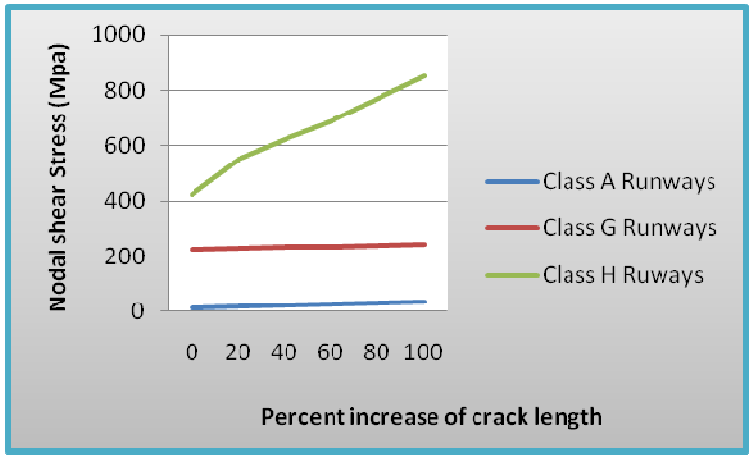

Figure 4.5. 8 *Nodal shear stress response for circumferential crack*

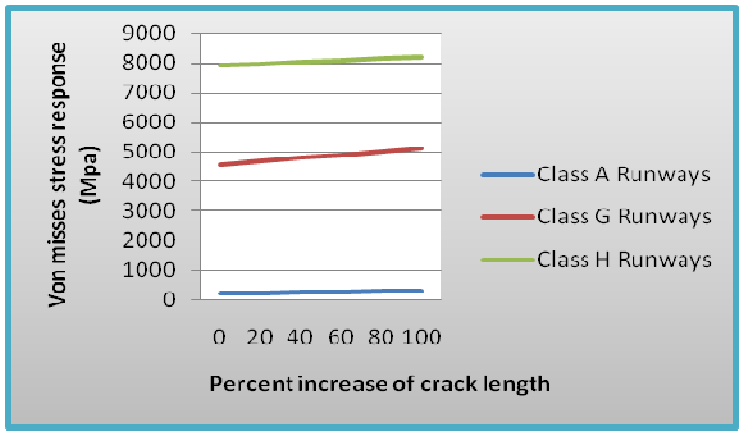

Figure 4.5. 9 *Von misses response for longitudinal crack orientation*

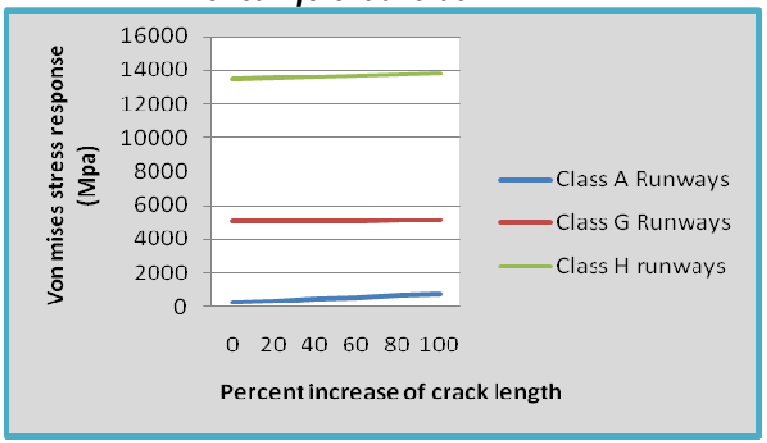

Figure 4.5. 10 *Von misses response for circumferential crack orientation*

Figure 4.5.5 and figure 4.5.6 respectively, represent *nodal shear stress response with* percentage increase *of crack length* for *longitudinal* and *circumferential crack orientation***,** for Class A, Class G and Class-H pavement input excitations. Figure 4.5.7 and figure 4.5.8 respectively, represent *Von misses stress response with* percentage increase *of crack length* for *longitudinal* and *circumferential crack orientation***,** for Class A, Class G and Class-H pavement input excitations.

Here again similar justifications discussed earlier are applied for nearly the linear variation of percentage increase of crack length with the various pavements, as we go through smooth then pastured and finally to plagued fields. On the other way we can also observe from the tables and graphs that the magnitude of stress response level is relatively small for smooth runway and higher for pastured fields and very high for plagued fields. Moreover, the magnitude of stress levels responded by the above pavements increase with increase of crack length. This is because of the linear variation of applied stress with crack length.

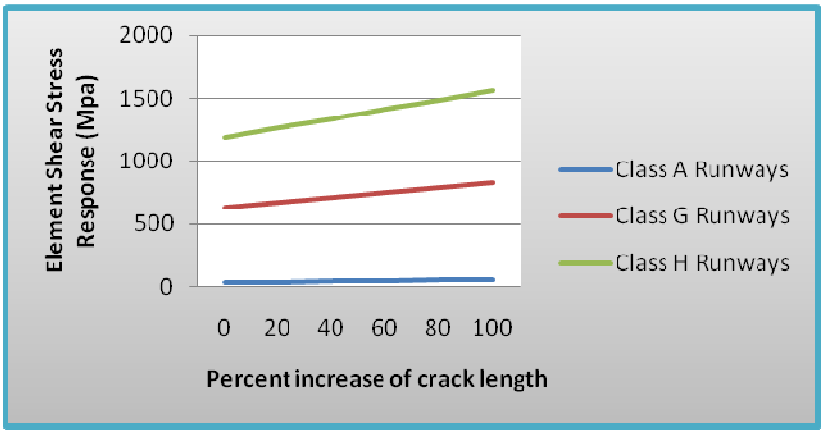

Figure 4.5. 11 ***Element shear stress response for longitudinal crack orientation***

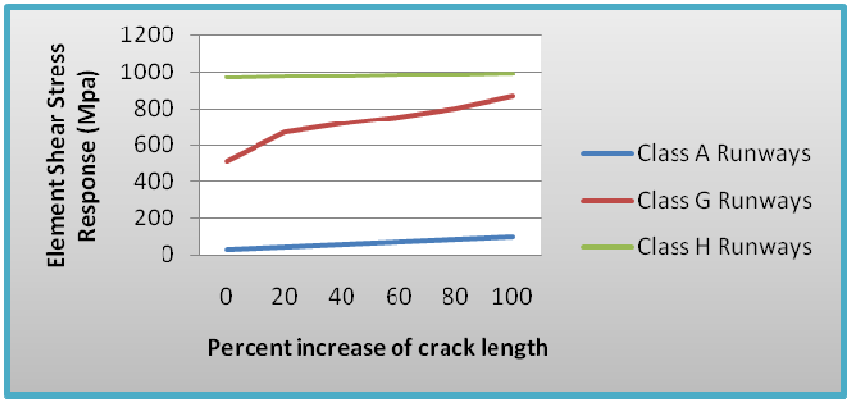

Figure 4.5. 12 *Element shear stress response for circumferential crack orientation*

Figure 4.5.9 and figure 4.5.10 respectively, show *element shear stress response with* percentage increase *of crack length* for *longitudinal* and *circumferential crack orientation***,** for Class-A, Class-G and Class-H pavement roughness excitations.

Here also as discussed earlier the magnitude of stress response increases with increase in crack length; and increase with increase in pavement roughness.

Chapter Five

5.1 Conclusion

In this study, the stress and strain responses of shell type aerospace materials having a crack with longitudinal and circumferential arrangement under dynamic loadings mainly random vibration loadings are determined, the results of which are believed to be significant to the aerospace material engineers. Dynamic analysis is a very important investigation when it comes to the composite materials, where these can exhibit diversity in material properties as well as shapes. This research addresses the effects of ground induced excitation on the stress and strain distribution on a surface cracked shell located on the outer most top part of the shell.

In actual life situations, performing random vibration is very difficult task and takes much time to calculate the results, so that the use of computer software's make it easy for printing out the results.

In all curves as the crack length increases the displacement and stresses response near the crack tips increases. We can see from the literature that the applied stress is directly proportional to the square root of the half crack length. This result was verified experimentally by Griffith for a wide range of crack length. This confirms both the analytical and experimental results obtained by Griffith's and other similar researchers.

From the curves we can observe that the shell responds relatively lowest stress and displacement response than Class G and Class H pavement. Class H has the worst stress and strain response near crack tips and much affects and severs the thin structure. So in the event of forced and emergency landing, the pilot has recommended to land as much as possible on Class G pavement than Class H pavement.

5.2 Future works

This work is done for finding the location of fracture on the all composite fuselage modeled as a shell with the presence of shock absorbing devices. Here a crack of having significant dimension is orientated longitudinally and circumferentially; and is placed externally on the outer most top part of the shell opposite to the direction of excitations. But fracture of composites basically ranges from debonding, delamination, matrix breakage and plasticity and so on. Modeling and performing analysis on such types of fracture is let for future researches. Moreover the various location and orientation of crack model with respect to the different types of pavement roughness inputs and varying the landing speed of the aircraft can also be proposed for future works. Since the fracture analysis is done by neglecting the effects of cutouts on the skin, consideration of these effects can be let for future works. Since the present work of fracture analysis is done for three point landing gear case, landing on a single leg, landing on two legs with or without the failure of the shock absorbing device and crack tip responses for loads due to impact loading are proposed for future works.

5.3 References

1. Jan R. Wright, Jonathan E. Cooper, **"**Introduction to Aircraft Aero-elasticity and Loads"
2. T.L. Anderson, (1995) "Fracture mechanics: Fundamentals and application", 2nd Ed, pp.12-18.
3. ANSYS Documentation manuals.
4. D.E. Newland "An introduction to, Random vibrations, Spectral and Wavelet analysis", Third edition.
5. Krautkramer, J and Krautkramer, H., (1990), "Ultrasonic testing of materials", 4th Ed., springer-Verlag, U.S.A.
6. Sansalon, M. and Carino, N.J., (1991), "Stress wave propagation methods," in Hand book on Nondestructive testing of concrete, Ed. V.M. Malhotra and N.J.Carino, pp. 275-304.
7. Sansalon, M. and Carino, N.J., (1986), "Impact-Echo: A method for flaw detection in concrete using transient stress waves," NBSIR 86-3452, National Bureau of standards, Sept., 222p.
8. J.Y. Wong, Ph.D, D.Sc, F.I. Mech.E, F.A.S.M.E, F.C.S.M.E, "Theory of Ground Vehicle", Third edition.
9. T.H.G. Megson "Aircraft structures for engineering students", Fourth edition.
10. Reza N. Jazar "Vehicle Dynamics: Theory and Applications"
11. Turkiy "Aircraft structures and constructions"
12. "Hand book of composite materials", voluem3. Polymer matrix composite, material usage, design, and analysis.
13. Mechanics of composite materials
14. Master's degree thesis, 2005. "Dynamic analysis of cracks in composite materials." Vidya Sagar Avadutala.
15. Master's degree thesis, 2008. "Static and dynamic analysis of a commercial vehicle with van body" Kassahun Mekonnen.

16. T. Stolarski, Y. Nakasone, S. Yoshimoto “Engineering analysis with ANSYS software.”

17. Alan T. Zehnder, Ph.D. “Lecture notes on fracture mechanics” June 23, 2009.
18. Alastair F. Johnson. “Impact and crash modeling of composite structures: Achallenging for damage mechanics.” Engineering Systems International GmbH Eschborn, Germany.
19. J. C. F Telles and C. A. R Vera-Tudela “A BEM NGF technique coupled with Operational quadrature method to solve Elastodynamic crack problems.” Federal University of Rio de Janeiro, COPPE/UFRJ Programa de Engenharia Civil.
20. Perrin et *al*. *(1995)* and Geubelle and Rice (1995) “A spectral method for Elastodynamic fracture analysis with out spatial replication of the rapture event”
21. Chen L.W., 1989. “Asymmetric dynamic stability of thick annular plates based on a high- order plate theory.” J. Sound Vibration, 130: 425-437.
22. Sérgio Frascino Müller de Almeida**,** Instituto Tecnológico de Aeronáutica – Mechanical Engineering Department. “Design and analysis of a composite fuselage.”
23. Internet resources.